UNIVERSITY OF INSUBRIA

Varese

A Thesis submitted for the degree of
Philosophiæ Doctor (Ph.D.) in Experimental and Clinical Physiology

XXVI cycle

Inward Rectifier Potassium Current in Dopaminergic Periglomerular Cells of Mouse Olfactory Bulb

Tutor Dr Elena Bossi
Co-tutor Prof. Ottorino Belluzzi
Coordinator Prof. Daniela Negrini

Ph.D. Student Dr. Mirta Borin

Academic Year 2012-2013

CONTENTS

ABBREVIATIONS AND ACRONYMS

ABC	– ATP-binding cassette
AMPA	– Amino-3-hydroxy-5-methyl-4-isoaxozole-propionic acid
ATP	– Adenosine-5'-triphosphate
cGMP	– Cyclic guanosine monophosphate
DF	– Driving Force
DG	– Dentate Gyrus
E_K	– Potassium equilibrium potential
EPL	– External Plexiform Layer
G protein	– GTP binding protein
G_{olf}	– Olfactory heterotrimeric G protein
$G_{\beta\gamma}$	– βγ subunit of G protein
GIRK	– G protein-coupled inwardly-rectifying potassium channel
g_{Kir}	– Kir Conductance
GL	– Glomerular Layer
GPCR	– G protein-coupled receptor
Gr	– Granule cell
GRL	– Granule Cell Layer
IP_3	– Inositol 1,4,5-trisphosphate
IPL	– Internal Plexiform Layer
JG	– Juxtaglomerular
K_{Ach}	– Muscarinic-gated K^+
K_{ATP}	– Adenosine-5'-triphosphate inhibited K^+
Kir	– Inwardly rectifying K^+
LC-CoA	– Long-chain acyl–coenzyme A
LV	– Lateral Ventricle
M	– Mitral Cell
MCL	– Mitral Cell Layer
NBD	– Nucleotide binding domain
NMDA	– *N*-Methyl-*D*-aspartic acid or *N*-Methyl-*D*-aspartate
NKCC2	– Na^+ -K^+ -2Cl^- co-transporter
OB	– Olfactory Bulb
ONL	– Olfactory Nerve Layer
OSN	– Olfactory Sensory Neuron
PA	– Polyamine
PIP_2	– Lipid phosphatidyl-4,5-bisphospate
PG	– Periglomerular Cell
PLC	– Phospholipase C
RGS	– Regulators of G protein signaling
RMS	– Rostral Migratory Stream
ROMK	– Renal outer medullary K^+
RPE	– Retinal pigmented epithelium
SA	– Short Axon Cell
SF	– Selectivity filter
SGV	– Subgranular Zone
SNr	– Substantia Nigra
SPD	– Spermidine
SPM	– Spermine
SUR	– Sulfonylurea Receptor
SVZ	– Subventricolar Zone
T	– Tufted Cell
TMD	– Transmembrane domain
V_M	– Membrane potential

ABSTRACT

Inward rectifier potassium (Kir) channels are important for neuronal signalling and membrane excitability. In this work, *patch-clamp* techniques were used to characterize Kir channels in mouse dopaminergic (DA) periglomerular (PG) cells. These interneurons are critically placed at the entry of the bulbar circuitry, in contact with terminals of olfactory sensory neurons and with dendrites of projection neurons.

Perforated-patch configuration was adopted to record Kir current in DA-PG cells in thin slice. I_{Kir} could be distinguished from the hyperpolarization-activated current by showing full activation in < 10 ms, no inactivation, suppression by Ba^{2+} in a typical voltage-dependent manner and reversal potential nearly coincident with E_K.

DA-PG cells are autorhythmic and are target of numerous afferents releasing a variety of neurotransmitters, although their properties and role remain elusive. Depolarization induced by Ba^{2+} blocks spontaneous activity, although the Kir current is not an essential component of the pacemaker machinery.

The current is negatively modulated by intracellular cAMP, as shown by a decrease of its amplitude induced by forskolin. Several neuromodulatory effects were tested on the Kir current of DA-PG cell. Activation of metabotropic receptors - known to be present on these cells - shows that the current can be modulated by a multiplicity of pathways. The Kir current can be increased, as observed with agonists of muscarinic, α1 noradrenergic and $GABA_A$ receptors, or I_{Kir} modulation can caused the opposite effect, i.e. agonists of D2, 5-HT and histamine receptors.

These characteristics of the Kir currents provide the basis for additional flexibility of DA-PG cells signaling and function.

1 INTRODUCTION

Sensory perception is a process by which information from the external world is reformatted into an internal state. A number of very different but elegant ways, based on distinct sensory channels, have risen according to the phylogenetic position of the species. Among them, communication with the environment and other organisms through chemical cues is an essential process for the survival of all multicellular systems.

The olfactory system recognizes a great numbers of odour substance and discriminates chemical signals with fine differences in their structural properties, which come from outdoor environment and can profoundly influence animal behaviour; so olfactory system provides essential information for animal survival.

The mammalian olfactory system regulates a wide range of multiple and integrative functions such as physiological regulation, emotional responses (anxiety, fear, pleasure), reproductive functions (sexual and maternal behaviours), and social behaviours (recognition of conspecifics, family, clan, or outsiders) (Lledo et al. 2005).

To achieve all these function, anatomically and functionally separate sensory organs are required (fig. 1.1). In mammals, the main olfactory system includes the olfactory epithelium, which represents the sensory organ recognizing more than a thousand airborne volatile molecules, called odorant compounds (or odorants). This neuroepithelium is connected to the next central station for processing olfactory information: the main olfactory bulb (OB). The olfactory epithelium contains several thousands of bipolar olfactory sensory neurons, each projecting to one of several modules in the olfactory bulb. These discrete and spherical structures, called olfactory glomeruli, are considered to be both morphological and functional units made of distinctive bundles of neuropil (Shipley & Ennis 1996). So, sensory inputs received by the cells in the glomerular unit result homogeneous, and this organization shows the degree to which the neurons in the same glomerular unit are interconnected.

In different species the number of olfactory glomeruli are different: rodent olfactory bulbs contain several thousand glomeruli, whereas fish and insects have 10-fold fewer, and glomerular structure can result from the convergence of 5,000 to 40,000 axon terminals that establish synapses with dendrites of bulbar output neurons and different local bulbar interneurons. Moreover, several and different mechanisms have evolved to ensure that only a single odorant receptor is expressed per sensory cell. In rodents, strict transcriptional control results in the choice of one among a possible thousand odorant receptor genes (Malnic et al. 1999).

After processing in the olfactory bulb, physiological signals are delivered directly to the secondary sensory centres in the primary olfactory cortex.

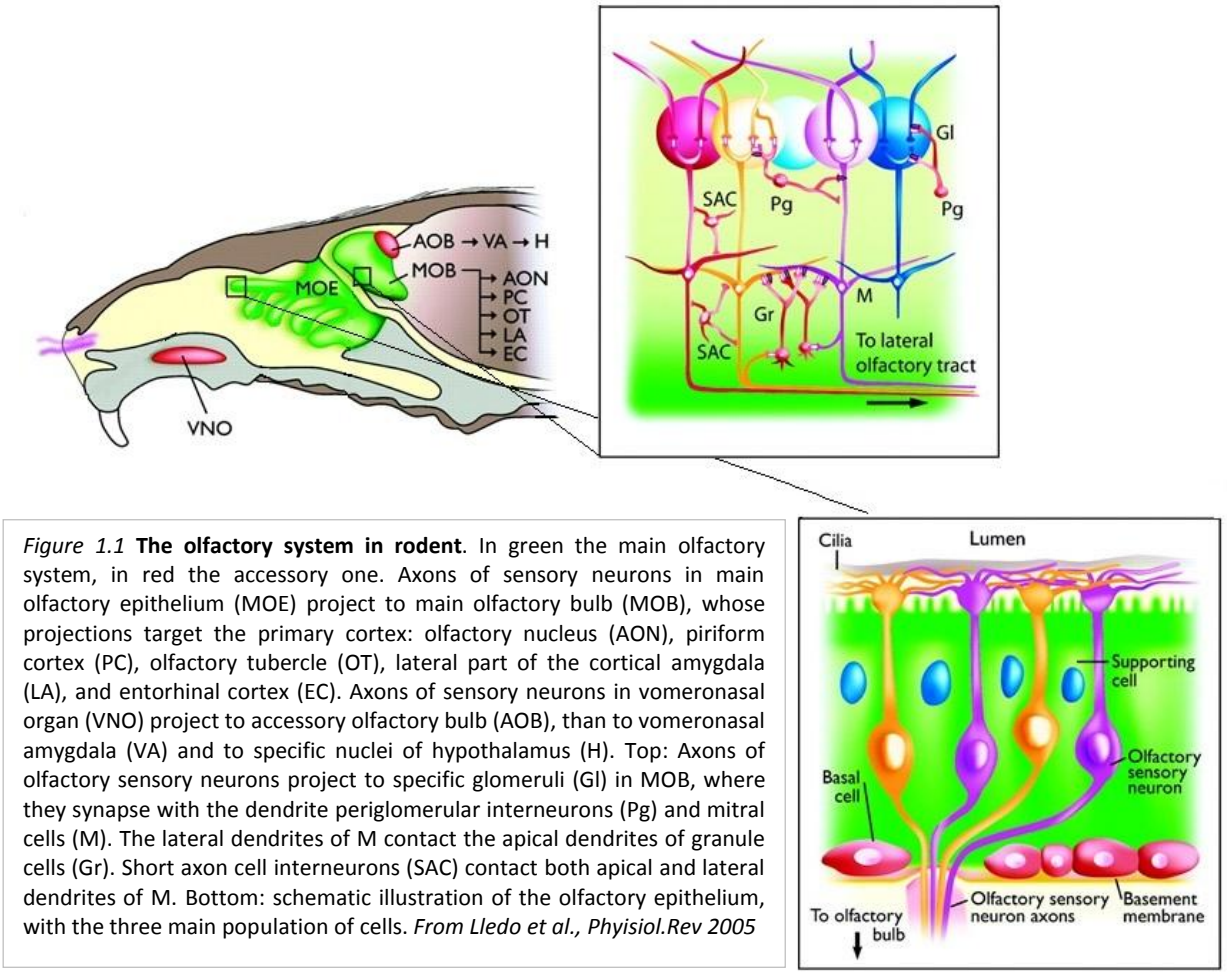

Figure 1.1 **The olfactory system in rodent**. In green the main olfactory system, in red the accessory one. Axons of sensory neurons in main olfactory epithelium (MOE) project to main olfactory bulb (MOB), whose projections target the primary cortex: olfactory nucleus (AON), piriform cortex (PC), olfactory tubercle (OT), lateral part of the cortical amygdala (LA), and entorhinal cortex (EC). Axons of sensory neurons in vomeronasal organ (VNO) project to accessory olfactory bulb (AOB), than to vomeronasal amygdala (VA) and to specific nuclei of hypothalamus (H). Top: Axons of olfactory sensory neurons project to specific glomeruli (Gl) in MOB, where they synapse with the dendrite periglomerular interneurons (Pg) and mitral cells (M). The lateral dendrites of M contact the apical dendrites of granule cells (Gr). Short axon cell interneurons (SAC) contact both apical and lateral dendrites of M. Bottom: schematic illustration of the olfactory epithelium, with the three main population of cells. *From Lledo et al., Phyisiol.Rev 2005*

The accessory olfactory system comprises the vomeronasal organ, which is specialized to sense chemical compounds (pheromones), and transfers information through the accessory olfactory bulb; this sensory organ provides information about the social and sexual status of other individuals within the species (Lledo et al. 2005).

However, recent evidence also suggests some cross-talk between the main and accessory systems. Indeed, the vomeronasal organ does not have an exclusive function with regard to pheromone recognition, but in rodents, it responds also to other molecules than pheromones (Luo et al. 2003).

1.1 The Main Olfactory System

The main olfactory system (referred to below simply as olfactory system) interfaces environment and central nervous system. It is responsible for correctly coding sensory information from thousands of odorous stimuli, which are processed throughout distinct levels. Each information processing level plays an important role in stimuli coding from the odorant receptors up to the level of the olfactory cortex (Lledo et al. 2005).

From Neuroepithelium to Olfactory Bulb

In mammals, the initial event of odor detection takes place at the periphery of olfactory system, the olfactory epithelium of the nasal cavity, which is located at the posterior end of the nose. This turbinate reach area detects an immense variety of volatile molecules of differing shapes and sizes present in the environment (Buck 1996, Firestein 1996). Olfactory transduction starts with about a thousand different types of odorant receptors located on the cilia of sensory neurons that comprise the olfactory neuroepithelium (Zhang & Firestein 2002). Three major cell types form this epithelium: sensory neurons, supporting cells, and several types of basal cells including the olfactory stem cells (fig. 1.1, bottom). Once mature, the sensory bipolar neurons extend a single dendrite to the neuroepithelial surface from the apical pole.

Sensory neurons dendrites present numerous cilia, which extensively invade the mucus layer of the nasal cavity. It appends in the nasal mucus that odor molecules bind to specific receptors on the cilia. Odorant receptors belong to the family of the G protein-coupled seven-transmembrane proteins, and in order to mediate odor detection tissue-specific downstream components are involved, such as the heterotrimeric G protein subunit (G_{olf}), type III adenylyl cyclase, and cyclic nucleotide-gated ion channels. In addition, several other second messenger cascades, which may involve Ca^{2+}, inositol trisphosphate (IP_3), or cyclic guanosine monophosphate (cGMP) regulate secondary events such as odorant adaptation. Activation of olfactory receptors induces a cascade of intracellular events resulting in an influx of both Na^{+} and Ca^{2+} that depolarizes the sensory neuron (Lledo et al. 2005).

On the other hand, each sensory neuron lengthens a single unmyelinated axon across the basal lamina and cribriform plate (of the ethmoid bone) in the olfactory bulb, through the olfactory nerve, where axons pack in fascicles, which transmit the electrical signals to the bulb. Throughout the olfactory pathway, a unique population of glia forms the bundles of axons that make up the olfactory nerve.

Upon reaching the olfactory bulb, axon terminals from olfactory sensory neurons expressing the same odorant receptor converge on a specific glomerulus (Lledo et al. 2005).

There is no strict spatial relationship between the arrangement of excitatory projections of the olfactory sensory neurons in the olfactory bulb and the regions of mucosa from which they originate, also bulbar outputs do not have point-to-point topographical projections to their target structures. This feature contrasts with the spatial organization of sensory systems in general, where afferent inputs are organized in a topographical mode. An activity-dependent mechanism seems rather to be responsible of bulbar extensive organization and targeting (Lledo et al. 2005). Recent reports highlight further mechanisms based on spontaneous and odorant-evoked neuronal activity in the establishment and maintenance of the sensory projections (Zou et al. 2004, Yu et al. 2004).

From Olfactory Bulb to Primary Cortex

Before the transmission to upstream centres odor information received by the olfactory bulb is processed and refined. According to the topographical organization of the bulbar circuit, two odor processing sites are involved: the glomeruli, where inputs arrived from sensory neurons, and the external plexiform where dendrite of output neurons stand.

Next processing occurs in primary and accessory olfactory cortex. These higher centers include the anterior olfactory nucleus, which connects the two olfactory bulbs through a portion of the anterior commissure, the olfactory tubercle, the piriform cortex (considered to be the primary olfactory cortex), the cortical nucleus of the amygdala, and the entorhinal area (Shipley & Ennis 1996).

The olfactory tubercle projects to the medial dorsal nucleus of the thalamus, which in turn projects to the orbitofrontal cortex, the region of cortex thought to be involved in the conscious perception of smell (Rolls 2001). Olfactory information must be relayed from convergent synapses in the olfactory bulb to higher brain centers, where it is decoded to yield a coherent odor image.

1.1.1 Neuronal Replacement in the Adult Olfactory System

The olfactory system is considered a good model for the study of adult neurogenesis because it exhibits lifelong turnover of peripheral sensory neurons and bulbar interneurons. Adult neurogenesis is present both in olfactory epithelium, where cell renewal persists throughout adult life to replace olfactory sensory neurons (Graziadei et al. 1978, Calof et al. 1998, Moulton 1974) and in the subventricular zone (SVZ), an area near the ventricle of the forebrain.

Globose and horizontal basal cells, deeply located in the olfactory epithelium are responsible of epithelial adult neurogenesis. Neurogenesis in the olfactory epithelium is tightly regulated by environmental factors: ablation of the olfactory bulb enhances neurogenesis (Carr & Farbman 1993), while blocking airflow through one side of the nasal cavity causes an ipsilateral reduction in cell proliferation. Also, differentiated neurons contribute to maintain cell population equilibrium sending back regulatory signals to inform progenitor cells about the number of new neurons that need to be produced. For this reason, studying mechanisms that control the rate of neuronal production is particularly interesting here.

In adult mammalian brain, the subventricular zone, which lines the lateral walls of the ventricles (LV), and the subgranular zone (SGV) of the dentate gyrus (DG) of the hippocampus constitute two sites of neuronal production (Altman 1963).

Bulbar interneurons are derived from neuronal precursor cells that migrate from the lateral ganglionic eminences, in embryo (Wichterle et al. 2001). Postnatally, they derive from neuronal precursor cells of SVZ that migrate in the rostral migratory stream (RMS) (Temple & Alvarez-Buylla 1999). Within the SVZ, the neural precursor cells are considered as stem cells since they proliferate and give rise to neuronal lineage cells: astrocytes, oligodendrocytes and neurons (Temple & Alvarez-Buylla 1999, Peretto et al. 1999). Mammalians continuous generation of SVZ neurons has been found not only in rodents (Lois & Alvarez-Buylla 1994, Altman & Das 1965, Hinds 1968) but also in primates (Kaplan 1983, Kobal & Kettenmann 2000, Kendrick et al. 1988, Pencea et al. 2001), and humans (Kukekov et al. 1999, Weickert et al. 2000).

It is still unknown the potency degree of SVZ neuronal stem cells: *in vitro* studies indicate forebrain periventricular stem cells as multipotency ones, controversial *in vivo* approaches underline the rather limited fate of this cells, which express neuronal markers(Gage 2000, Temple 2001). In addition, precursor cells of the SVZ can migrate tangentially, going on dividing during their migration along the RMS, to populate the olfactory bulb, where they differentiate into local neurons (Lois &

Alvarez-Buylla 1994(Luskin 1993). For this reason there is a prominent interest in studying chemical factors (fig.1.2) that inhibit or promote neurogenesis, neuronal differentiation and migration, or actively produce apoptotic cascades, since apoptosis seems to play an important role in controlling neuron numbers (Lledo et al. 2006). When neuroblasts reach the olfactory bulb, they migrate radially, and 90% differentiate into GABAergic and 10% into dopaminergic interneurons of the glomerular and granule cell layers (Betarbet et al. 1996).

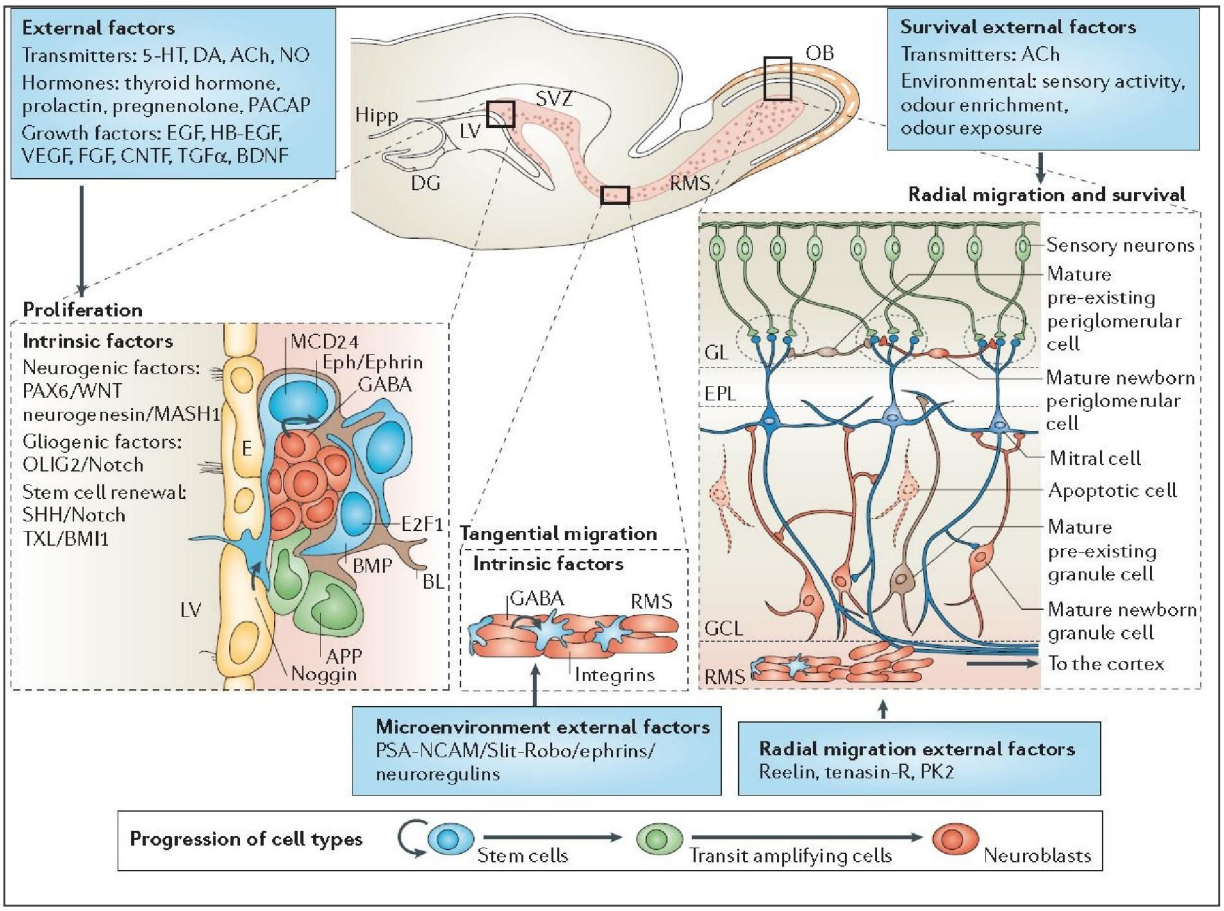

Figure 1.2 **Neurogenesis in adult olfactory bulb** Proliferation in the subventricular zone (SVZ) takes place in the medial wall of the lateral ventricle (LV), where stem cells divide to generate transit amplifying cells. In turn, they give rise to neuroblasts that migrate in the rostral migratory stream (RMS) to their final destination in the olfactory bulb (OB). Intrinsic and external factors control newborn cell proliferation and fate. The tangential migration along the RMS is regulated by contact-mediated repulsion or attraction interactions between neuroblasts and the microenvironment. Chain detachment and radial migration are regulated by external factors reelin, tenascin-R, and prokineticin 2 (PK2). When neuroblasts reach their last localization, radial migration trough the different layer of the olfactory bulb stops. Here they differentiate into two local interneuron subtypes: granule cells and periglomerular neurons. Sensory input establish cells survival and fate.

5-HT, 5-hydroxytryptamine (serotonin); ACh, acetylcholine; APP, amyloid precursor protein; BDNF, brain-derived neurotrophic factor; BL, basal lamina; BMI1, polycomb family transcriptional repressor; BMP, bone morphogenetic protein; CNTF, ciliary neurotrophic factor; DA, dopamine; DG, dentate gyrus; E, epidermal cell; E2F1, E2F transcription factor 1; EGF, epidermal growth factor; EPL, external plexiform layer; FGF, fibroblast growth factor; GABA, gamma-aminobutyric acid; GCL, granular cell layer; GL, glomerular layer; HB-EGF, heparin-binding EGF; Hipp, hippocampus; MASH1, mammalian achaete-scute homologue 1; MCD24, glycosylphosphatidyl-inositol-anchored highly glycosylated molecule; NO, nitric oxide; OLIG2, oligodendrocyte transcription factor 2; PACAP, pituitary adenylate cyclase-activating polypeptide; PAX6, paired box 6; PSA-NCAM, polysialic acid–neuronal cell adhesion molecule; SHH, sonic hedgehog; TGFalpha, transforming growth factor-alpha; TXL, thioredoxin-like 1; VEGF, vascular endothelial growth factor.

From Lledo PM et al., Neurosci. 2006.

1.2 Olfactory Bulb

Olfactory bulb, one of the most interesting parts of the brain, is an excellent model for understanding the neural mechanisms of sensory information processing, moreover it constitutes a site in which interneurons are added in postnatal and adult life.

Since first studies, it has known that "the olfactory bulb is not merely a 'ganglion' in which the olfactory pathway is synaptically interrupted, but is indeed a centre of great complexity containing associative connections at several levels, intrinsic neuronal circuits of varying length, and a 'centrifugal' as well as the sensory input" (Nieuwenhuys 1967).

The first relay station for transmission of olfactory information is, indeed, olfactory bulb, which receives and processes the information from the olfactory sensory neurons in the nasal mucosa and it sends this information to different parts of the primary olfactory cortex in the forebrain.

Axonal termini of olfactory sensory neurons (OSNs) from the olfactory epithelium synapse directly onto second order neurons within the forebrain. In the olfactory bulb, OSNs form both synapses with output (second order) neurons and local interneurons in the glomerular layer (GL). Sensory neurons expressing a given receptor project to a specific subset of glomeruli, making a topographical organization highly conserved in different species across phyla (Lledo et al. 2006).

A given glomerulus can respond to multiple odorants, and a given odorant activates multiple glomeruli. As a result, odor identity is represented by patterns of glomerular activation, depending on properties of synaptic transmission between sensory neurons and their postsynaptic targets in OB.

In the glomeruli, OSN termini form excitatory glutamatergic synapses with the apical dendrites of the bulbar output cells (Aroniadou-Anderjaska et al. 1997), and with periglomerular interneurons (Keller et al. 1998). These types of olfactory nerve-evoked excitatory response comprise fast AMPA and slow NMDA components (Aroniadou-Anderjaska et al. 1997, Berkowicz et al. 1994, Chen & Shepherd 1997). Complex mechanisms take place in order to reliably transmit information contained in the odorant-evoke firing of sensory neurons to the brain. Under normal condition, glutamate release from OSN termini is high (Aroniadou-Anderjaska et al. 2000, Hsia et al. 1999); this feature makes the olfactory system able to detect extremely faint sensory signals. In presence of threshold odorant concentration, the ability of amplify low signals of olfactory nerve-evoked excitatory responses, by high glutamate release, ensures transmission of information contained in sparse sensory

neuron firing and it provides a mechanism by which afferent inputs to the bulb are highly reliable (Murphy & Isaacson 2003, Murphy et al. 2005). On the other hand, at high concentration of odorants expected burst response does not take place due to the strong paired-pulse depression, which avoids system saturation ensuring system modulation. High level of odorants reduce but never strengthen the synaptic transmission between olfactory sensory neurons and olfactory bulb (Ennis et al. 1996, Aroniadou-Anderjaska et al. 2000), by activation of presynaptic metabotropic receptors present on olfactory sensory neurons. In this mechanism, periglomerular local neurons play a key role releasing dopamine and GABA within olfactory bulb glomeruli (McLean & Shipley 1988, Smith & Jahr 2002). These local neuromodulators reduce both the transmitter release from olfactory nerve terminals and *paired-pulse* depression - via activation of presynaptic D2 dopamine and GABAB receptors. They could further maintain relative response magnitudes across a wide range of input intensities, reducing sensory noise and improving contrast between neighbour-activated glomeruli (Aroniadou-Anderjaska et al. 2000, Ennis et al. 1996) (Hsia et al. 1999, Lledo & Gheusi 2003).

1.2.1 Synaptic Processing within the Olfactory Bulb

Although, odorants induce a well-organized pattern of activation in glomeruli across the surface of the olfactory bulb, transduction mechanisms, which transform input signals into a specific odor code, remain still unclear.

Principal output neurons

The main output neurons are located in a single lamina (figure 1.3), the mitral cell layer (MCL), and they extend the primary dendrite vertically to contact one glomerulus, where interactions with bulbar interneurons and olfactory nerve terminals occur (Mori et al. 1999). Mitral cell secondary (or basal) dendrites (two to nine) radiate horizontally the bulb branching in the external plexiform layer (EPL). Two type of mitral cells (M) are identified (Orona et al. 1984, Mori et al. 1983, Macrides & Schneider 1982). More numerous type I mitral cell have basal dendrites in deep EPL, displaced type II mitral cells have basal dendrites near the middle of EPL and their somata lie more superficially than type I.

The other kind of output neuron, Tufted cells (T), can be separated in three groups as a function of their cell body location: middle and internal tufted cells have their somata in the EPL, near the middle and in deep respectively, while external tufted cells stand in the glomerular layer. Middle and internal tufted cells present basal dendrites and an apical dendrite that terminates within a single

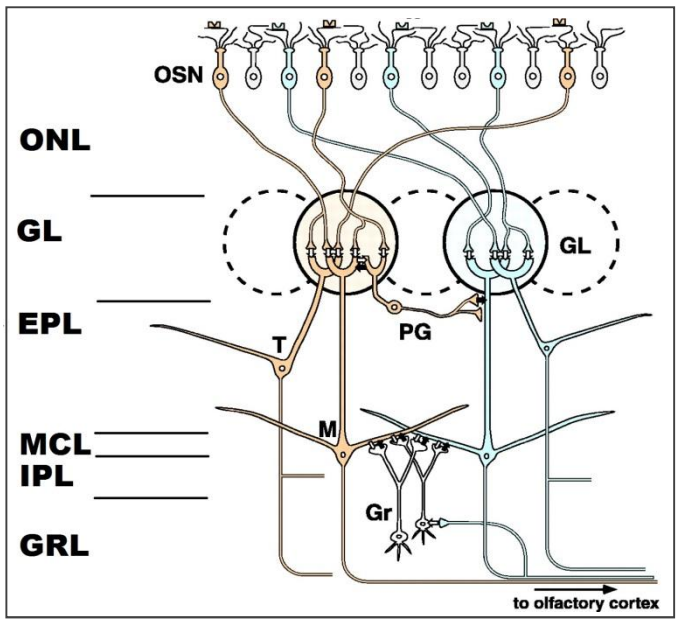

Figure 1.3 **Basic circuit diagram of olfactory bulb**.
In two different colors are showed glomerular modules representing two different types of odorant receptors. White arrows denote excitatory synapses, while black arrows denote inhibitory synapses. Mitral cells (M) and tufted cells (T) are output neurons, and granule cells (Gr) and periglomerular cells (PG) are local interneurons. OSN, olfactory sensory neuron, ONL, olfactory nerve layer; GL, glomerular layer; EPL, external plexiform layer; MCL, mitral cell layer; IPL, internal plexiform layer; GRL granule cell layer.
From Mori K. et al., Science 1999

glomerulus. Axons of these cells project to the primary olfactory cortex. An external tufted cell has short apical dendrite, which terminates in a glomerulus, and basal dendrites extending below glomerular layer. Some external tufted cells send their axon to the cortex, whereas axons of others terminate in the bulb (Macrides & Schneider 1982, Macrides & Davis 1983).

Mitral and tufted cells show several differences starting from the position of their cell bodies, the distribution of basal dendrites and their specificity for transmitters. They have different projection pattern in the olfactory cortex, and they are connected to different particular groups of granule cells (Schoenfeld & Macrides 1984, Schoenfeld et al. 1985, Scott et al. 1980).

The external plexiform layer presents relatively few cell bodies, but it is a very dense neuropil layer, where basal dendrites of principal cells have synaptic contacts with peripheral dendrites of granule cells.

Local interneurons

Both sensory excitatory inputs and intra-bulbar circuit stimuli control tightly the firing activity of output neurons. Two distinct connections are implied in the intra-bulbar circuit stimuli: the first occurs between primary dendrites and periglomerular cells (PG), the second between secondary dendrites and granule cells (Gr) (Shipley & Ennis 1996). Granule cells and periglomerular cells are interneurons which extend their projections within the olfactory bulb.

Most of the periglomerular interneurons have dendrites restricted to one glomerulus and contact olfactory nerve terminals or mitral cell primary dendrites, so the glomerulus becomes a complex structure consisting of axonal and dendritic compartments (Kosaka et al. 1997, Kasowski et al. 1999).

Each glomerulus is surrounded by numerous periglomerular cells with small somata (6-8 μm). PG cell dendrite ramifies and terminates within one or two

glomeruli, and they take contact with olfactory axons and dendrites of principal cells; PG cell axon can extend across three to five glomeruli (Pinching & Powell 1971, Macrides & Davis 1983, Halasz & Greer 1993). PG cells constitute a heterogeneous population, which differs in neurochemical, morphological and physiological features (Kosaka et al. 1995, Kosaka et al. 1997, Puopolo & Belluzzi 1998, Toida et al. 1998, Toida et al. 2000).

In the external plexiform layer, principal cells interact with axonless interneurons named granule cells, the most numerous cellular populations within the bulb. Granule cells are densely packed in the Granule cell layer (GRL). They can present a rounded or fusiform somata and they constitute aggregates of three to five cells each ones, in which gap junctions are present as their activity can be synchronized. Each cell gives rise to a thick peripheral dendrite, that ramifies and terminate in the EPL and to fine deep (one to four) dendrites which terminates within the GRL (Price & Powell 1970). The main difference between periglomerular and granule cells is that the former mediate mostly interactions between cells within the same glomerulus, while granule cells mediate interactions between output neurons projecting to many different glomeruli.

Neuronal communication within the olfactory bulb has some unusual features. Many bulbar neurons present reciprocal dendrodendritic synapses. In addition, several bulbar neuronal type can modulate their own activity through the transmitter that they themselves release. The reciprocal circuit via dendrodendritic synapses provides a spatially localized inhibition. It is suggested that a mechanism for lateral inhibition is provided between output neurons that innervate different glomeruli. Indeed, the projection field of interneuron is large enough to contact dendrites of several output cells. Bulbar principal neurons are connected to different glomeruli and they respond to a wide range of odor molecules, moreover they receive inhibitory inputs from neighbouring glomerular units - via lateral inhibition at dendrodendritic connections. This inhibition is proposed to refine the process of odor information. These features make the olfactory bulb a structure where information is transmitted vertically, across the glomerular relay between sensory neurons and output neurons, and horizontally through local interneuron connections, which are activated in odor-specific patterns (Lledo et al. 2005).

This kind of inter-glomerular communication is also mediated by a distinct interneuronal population: the so called “short axon” cells (SA). Short axon cells located in the glomerular layer have an oval cell body and dendrites ramifying between or around glomeruli. Their inter-glomerular axons extend from one to three

glomeruli to excite inhibitory PG cells (Aungst et al. 2003). Really, short axon interneurons are equivalently spread along bulbar layers, so they are also present in EPL, MCL, IPL and they are relatively numerous in granule cell layer. Thanks to Golgi impregnation technique several type of SA are identified; this neurons have an intermediate size between Gr and M and they present three to eight dendrites (Ramon y Cajal 1911, Price & Powell 1970, Pinching & Powell 1971, Schneider & Macrides 1978, Shepherd & Greer 1998).

In view of the above, glomeruli can respond to a wide range of related odorants but also receive inhibitory inputs from neighbouring glomerular units through lateral inhibition. Odor perception quality is firstly ensured by sensory neuron termini transmitting sensory inputs to glomeruli. Following improvements in odor stimulus refinement are encoded by mitral cell activity patterns, in other words by a specific combination of activated mitral cells, that in turn critically depend on GABAergic inhibition.

1.3 Periglomerular Cells

In the Olfactory Bulb, interneurons are generated continuously in the postnatal and adult periods from the progenitor cells located in the subventricular zone of the lateral ventricle. These new generated cells migrate tangentially through the rostral migratory stream, then radially across bulbar layers until they find their final position building the right synaptic interactions (Altman 1969, Lledo et al. 2008).

Periglomerular layer is populated by three types of interneurons (as seen above): periglomerular cells, short axon cells and external tufted cells (Halász 1990). Among these interneurons, periglomerular cells and external tufted cells send dendrites into glomeruli, while superficial short axon cells are believed to send dendrites in the periglomerular region but not into glomeruli (Kosaka et al. 1998).

PG cells constitute high chemically heterogeneous cell population as T. Kosaka and K. Kosaka morphological and immunocytochemical studies reveal.

Glutamic acid decarboxylase (GAD), γ-aminobutyric acid (GABA), tyrosine hydroxylase (TH), calretinin and calbindin D28k characterize the four major chemically identified groups of PG cells, in main olfactory bulb of C57B/6J strain mice (Kosaka & Kosaka 2007).

Each glomerulus is regarded to consist of two compartments (or zones): the olfactory nerve (ON) zone and the non-olfactory nerve (non-ON) zone (Kosaka et al. 1997). The borders of these compartments cannot be strictly define. The ON zone is mainly occupied by olfactory nerve terminals as well as fine dendritic processes of

intrinsic neurons, so the ON zone is the site where olfactory receptor cells make synapses on their targets. The non-ON zone is occupied by dendritic processes of intrinsic neurons, where dendrodendritic interactions between intrinsic neurons mainly occur. PG cells can be classified into two types - type 1 and type 2 - on the basis of the distribution of their intraglomerular dendrites. Type 1 cell dendrites (the blue ones in figure 1.4) are located both in the ON and the non-ON zones, whereas type 2 cell dendrites (the green ones) are located in non-ON zone but rarely in the ON zone (Kosaka et al. 1998). However, it is required to keep in mind that this scheme simplifies the classification of PG neurons. Considering the high heterogeneous PG population some cells might overcome this representation.

In mouse olfactory bulb, type 1 PG cells include both GAD/GABA-positive and tyrosine hydroxylase-positive cells and type 2 PG cells include both calretinin-positive and calbindin D28k-positive cells.

All of the tyrosine hydroxylase positive neurons exhibited GAD/GABA immunoreactivity, but neither are calretinin-positive nor calbindin D28k-positive. These tyrosine hydroxylase-positive neurons varied in size, and also in the intensity of the tyrosine hydroxylase immunoreactivity and GAD/GABA immunoreactivity. This suggest that GAD/GABA- and TH-positive group may consist of two or more subgroups of neurons with different sizes.

All of the calbindin D28k-positive somata are GAD/GABA-positive.

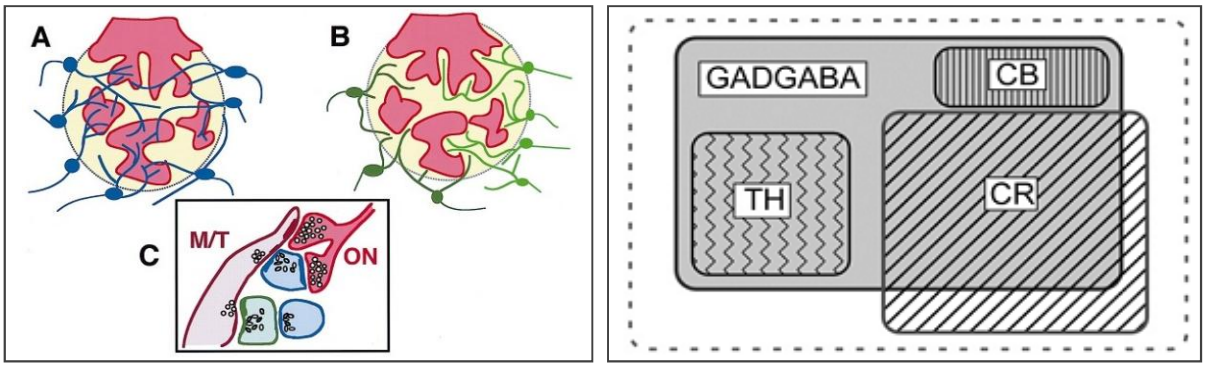

Figure 1.4 On the left: **type 1 (blue) and 2 (green) PG cells**. Simplified scheme of the neuronal organization in the glomerular unit. In red the ON zone and in yellow the non-ON zone of a glomerulus (A,B). (C): Synaptic connections of types 1 and 2 PG cells in the glomerulus. ON, olfactory nerve; M/T mitral/tufted cell.
From Kosaka et al., Neurosci. Res 1998.
On the right: **Cellular composition in the juxtaglomerular region of mouse OB.** Total cells in the juxtaglomerular region are represented by dashed rectangle. All TH-positive cells, CB-positive cells and about 65% of the CR-positive cells are included in the GAD/GABA-positive cells. TH, CB and CR characterize groups of PG cells.
From Kosaka K. et al., Brain Res. 2007.

In the mouse olfactory bulb, these calbindin D28k positive somata usually exhibite strong calbindin D28k immunoreactivity and intermediate GAD/GABA immunoreactivity.

A large part but not all, of the calretinin positive somata are also GAD/GABA-positive. Some of these GAD/GABA-positive calretinin-positive somata exhibit a faint calretinin immunoreactivity and an intermediate GAD/GABA immunoreactivity, whereas others show a strong calretinin immunoreactivity and a faint GAD/GABA immunoreactivity.

None of the calbindin D28k-positive somata are calretinin-positive and vice versa.

The TH-positive somata, which are always GAD/GABA-positive, consist of about 20% of the GAD/GABA-positive somata. About 65% of the calretinin-positive neurons and, all of the calbindin D28k-positive neurons, are also GAD/GABA-positive. For the GAD/GABA-positive somata, the 35% are calretinin-positive and the 10% are calbindin D28k-positive. None of the somata expresses both calretinin and calbindin D28k immunoreactivities (Kosaka & Kosaka 2007).

1.3.1 TH- and GABA-positive JG Cells

There are two types of TH-positive juxtaglomerular (JG) neurons with different soma sizes, see figure 1.5 (Kosaka & Kosaka 2008, Halász et al. 1981, Pignatelli et al. 2005). As specified by Kosaka and Kosaka's work, the term juxtaglomerular neuron "*indicates neurons located around glomeruli irrespective of neuron types, including PG cells, external tufted cells and SA cells. Thus the term 'JG neurons' is usually used when the neuron types are not distinguished or un-identified or controversial*" (Kosaka & Kosaka 2011).

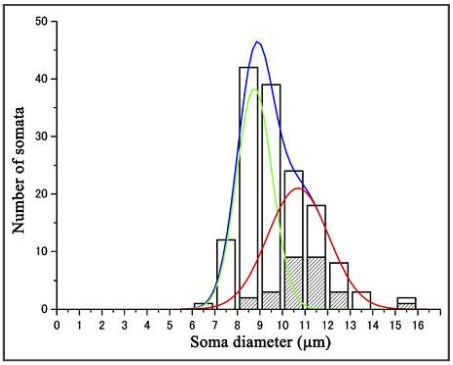

Figure 1.5 **TH+ cell soma size histogram**. Two Gaussian curves (green and red) describe the TH-positive soma size histogram, as well as their combined curve in blue.
From Kosaka T. et al., Neurosci Res 2008)

Between the two TH-positive cell population distinguished by cell soma size, the biggest one seems to be the main source of the long inter-glomerular connections in mouse olfactory bulb: DA - GABA periglomerular cells are candidate to play this role (Kosaka & Kosaka 2007).

In literature (De Marchis et al. 2007, Ventura & Goldman 2007, Kohwi et al. 2007), TH-positive juxtaglomerular neurons are reported to be one of the major groups of juxtaglomerular neurons generated continuously in the postnatal and adult periods. Kosaka and Kosaka suppose that this TH+ JG neurons continuously supplied in adult life are different from those participating in the long inter-glomerular connections. In addition, those TH-positive neuron postnatally generated appear to be the small type of TH-positive periglomerular cells rather than the large type of TH-positive ones (Kosaka & Kosaka 2008).

1.3.1 Electrophysiological characterisation of TH-positive PG cells

An estimated 10% of juxtaglomerular neurons in adulthood are positive for tyrosine hydroxylase (TH), which is the rate-limiting enzyme for dopamine synthesis (McLean & Shipley 1988, Kratskin & Belluzzi 2003). Moreover, DA cells are among interneurons added in adult life (Betarbet et al. 1996, Baker et al. 2001). In absence of synaptic inputs, as many DA neurons in the CNS can generate rhythmic action potentials (Grace & Onn 1989, Yung et al. 1991, Neuhoff et al. 2002), also DA cells in the glomerular layer of the olfactory bulb possess a pacemaker activity (Pignatelli et al. 2005).

Thanks to use transgenic mice carrying green fluorescent protein (GFP) under the control of TH promoter (TH-GFP cells) (Sawamoto et al. 2001, Matsushita et al. 2002) a first electrophysiological characterization of these cells was outline (Pignatelli et al. 2005). For the first time, the difficulty of discerning DA PG cells in living brain slice is overcome thanks to this animal model, which is an invaluable tool to obtain functional studies of DA cells in the OB.

The main source of TH-GFP cells is in the glomerular layer of olfactory bulb, where it is possible to distinguish two population of TH-GFP cells basing on the distribution of the mean cell diameter of GFP+ cells. This result is confirmed by the frequency distribution of the membrane capacitances, although no significant differences in the properties of the two population is found (Pignatelli et al. 2005).

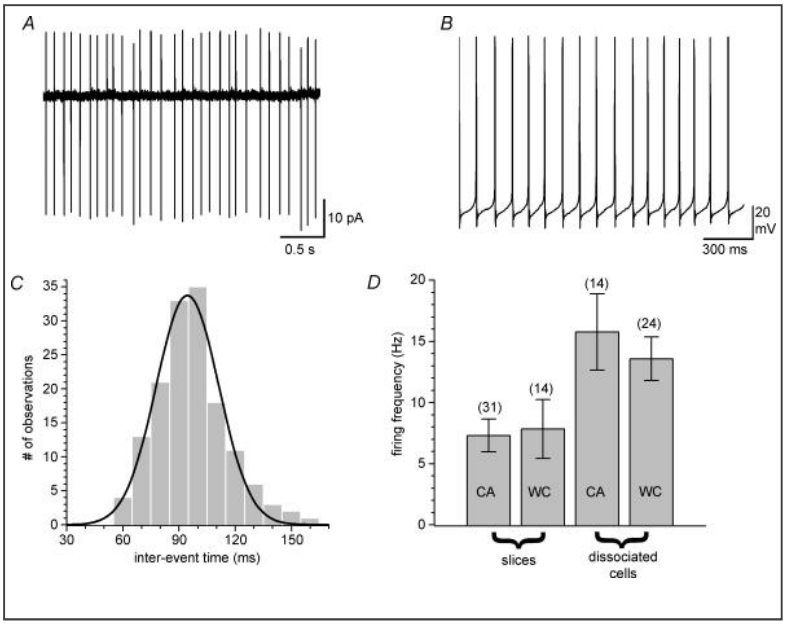

Figure 1.6 **Spontaneous firing in TH-GFP+ cells.**
The presence of autorhythmic activity is the most salient feature of DA cells in the olfactory bulb. Example of action current recording is showed in A, in *voltage-clamp cell-attached* mode.
In B, action potentials are showed in *whole-cell* mode and *current-clamp* configuration.
In C, frequency distribution of the inter-event time for the cell shown in B. The firing activity is rather constant in the most of cells.
In D the frequency of spontaneous firing in TH-GFP cells is summarized under the indicated experimental conditions.
CA, cell attached; WC, whole cell.
From Pignatelli et al., J.Physiol 2005

About 80% of DA neurones are spontaneously active. This feature persists after blocking glutamatergic and GABAergic synaptic transmission. It is an intrinsic properties of the cell membrane and is independent from external synaptic input

presence. This result is further supported by the observation that also dissociated TH-GFP cells conserved their capacity of generating rhythmic activity, both in whole-cell and cell-attached mode (fig. 1.6).

DA neurons in the mice OB have a complement of voltage-dependent currents, which have been kinetically characterized in order to understand the mechanism of spontaneous firing. The slow depolarization between spikes is sustained by the persistent tetrodotoxin-sensitive sodium current ($I_{Na(P)}$) and by the T-type calcium current ($I_{Ca(T)}$). Both $I_{Na(P)}$ and $I_{Ca(T)}$ are necessary to sustain spontaneous firing as the selective block of one or both abolish spontaneous activity.

In these cells, five main voltage-dependent conductances are identified: the two having largest amplitude are a fast transient Na^+ current and a delayed rectifier K^+ current. In addition, three smaller inward currents, sustained by Na^+ ions (persistent type) and by Ca^{2+} ions (LVA and HVA), are observed (Pignatelli et al. 2005).

Also two hyperpolarization-activated currents with inward rectifying properties are present in TH-GFP+ neurons. The recently characterized first type current is I_h (or I*f* in cardiac tissue) hyperpolarization-activated current, a mixed cation current with a reversal potential substantially positive to E_K. DA PG I_h has a relatively slow activation kinetics, and it is insensitive to Ba^{2+}, while it is blocked by high selective drug such as ivabradine and ZD7288 (Pignatelli et al. 2013).

The second has fast kinetics, is permeable primarily to K^+, is blocked by extracellular barium and cesium, has a voltage-dependence on extracellular K^+ concentration, and it has been identified as a classical potassium inward rectifier current (Kir).

It is the matter of my work.

1.4 Kir Channels

Inwardly rectifying potassium (Kir) channels belong to potassium channel family which is expressed in many cell types and contribute to a wide range of physiological processes. Potassium channels are classified into three groups in terms of their predicted membrane topology. The first group includes six transmembrane domain (TMD) proteins such as voltage-gated and Ca^{2+}-activated K^+ channels, while the second group holds "Leak" K^+ channels which are formed by four transmembrane domain proteins. Two transmembrane domain proteins belong to the third group, where you can find inward rectifier K^+ channels. Each group of principal subunits is divided into families and further subdivided into several subfamilies based on structural properties, which are resumed in figure 1.7. In addition of principal K^+ channel subunits, many K^+ channels present auxiliary proteins that can modify the channel properties. In some cases, principal subunits do not form functional homomultimeric channels: in order to give functional channels, they must coassemble with subunits belonging to a different subfamily. Figure 1.7 A also shows auxiliary subunits grouped together with the principal subunits with which they have been shown to interact (Coetzee et al. 1999).

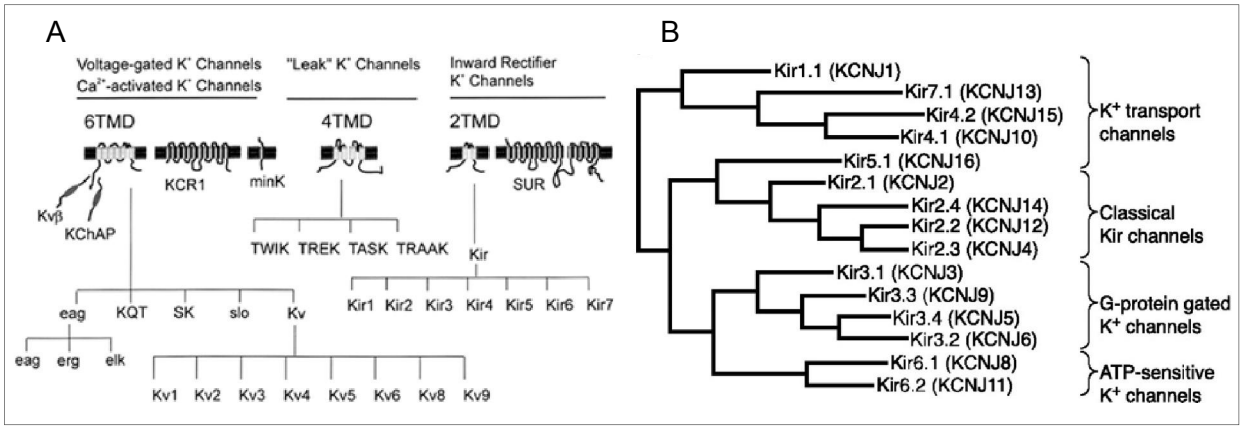

Figure 1.7 A) **Schematic representation of the three groups of K^+ channel principal subunits**. A functional classification places the voltage- and Ca^{2+}- regulated K^+ channels in the 6TMD group, the "leak" K^+ channels in the 4TMD group, and the inward rectifier K^+ channels in the 2TMD group. *From Coetzee W.A.et al., Ann.N.Y.Acad.Sci.1999*
B) **Kir channel phylogenetic tree**. Phylogenetic analysis of the 15 known subunits of human Kir channels. These subunits can be classified into four functional groups. *From Hibino H. et al., Physiol Rev 2010*

Inwardly rectifying potassium channels have a principal subunit of two TMDs (M1-M2) and a pore domain, analogous to S5-P-S6 of the 6TMD K^+ channel subunits, and it is thought to assemble as tetrameric proteins to form functional channels (Coetzee et al. 1999, Hibino et al. 2010, Bichet et al. 2003, van der Heyden et al. 2013).

Inwardly rectifying potassium currents were originally described as “anomalous” rectifier K^+ currents that refers to the ability of an ion channel to allow greater influx than efflux of ions. In general, inward rectifier channels allow small amounts of outward current at membrane potential (V_M) positive to the potassium equilibrium potential (E_K) compared to currents generated at stimuli negative to the potassium equilibrium potential (Hibino et al. 2010).

There are 15 Kir subunit genes, known to date, which are classified in seven subfamilies (Kir 1.x to Kir 7.x) in turn organised into four functional groups:

1) Classical Kir channels
2) G-protein gated Kir channels (GIRK)
3) ATP-sensitive K^+ channels
4) K^+-transport channels.

Members of Kir 2, Kir 3, Kir 5 (having only a single member) and Kir 6 subfamilies fall into their own expected group, as shown in figure 1.7 B, on the other hand the remaining members of Kir 1, Kir 4, and Kir 7 subfamilies are all part of the fourth functional group (Hibino et al. 2010).

A threshold identity values of > 55 % exists among members of individual Kir subfamilies (organised in the phylogenetic tree of 2 TMD inward rectifier potassium channels as shown in figure 1.7 B), except for Kir 1, Kir 4, and Kir 7 subfamilies which score an identity lower than 36%, suggesting that their genes might belong to different subfamilies. Moreover, ambiguity arose in the naming of these genes, so Kir 4.1 is also known as Kir 1.2, because of its apparent similarity to Kir 1.1; similarly there is a certain unclearness in the naming of Kir 4.2/Kir 1.3. The last cloned gene is supposed to be a new subfamily member and for this reason it is defined Kir 7.1, but it is also named as Kir 1.4 by others (Coetzee et al. 1999).

1.4.1 Architecture of Kir Channels

A four identical (homotetrameric) or homologous (heterotetrameric) Kir subunits tetrameric structure is organized on the membrane in order to surrounding a water-fill pore, through which K^+ ions can move following their electrochemical gradient. Each subunit includes two transmembrane helices, a pore forming region and a cytoplasmic domain formed by the ammino (N) and carboxy (C) termini, as schematically shown in figure 1.8 A. An interesting feature is that N and C termini, belonging to neighbouring subunits, interact through two parallel β-strands (figure 1.8 B).

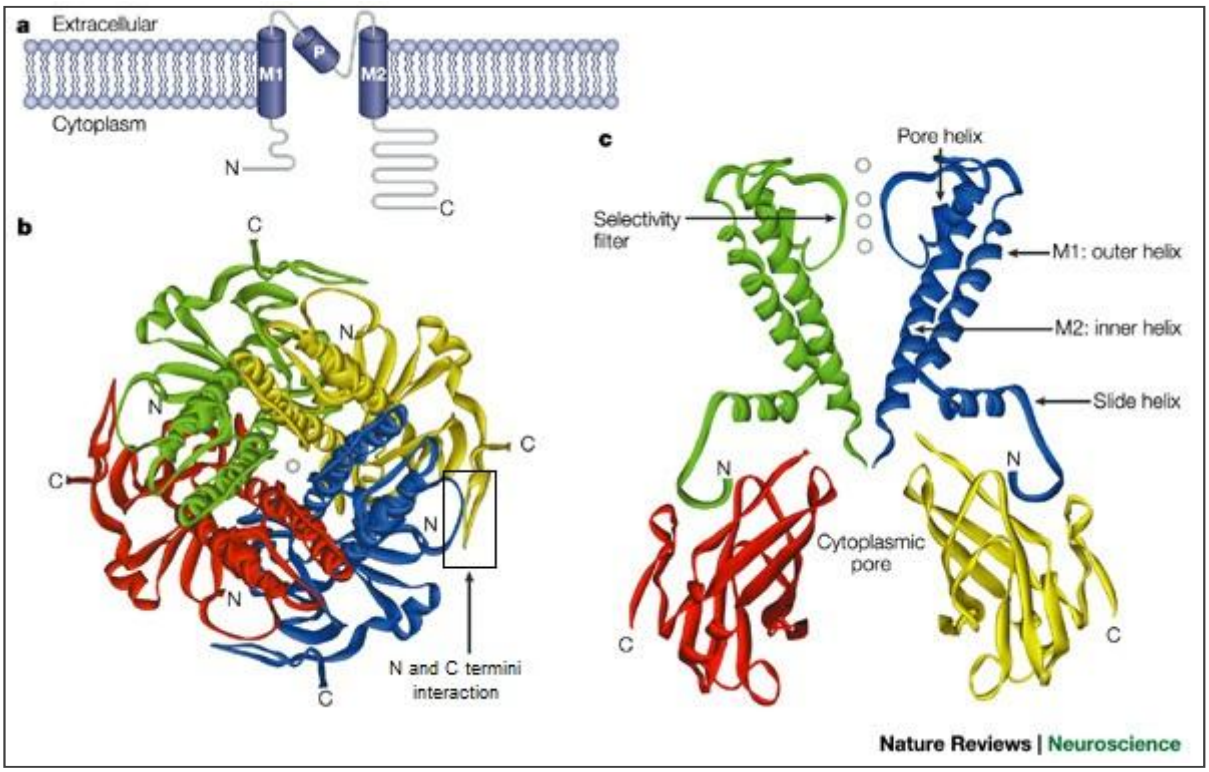

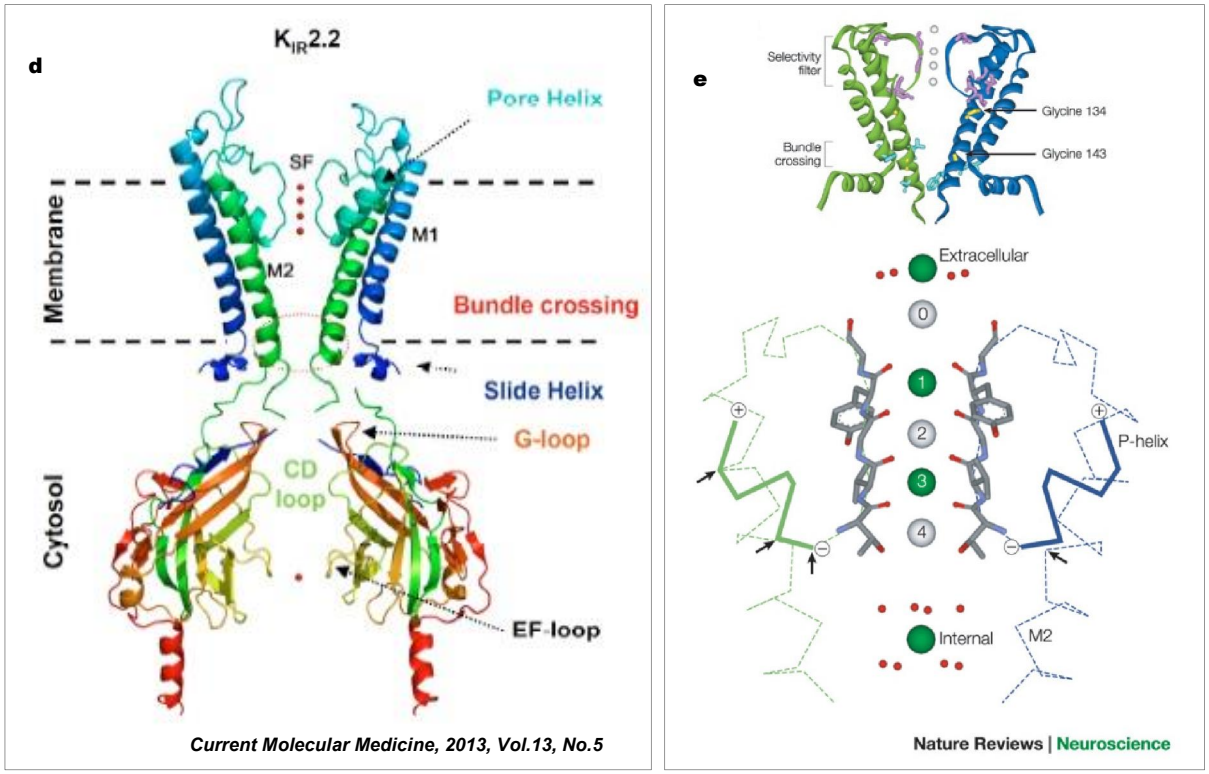

Figure 1.8 ***Overall architecture of inwardly rectifying K+ (Kir) channels.*** In ***a,*** schematic draw of a single channel subunit showing transmembrane helices (M1,M2) and the pore forming region (pore-helix, P). In ***b*** and ***c,*** above and side view of KirBac 1.1 tetrameric structure, where monomers are differently colored and K^+ ions are white. *From Bichet D. et al., Nat.Rev.Neurosci 2003*.

In ***d***, structure of Kir 2.2 where two subunits have been remove for clarity; red spheres are K^+ ions and the bundle crossing region is shown by the red dot circle. SF: narrow selectivity filter region; G-loop: a belt around the central pore (also known as H-I loop); CD- and EF-loop, coming from βstrands C and D and βstrands E and F, constitute the cytoplasmic pore permeation pathway. *From Van der Heyden et al., Curr.Mol.Med. 2013.*

In ***e,*** selectivity filter of KcsA emphasizes the linear array of K^+ binding sites. Only residues of the K^+ channel signature sequence (TVGYG) are shown in ball-and-stick representation. At the enter of filter, K^+ ion hydration shell is progressively replaced by interactions with backbone carbonyls (positions 0 to 4). The filter can contain two K^+ ions simultaneously, either at positions 1 and 3 (green spheres), or at 2 and 4 (white spheres). Black arrows show mutations that affect selectivity filter. *From Bichet D. et al., Nat.Rev.Neurosci 2003*.

The transmembrane domain is formed by two transmembrane helices M1 and M2 separated by an extracellular loop that form a K^+ selectivity filter (van der Heyden et al. 2013). This pore loop, located between the M1 and the M2 helices, contains the descending pore helix and the ascending K^+ channel signature sequence (figure 1.8) (Bichet et al. 2003). At the bound between membrane and cytoplasm the M2 forms a shrinkage the "*bundle crossing region*" in order to prevent ion flux when channel is closed. It is showed in figure 1.8 D by the red dot circle. The bundle crossing opens to 17 Å. It moves in a kinking way, turning 25° around the helical axis and using as hinge a conserved glycine (van der Heyden et al. 2013).

The intracellular domain is formed by two-third of the Kir channel ammino-acid sequence and it is organized in order to give the "*cytoplasmic pore"*, which is 30 Å long and 7-15 Å in diameter. The wall of β-sheets, containing many polar and charged and surrounding the pore channel, makes a crucial region for channel modulation by intracellular regulator and for establishing the strong voltage dependence of inward rectification (Bichet et al. 2003).

1.4.2 Ion Selectivity

Selectivity for K^+ is given by selectivity filter (SF)(figure 1.8 E), defined as the narrowest part of the conduction pathway in the open channel. The conserved K^+ channels signature sequence (TXGYG or TXGFG) is located in the P-loop. The main chain carbonyl oxygens of the signature sequence form the selectivity filter (Bichet et al. 2003). Point mutations in the K^+ channels signature sequence abolish K^+ selectivity (Heginbotham et al. 1994). K^+ channel signature sequence is conserved between all K^+ channels and interestingly the bacterial KcsA pore can substitute for the pore of other K^+ channels (Lu et al. 2001). This suggests that the mechanism of ion selectivity filter is similar in all K^+ channels. In figure 1.8 E, a close-up view of the selectivity filter of KcsA is shown and the ball and stick representation defines the K^+ channels signature sequence. At the extracellular and internal ends of the filter, K^+ ions are surrounded by water molecules which are progressively replaced by interactions whit the backbone carbonyls of the selectivity filter. The filter can contains two K^+ ions simultaneously either at position 1 and 3 or at 2 and 4 (Bichet et al. 2003). Other than the K^+ channel signature sequence, structural features are also important for K^+ selectivity in Kir channels. Differences in the residues that surround the selectivity filter account for the reduced K^+ selectivity, as demonstrated in mutagenesis studies in the pore helix or in M2 of Kir 3 family

members (Lu et al. 2001, Slesinger 2001). The idea that the surrounding structure contributes to stabilize the SF is suggested by the presence of a salt bridge between conserved charged residues. It seems to anchor and stabilize the K+ channel signature sequence in most Kir channels (Yang et al. 1997).

1.4.3 Inward Rectification

Inward rectification was originally termed *anomalous* rectification: indeed it is opposite to the normal outward rectification that is seen in delayed rectifier K channels (Nichols & Lopatin 1997). For K^+ channels, inward rectification means that at any given driving force (voltage), the inward flow of K^+ ions is greater than the outward flow for the opposite driving force (Nichols & Lopatin 1997). K^+ ions could pass selectively in both direction in Kir channels, while cytoplasm Mg^{2+} and polyamines interact with pore channel, blocking K^+ efflux at membrane potentials which are more positive than the E_K (Bichet et al. 2003).

The functional role of inward rectifier channels depends critically on their degree of rectification. The degree of rectification is correlated with the binding affinity of the channel for blocking cations. Among Kir family members, there are strong (Kir 2 and Kir 3) and weak (Kir 1 and Kir 6) rectifiers (figure 1.9).

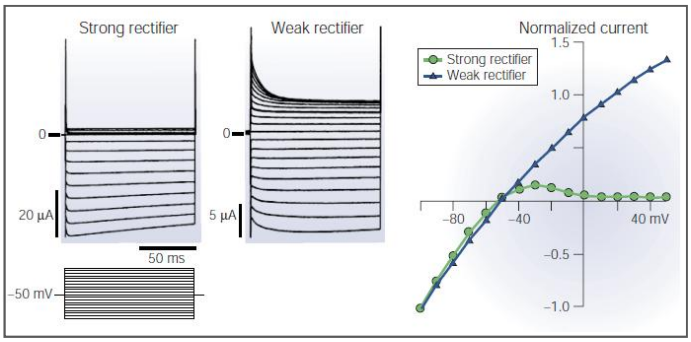

Figure 1.9 **Inward rectification.** Current traces and current–voltage curves of a strong and a weak inward rectifier. The examples were obtained under a two-electrode voltage clamp of Xenopus oocytes expressing wild-type (left) Kir2.1 and E224G/E299S mutant (right) channels. The protocol consists of voltage steps of 10 mV increments from - 140 mV to 50 mV from a holding potential of - 50 mV.
From Bichet D. et al., Nat.Rev.Neurosci 2003.

Classical (Kir 2.X) strong inward rectification is present in skeletal muscle, in glial cells and neurons of central nervous system. It is essential for the stable resting potential and long plateau, which are features of the cardiac action potential. The high conductance at negative voltages allows cells to maintain a stable resting potential, while the greatly reduced conductance at positive potentials avoids short-circuiting the action potential. Others Kir channels display weak rectification and they allow substantial outward current to flow at positive potentials: this category involves Kir 6.X family (also known as ATP-sensitive K^+ (K_{ATP}) channels) which is present in all muscle cell types, in the brain, and in pancreatic cells where it is centrally involved in the regulation of insulin secretion.

Between these extremes, you can find Kir channels that have intermediate rectification properties which populate in particularly the brain and many of these depend on ligand activation (Kir 3.X family), often through G proteins or other second messenger systems (Nichols & Lopatin 1997).

Some specific terms are used to describe voltage-dependent transitions of a depolarization-activated channel: the term *activation* is used to describe the opening upon depolarization, *inactivation* to indicate the following closing of the channel at such voltage, *deactivation* to refer to the reversal process of activation at negative voltages, and *recovery from inactivation* to mean subsequent recovery of availability of channel at negative voltages. In Kir channels, the increase of current flow following hyperpolarisation is referred to as activation, while the reduction of channel current at positive potentials is generally described as rectification.

Extrinsic Mg^{2+}-induced gating

Originally it is suggested that inward rectification might result from a positively charged substance blocking the channel in a voltage-dependent manner from the internal side of the membrane (Armstrong 1969). Indeed, it has been shown that the divalent magnesium (Mg^{2+}) caused inward-rectification by blocking the channel pore in a voltage-dependent manner. Extensive work on native inwards rectifier channels from cardiomyocytes shows that in absence of the block by Mg^{2+} the channel conductance is ohmic: in I-V relations both inward and outward currents are measured and the fitted line crosses the voltage axis at around E_K.

On the other end internal Mg^{2+} on the cytoplasmic side at physiological concentrations blocks the outward current, and the channel remains close to value more positive than E_K, without affecting the inward current (Matsuda et al. 1987, Matsuda & Stanfield 1989). Mg^{2+} ions prevent K^+ efflux by moving into the inner mouth of the K^+ channel, than they are driven intracellularly again by negative voltage by inward moving K^+ (Matsuda 1991).

Crystallographic and electrophysiological analyses show the existence of selective binding of cations at the cytoplasmic pore. This binding accelerates channel modification and lowers the probability the pore being open. Kir channel permeability is regulated by the membrane-embedded domain, which gates at the bundle crossing (formed by the inner helices near the cytoplasm) and at the selectivity filter (near the extracellular vestibule). The cytoplasmic domain plays a key role in channel gating too. Its conformational change alters the electrostatic field potential in the cytoplasmic pore (figure 1.10). In its closed state, the pore tends to bind Mg^{2+}, and this prevents diffusion of K^+ ions. When the channel is

open, expansion of the cytoplasmic pore lowers the electrostatic field potential and liberates bound Mg^{2+} to permit movement of K^+ (Inanobe et al. 2011).

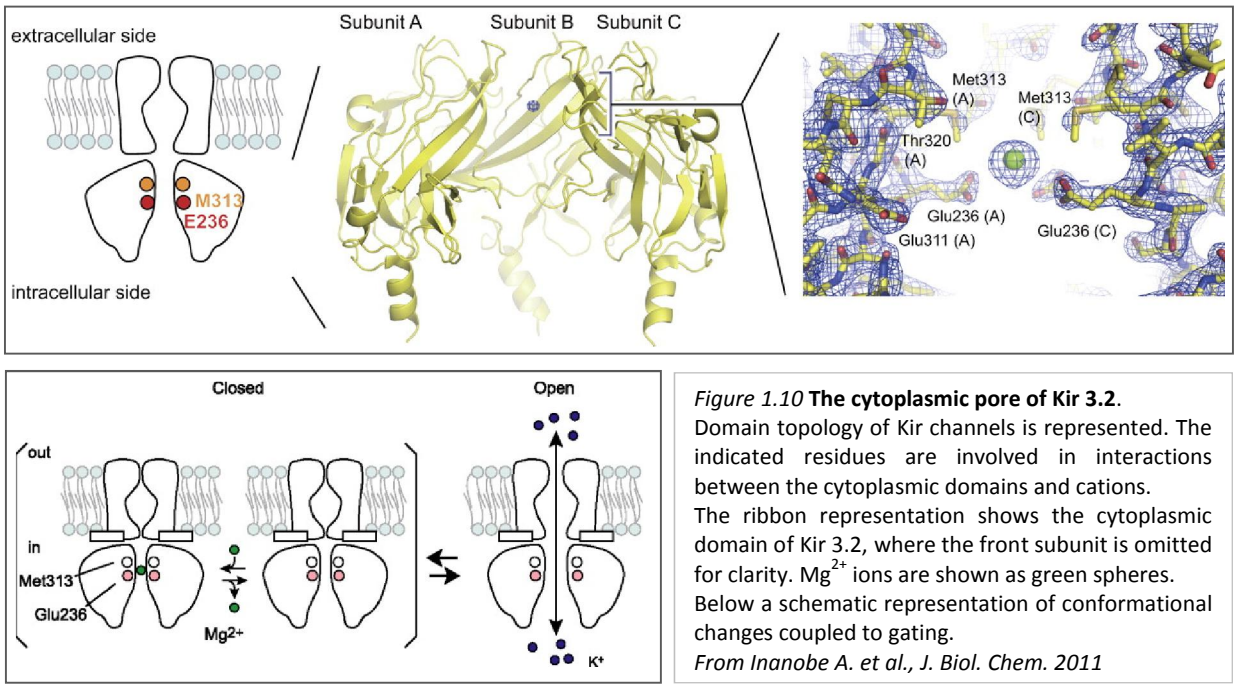

Figure 1.10 **The cytoplasmic pore of Kir 3.2**.
Domain topology of Kir channels is represented. The indicated residues are involved in interactions between the cytoplasmic domains and cations.
The ribbon representation shows the cytoplasmic domain of Kir 3.2, where the front subunit is omitted for clarity. Mg^{2+} ions are shown as green spheres.
Below a schematic representation of conformational changes coupled to gating.
From Inanobe A. et al., J. Biol. Chem. 2011

Even in the absence of intracellular Mg^{2+} inward-rectification is present. This remaining voltage-dependent rectification was ascribed to a mechanism intrinsic to the channel protein and termed *intrinsic gating* to distinguish it from the *extrinsic* Mg^{2+}-induced pore block (Oliver et al. 2000).

Intrinsic gating

Experiments (Lopatin et al. 1994) on Kir 2.3 channels (expressed in *Xenopus* oocytes) show the gradually disappearance of Kir 2.3 rectification after patch excision. Rectification is restored by placing excised membrane patches close to the surface of cells, confirming that it is caused by soluble intrinsic factors: polyamines.

Polyamines (putrescine, cadaverine, spermidine and spermine) are organic compounds having two or more primary amino groups which can bind to DNA (Tabor & Tabor 1984). These molecules are essential for normal and neoplastic cell growth: if cellular polyamine synthesis is inhibited, cell growth is stopped or severely retarded. The provision of exogenous polyamines restores the growth of these cells. Most eukaryotic cells have a polyamine transporter system on their cell membrane that facilitates the internalization of exogenous polyamines. This system is highly active in rapidly proliferating cells and is the target of some chemotherapeutics currently under development (Wang et al. 2003). Although many other functions remain undefined, it is known they act as promoters of programmed ribosomal frameshift during translation (Rato et al. 2011), and they are important

modulators of a variety of ion channels, including NMDA receptors and AMPA receptors.

Spermine (SPM) and spermidine (SPD) are identified as the "*rectifier substance*" of Kir channels. These naturally intracellular polyamines are present at micromolar concentrations and block Kir current in a voltage-dependent manner steeper than Mg^{2+} (Oliver 2000).

To block Kir channels, polyamines enter and occlude the central K^+-selective pore of the channel. The affinity and voltage dependence of block varies with the identity of the blocking polyamine: spermine are the most potent and voltage-dependent blocker whereas shorter polyamines (e.g., spermidine, cadaverine, and putrescine) exhibit weaker affinity and voltage dependence (Nichols & Lopatin 1997, Lopatin et al. 1995, Guo & Lu 2003, Pearson & Nichols 1998). The steep voltage dependence of polyamine blockade arises in part from interactions of the blocking molecule with permeating ions. Movement of the blocker through the channel pore forces occupant permeating ions to traverse the membrane electric field (Pearson & Nichols 1998, Spassova & Lu 1998).

Crystal structures have revealed that, the pores of inwardly rectifying potassium channels are considerably longer than an individual spermine molecule and are lined by multiple rings of negative charges (Kuo et al. 2003).

Some studies have suggested a model of "shallow" spermine block of Kir channels: spermine binds between the "rectification controller" residue and several rings of negatively charged residues located in the cytoplasmic domain of the channel (figure 1.11, Model A)(Guo & Lu 2003). Others have proposed a "deep" model of spermine block, suggesting that spermine binds between the "rectification controller" residues and the selectivity filter (figure 1.11, Model B)(Kurata et al. 2004, Kurata et al. 2006).

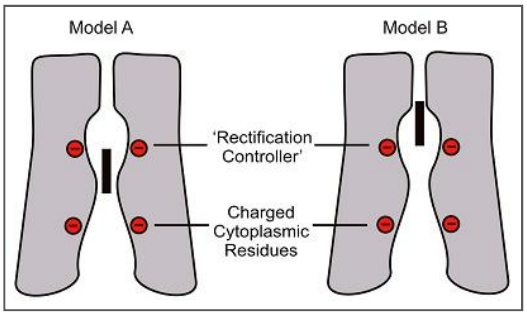

Figure 1.11 **The polyamine binding site in the Kir channel pore**. (A) Different model cartoons of *shallow* (Model A) versus *deep* spermine binding (Model B). Red bottom circles indicate rings of negative charges in the cytoplasmic domain, while the top circles show the inner cavity ones of strongly rectifying Kir channels. The black rectangle represents a spermine molecule in the Kir pore.
From Kurata H.T. et al.,J. Gen. Physiol 2006.

More recent studies have shown that these *shallow* and *deep* sites are generally understood to be sequentially coupled: firstly, blockers interact with the cytoplasmic domain and subsequently they migrate towards the rectification controller site to generate steep voltage-dependence (Shin & Lu 2005). Results demonstrate polyamine block of Kir channels involves migration of blockers through the long Kir channel pore (> 70 Å). This way involves

intermediate binding sites before the blocker reaches a stable binding site in the deep transmembrane region of the channel (Shin & Lu 2005, Kurata et al. 2006).

Finally Kurata's 2013 work solidifies a structural interpretation of a deep spermine binding site, thanks to inclusion of multiple cysteine substituted sites in Kir channels and progressively longer blockers tests (Kurata et al. 2013).

1.4.4 Cytoplasmic Regulatory Factors

Several cytoplasmic factors can modulate Kir channels activity: first of all phosphoinositides are critical determinants of ion channels activity. In particular phosphatidylinositol-4,5-bisphosphate (PI-4,5-P_2 or PIP_2) seems to be the most important in controlling all type of inward rectifier potassium channels (Hilgemann & Ball 1996, Fan & Makielski 1997), although trough different affinities and stereo-specificities (Du et al. 2004, Rohacs et al. 2002).

The direct interaction between negative phosphate head-groups of PIP_2 and positively charged residues in N- and C- termini are essential for activation of channels (Fan & Makielski 1997, Shyng et al. 2000, Lopes et al. 2002). Each PIP_2 molecule consists of an inositol head group and fatty acid side chains. In contrast to naturally occurring PIP_2 in the cell membrane, short chain water soluble diC4 PIP_2 does not activate Kir channels. This suggest that the long fatty acid chains are required to activate Kir channels by incorporating PIP_2 into the membrane (Rohacs et al. 2002). The presence of channel-PIP_2 interaction is particularly important for activation of Kir channels and it is considered as a final step in the transitions between the closed and the open state of Kir channels (Logothetis et al. 2007).

Other modulators - such as phosphorylation, pH, heterotrimeric G proteins (specifically Gβγ subunit), and ATP - operate their regulatory role showing great dependence on strength of channel-PIP_2 interaction. It seems that these modulators act by adjusting channel-PIP_2 interaction (Du et al. 2004).

Other negatively charged membrane lipids and derivates play a role in regulating the Kir channels. Long-chain acyl–coenzyme A (LC-CoA) esters and phosphatidic acid active K_{ATP} channels, whereas LC-CoA inhibits other Kir channels such as Kir 1.1, Kir 2.1, Kir 3.4, and Kir 7.1.

Biochemical studies show that PIP_2 and LC-CoA bind competitively to the C-terminal domains of Kir channels with similar affinity. Therefore the mechanism of LC-CoA inhibition of Kir channels - other than Kir 6.2 - is attributed to their competitive displacement of PIP_2 (Logothetis et al. 2007).

Protein kinase phosphorylation regulates activity of various channel types including Kir channels. Protein kinase A has been shown to activate Kir 1.1 channels in a PIP2-dependent manner.

ATPγS is a useful tool to investigate the ATP-requiring steps, indeed it is an analog of ATP with a sulfur atom replacing one of the oxygen atoms in the γ phosphate area. Using this compound, it is possible to provide a substrate for PKA without activating phosphoinositide kinases and affecting PIP_2 levels in membrane. To test the fully reactivation of Kir channels after their rundown in membrane depleted of PIP_2, PIP_2 and PKA + ATPγS are applicated separately. 10μM PIP_2 is the required concentration to fully reactivate Kir 1.1, whereas PKA + ATPγS does not restore channel activity, but after a pretreatment with PKA + ATPγS the PIP_2 concentration required to reactivate the channel is reduced to 1μM. These data suggest that PKA phosphorylation alone is not sufficient for channel reactivation, but also that the sensivity of Kir channels to activation by PIP_2 is increased in phosphorylated channels. The enhancement of PIP2–KIR1.1 interaction by PKA phosphorylation (Fig. 1.12) is likely due to an allosteric effect (Liou et al. 1999).

It has also been reported that protein kinase C can regulate Kir 1.1 channels in a PIP_2-dependent manner. Unlike PKA, PKC appears to inhibit Kir 1.1 channels by reducing membrane PIP_2 levels (Zeng et al. 2003).

Polyamine (PA) block has been most intensively studied in strong inward rectifier Kir 2.1 channels, and exhibits a complex dependence on both voltage and polyamine concentration (Lopatin et al. 1994, Lopatin et al. 1995, Guo & Lu 2003, Xie et al. 2002, Xie et al. 2003). Indeed, voltage-dependent block by intracellular polyamines and Mg^{2+} is the common mechanism underlying the inward rectification in all the Kir channels (Lopatin et al. 1994, Lopatin et al. 1995). It is known that positively charged polyamines can bind to the cytoplasmic region of Kir channels without occluding the pore. This kind of interaction facilitates entry of other polyamines into a deeper binding site located within the membrane pore (Xie et al. 2002, Xie et al. 2003). Moreover, it was shown that long polyamines also strengthen the interaction of PIP_2 with Kir 2.1 channels (figure 1.12), acting to maintain channel availability (Xie et al. 2005).

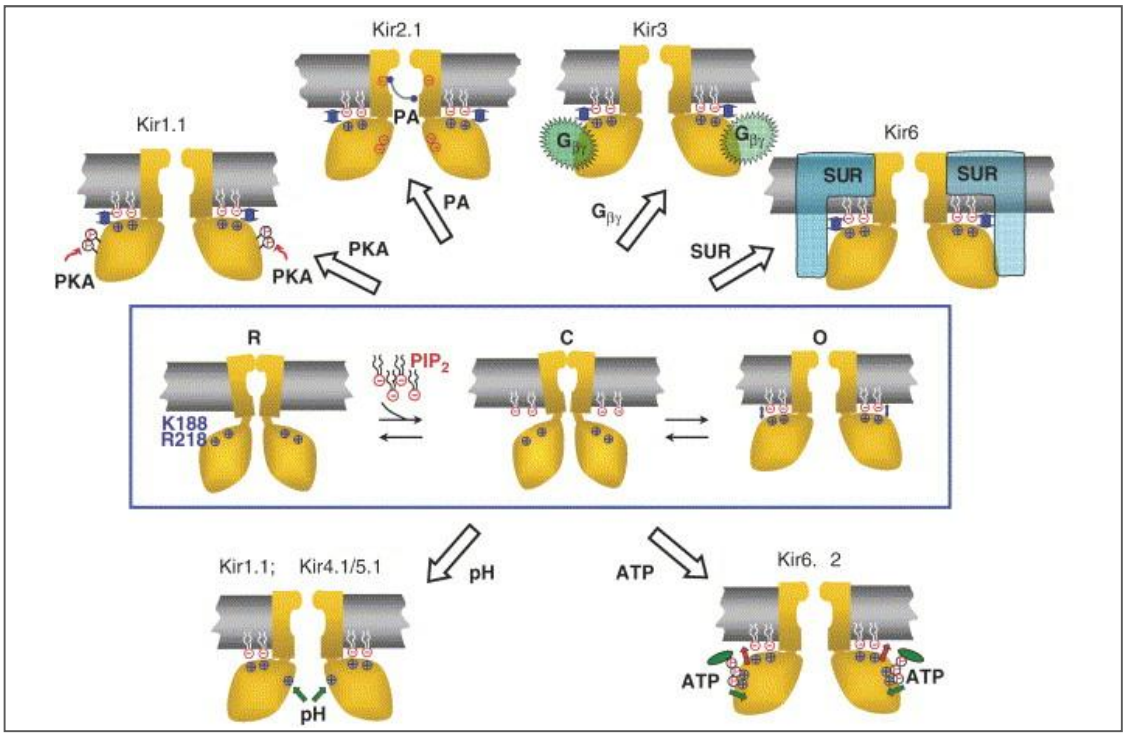

Figure 1.12 **PIP_2 activation and co-regulators of Kir channels.** The scheme in the middle box shows transitions between open (O), close (C), and rundown (R) states in relation to the PIP_2-channel interaction. Other regulators are shown above and below: in Kir 1.1, PKA phosphorylation of S219 and S313; in Kir 2.1, polyamines (PAs) interaction with D172; in Kir 3, Gβγ interaction with the N- and C-termini; in Kir 6.2, SUR interaction with N terminus. PIP_2 affects ATP sensitivity in the Kir 6.2 channel, and pH sensitivity in other numerous Kir channels. *From Xie et al., Progress in Biophysics and Molecular Biology 2006.*

It has been suggested that PIP_2 binding causes conformational changes at the bundle crossing formed by the M2 helix or the G-loop (girdle) near the junction between transmembrane pore and cytoplasmic pore domains. These changes in turn promote the open state. The channel closes when the interaction with PIP_2 is lost. When long polyamines are present, they seems stabilize the bundle crossing in its open configuration, enhancing the interaction with PIP_2 at the cytoplasmic side of the membrane. So long polyamines are capable of stabilizing the channel in an open configuration by strengthening channel–PIP_2 binding affinity. Long polyamines serve a dual role as both blockers and co-activators (with PIP2) of Kir 2.1 channels (Xie et al. 2005).

G protein βγ subunit plays a key role in Kir channels modulation. There is a whole Kir family (Kir 3.x) activated after the binding of $G_{\beta\gamma}$ subunit (figure 1.12). They are named GIRK channels as G protein-coupled inward rectifier K^+ channels (Walsh 2011). Therefore G-proteins can modulate ion channels directly - through membrane delimited pathways - or indirectly via various second messenger signaling pathways. It is well accepted that a direct interaction between the N- and C-termini of Kir 3.x channels with $G_{\beta\gamma}$ is necessary for G-protein modulation of the

channel. In addition, Kir 3.1 and Kir 3.4 subunits form an heterotetrameric channel, the K_{ACh} channel, which is activated after the direct binding of $G_{\beta\gamma}$ to the N- and C-termini (Xie et al. 2007).

Data suggest the necessary requirement of PIP_2 for the $G_{\beta\gamma}$ stimulation of the channel activity. Indeed, when $G_{\beta\gamma}$ is directly applicate to the cytoplasmic side, it slows the inhibition effect of channel induced by the lack of available PIP_2, and it increases the channel activation in presence of PIP_2. When K_{ACh} channels run down completely, they cannot be activate by addition of $G_{\beta\gamma}$ alone (Xie et al. 2007).

Intracellular Na^+ ions

The most likely mechanism for Na^+ activation of Kir 3 channels (3.2 and 3.4) is mediated by the interaction between Na^+ ions and an aspartate residue within the C-termini region of channels. This interaction reduces the negative electrostatic potential in the vicinity of the PIP_2 binding site and enhances the PIP_2–channel interaction. Similar activation effect by Na^+ is also suggested for Kir 6.2 channel, and it implies a corresponding aspartate residue (Logothetis et al. 2007).

Na^+ activation of Kir 3 channels is a mechanism strictly linked to $G_{\beta\gamma}$ subunit presence. It seems that there are two distinct gates at the channel pore, one sensitive to $G_{\beta\gamma}/Na^+$ complex and another to PIP_2. Data reveal that both PIP_2 and $G_{\beta\gamma}/Na^+$ are necessary to open the channel and to make it permeable to K^+ ions (Logothetis et al. 2007).

Sulfonylurea receptor and ATP sensitivity

K_{ATP} channels are heteromultimers composed of the pore-forming Kir subunit Kir 6.1/6.2 and the sulfonylurea receptor (SUR). SUR is a member of the ATP-binding cassette (ABC) transporter family and has 17 transmembrane helices arranged in groups of 5, 6, and 6 which form the transmembrane domains 0, 1, and 2. SUR also has two nucleotide binding domains (NBDs), which are large intracellular loops responsible for nucleotide binding and hydrolysis (Xie et al. 2007).

Due to the complexity of their organization, K_{ATP} channels are regulated by several compounds which interact with various subunits and binding sites - such as ligands, drug, K^+ channel openers, nucleotides and sulfonylureas (Xie et al. 2007). SUR subunits are the main responsible of K_{ATP} channel regulation. They mediate stimulation by K^+ channel openers and block by sulfonylureas.

Also the intracellular ATP modulates K_{ATP} channels activity, causing at high concentration the inhibition of the channel (Nichols & Lopatin 1997). In absence of PIP_2, K_{ATP} channel is able to bind ATP, this cause the channel closure. On the other hand, the negatively charged head group of membrane PIP_2 interacts with positive

charged residues in the cytoplasmic domain of the K_{ATP} channel: this interaction may distort the ATP-binding site and prevent ATP from binding and channel from closing (fig. 1.12). This regulatory system adjusts finely the *in vivo* response to various signaling pathways by modifying level of membrane PIP_2. Data show that activation of phospholipase C (PLC), which breaks down PIP_2 and decreases its intracellular concentration, increases the ATP mediated inhibition effect. Stimulation of PI-kinase, which increases PIP_2 intracellular level, reduces K_{ATP} channel ATP sensivity (Xie et al. 2007).

pH sensitivity

Kir 1.1 and Kir 4.1 are the most sensible to pH changes than the others (2.3, 5.1, and 6.2). Intracellular acidification reduces Kir 1.1 probability to be in the open state. In Kir1.1 channels, this pH gating has been attributed to a discontinuous arginine-lysine-arginine triad in the N and C termini. It seems that the lysine in the N terminus plays the major role in pH regulation, and they are missing in pH-insensitive Kir channels. In the Kir 4.1 channel, the equivalent lysine residue is critical for the pH sensitivity (Xie et al. 2007).

PIP_2 plays an important role in the pH regulation of Kir channels. It is suggested that PIP_2 binding to Kir 1.1 alters the pKa for pH gating. Evidence indicates that low affinity PIP_2 interaction is a prerequisite for pH sensitivity in some Kir channels and that the N-terminal PIP_2 interaction site must be absent for pH gating in the physiological range. The PIP_2 dependence for pH inhibition was also observed in Kir 2.x (Du et al. 2004), heteromeric Kir 4.1–Kir 5.1 channels (Yang et al. 2000), and in Kir 6.2 channels (Schulze et al. 2003). Thus, channel–PIP_2 interactions may act like a switch that controls pH-induced inhibition of Kir channels (Xie et al. 2007).

Taken together, these findings on the regulation Kir 1.1 by PKA, Kir 2.1 by PA, Kir 3 by $G_{\beta\gamma}$, and Kir 6.2 by SUR suggests a mechanism, where various intracellular regulatory particles bind to, or interact with the N- and/or C-termini of these channels, causing a conformational change which modulates gating. These allosteric changes alter the structure or position of the PIP_2 binding region and affect the channels interaction with PIP_2.

1.5 Inward rectifier family members

Kir Family	*Alias*	*Protein*	*Gene*
Classical Kir Channels	IRK 1	Kir 2.1	KCNJ 2
	IRK 2	Kir 2.2	KCNJ 12
	IRK 3	Kir 2.3	KCNJ 4
	IRK 4	Kir 2.4	KCNJ 14
G-protein gated Kir Channels	GIRK 1	Kir 3.1	KCNJ 3
	GIRK 2	Kir 3.2	KCNJ 6
	GIRK 3	Kir 3.3	KCNJ 9
	GIRK 4	Kir 3.4	KCNJ 5
ATP-sensitive K+ channels	K_{ATP}	Kir 6.1	KCNJ 8
	K_{ATP}	Kir 6.2	KCNJ 11
	*SUR subunits**	*SUR 1*	*ABCC8*
	*SUR subunits**	*SUR 2a*	*ABCC9*
	*SUR subunits**	*SUR 2b*	*ABCC9*
K+-transport channels	ROMK 1	Kir 1.1	KCNJ 1
	K_{IR} 1.2	Kir 4.1	KCNJ 10
	K_{IR} 1.3	Kir 4.2	KCNJ 15
	K_{IR} 1.4	Kir 7.1	KCNJ 13
	BIR 9	Kir 5.1	KCNJ 16

Table 1 **Inward rectifier family members**. *Although SUR subunits are not members of Kir family, they are shown in table, due to the essential role they play in K_{ATP} channel activity.

1.5.1 Classical Kir channels

The classical K^+ inward rectifier channels, also known as strongly rectifier, are formed by *Kir 2* (Kir 2.1 – Kir 2.4) proteins, mainly as homotetramers but also they exist as heterotetramers. The differences within the Kir 2 family depend on both specific biophysical properties - such as single channel conductance, rectification, barium block - and regulatory pathway like phosphorylation and second messenger signalling (arachidonic acid or phosphatidyl inositol phosphates). Therefore, the properties of homo- and heteromeric Kir 2.x channels may strongly depend on the cellular coexpression of Kir 2 subunits (Pruss et al. 2005).

Dominant negative mutations in Kir 2.1 underlie Andersen–Tawil syndrome, an autosomal dominant desease characterized by periodic paralysis, cardiac ventricular arrhythmias related to prolonged QT interval and dysmorphic facial features. Thus, Kir 2.1 is an unlikely candidate for drug-development efforts (Bhave et al. 2010).

Classical Kir channels are widely expressed in the working myocardium, but almost absent in nodal tissues. They sets the resting membrane potential close to the potassium equilibrium potential, and contributes outward potassium current

during repolarisation (van der Heyden et al. 2013). The first three members of the Kir 2 family show expression in many different tissues and cell types, whereas Kir 2.4 seems to be specific for neuronal cells (Pruss et al. 2005).

Immunocytochemical localization and situ hybridization data show all four Kir 2 subunits are expressed in the olfactory bulb. Kir 2.1 immunostaining is most prominent in the glomerular layer. Kir 2.2 immunoreactivity is also very prominent in the glomerular layer but only weakly detectable in the mitral cell layer. The external plexiform layer of olfactory bulb displays the highest Kir 2.3 signal, while the channel is virtually absent from the periglomerular cells (figure 1.13). Only a small subset of granular cells in the granule cell layer express the Kir 2.4 subunit, but many other olfactory bulb neurons display the Kir 2.4 channel with prominent immunostaining of mitral and tufted cells (Pruss et al. 2005).

Distribution of individual Kir2 subunits in different brain regions

Brain region	Kir2.1	Kir2.2	Kir2.3	Kir2.4
Telencephalon				
Olfactory bulb				
Glomerular layer	++++	+	0	+
External plexiform layer	+	0	++++	0
Mitral cell layer	+	+	+	++
Granule cell layer	++	0	+	+

H. Prüss et al. / Molecular Brain Research 139 (2005) 63–79

Figure 1.13 **Kir2.x in the Olfactory Bulb.** Focus on table 1 *from Prüss H. et al., Brain Res.Mol.Brain Res., 2005*.
Data come from the use of polyclonal monospecific affinity purified antibodies against the less conserved carboxy-terminal sequences of Kir 2.1, 2.2, 2.3, and 2.4. The detailed distribution of all members of the Kir 2 family in the rat central nervous system is given.

1.5.2 G - protein gated Kir channels (GIRK)

Kir 3 channels are distinguished from other inward rectifiers because of their activity is critically regulated by G protein-coupled receptors (GPCRs). For this reason they are called GPCR-activated inward rectifier K^+ channels (GIRK) (Bhave et al. 2010). GIRK channels responsible for G protein–coupled receptor-activated currents are important elements in controlling cellular excitability in heart, in central and peripheral nervous system. They play a key role controlling slow postsynaptic inhibitory signaling and hormone secretion via *pertussis* toxin sensitive GPCRs in endocrine tissue (Sadja et al. 2003).

These channels exhibit a low open-state probability under basal conditions, but are activated through a $G_{\beta\gamma}$-dependent pathway following GPCR stimulation (Nichols & Lopatin 1997). Upon GPCR stimulation, the α subunit of the G protein replaces its bound GDP with GTP. This causes the βγ subunits to dissociate from the α subunit; as a result $G_{\beta\gamma}$ and G_{α} can act as two independent down-stream signaling effectors.

In the case of the GIRK channel, the $G_{\beta\gamma}$ subunit direct binds and actives the channels. The $G_{\beta\gamma}$ activation signal burns out when G_{α}-GTP is hydrolyzed into G_{α}-GDP, which can reassemble G protein binding to $G_{\beta\gamma}$ subunit.

Regulators of G protein signaling (RGS) proteins, which accelerate the GTPase activity of the G_{α} subunit, are involved in important modulation of GIRK current. The expected decrease in current amplitude, after RGS induced GTPase activity, does not occur in experimental observations. For this reason a complex GPCR- G protein- RGS- GIRK interaction net has been proposed (fig 1.14)(Sadja et al. 2003).

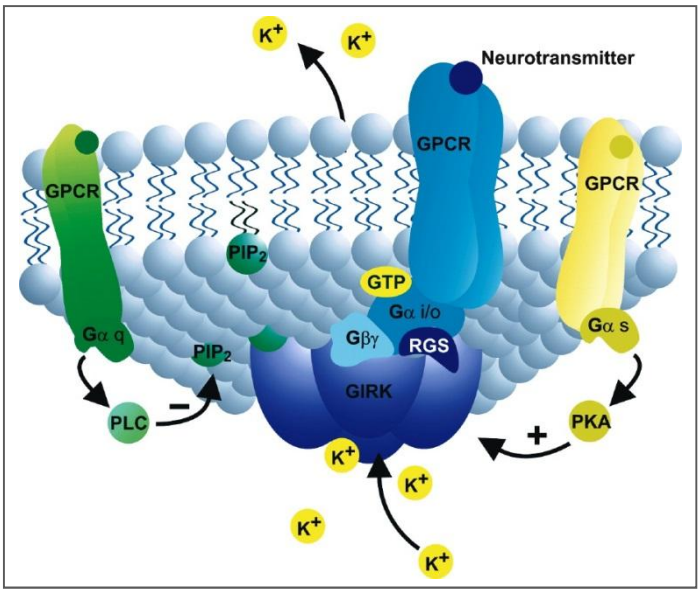

Figure 1.14
Schematic representation GIRK channel signaling complex.
GIRK channels gate after the activation of GPCRs. *Pertussis* toxin-sensitive G proteins (Gi/o) releases $G_{\beta\gamma}$ dimers to directly gate the channel (blue).
The phospholipid PIP_2 is closely associated with the channel to stabilize its functional integrity. GPCRs that are associated with G_q proteins (green) can reduce channel activity through phospholipase C (PLC), which breaks down PIP_2. On the other hand, GPCR linked to $G_{\alpha s}$ proteins (yellow) increase channel activity by protein kinase A (PKA). Both PLC and PKA may be soluble and thus do not have to directly associate with the GIRK channel activation complex.
From Sadja et al., Neuron 2003.

In mammals, the GIRK family is comprised of four members: Kir 3.1, 3.2, 3.3 and 3.4. GIRK channels exist primarily as heterotetramers, with Kir 3.1/3.2 predominating in the nervous system and Kir 3.1/3.4 in the heart (Bhave et al. 2010). Expression of GIRK 2, GIRK 3, or GIRK 4 alone yield G protein–activated inwardly rectifying K^+ conductances. On the other hand, when GIRK 1 subunit is expressed alone no channel activity can be detached, despite the protein expression. For this reason, it is suggested that GIRK 1 forms native channels together with the functional homologs GIRK2, GIRK3, and/or GIRK4, depending on which subunits are available in a given cell (Bhave et al. 2010).

Kir 3.1/3.4 heteromeric channels are expressed primarily in atrial myocytes of the heart where they are functionally coupled to M2 muscarinic GPCRs. Release of acetylcholine onto M2 receptors, due to vagal nerve stimulation induces an outward K^+ current through Kir 3.1/3.4 channels, which hyperpolarizes the cell membrane potential. The classical term for this acetylcholine-activated inward rectifier K^+ current is I_{KACh} (Bhave et al. 2010). The muscarinic-gated K^+ (K_{Ach}) channel is so called because of the first identified agonist, although other several

neurotransmitters can active it, including somatostatin, GABA and adenosine (Bhave et al. 2010).

Kir 3.1/3.2 heteromeric channels are broadly expressed in the nervous system, where they act as effectors for several neurotransmitter systems including GABA, opioid, glutamate, adenosine, and dopamine. GIRK activation leads to membrane hyperpolarization and weakening of postsynaptic excitation (Bhave et al. 2010).

1.5.3 ATP-sensitive K^+ channels

Kir 6 (Kir 6.1 and Kir 6.2) constitute the pore-forming subunits of ATP-sensitive potassium (K_{ATP}) channel. It couples cellular metabolism to membrane excitability in several key cell types: in pancreatic β cells with insulin release control, in vascular smooth muscle whit blood flow control, in cardiac sarcolemma and in brain.

K_{ATP} channels are extensively expressed in various regions of the mammalian brain, including the substantia nigra (SNr), neocortex, hippocampus, and hypothalamus. In the adult brain, Kir 6.2 subunits have been found in hippocampal, cortical, and hypothalamic neurons, as well as in the SNr pars reticulata. Immunohistochemical studies showed that Kir 6.2 subunits are mainly located in the somata and dendrites of the central neurons.

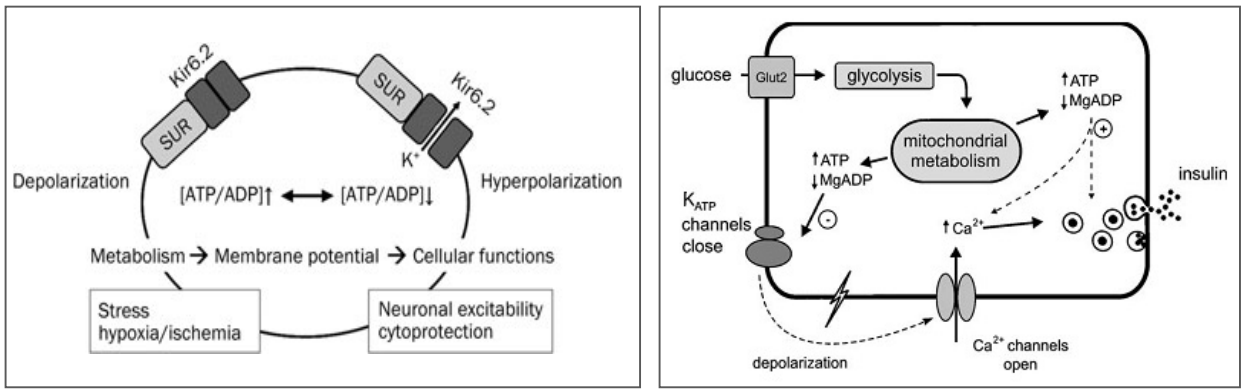

Figure 1.15 **Schematic illustration of K_{ATP} channels function in neurons and β cells**.
In neurons (right) K_{ATP} channels serve as metabolic sensors to couple electrical activity of neurons. Under normal physiological conditions, K_{ATP} channels remain close, due to the high ATP/ADP ratio. Reducing the ATP/ADP ratio opens the channel and allows K^+ ions to exit the cells, thus hyperpolarizing the neurons. *From Sun and Feng, Nature 2013.*
In pancreatic β cells (left) K_{ATP} channels contribute to insulin secretion.
Under resting conditions, K_{ATP} channels are open, producing hyperpolarization of the β cell plasma membrane and so preventing insulin secretion. Glucose enters the β cell by way of the GLUT2 glucose transporter. Once inside the cell, glucose is metabolized, ATP level increases whereas Mg-ADP level decreases, causing K_{ATP} channels to close. This produces a membrane depolarization that activates voltage-gated Ca^{2+} channels, causing Ca^{2+} influx and a rise in cytosolic Ca^{2+} that triggers release of insulin granules. *From Freeman et al.,2006.*

The metabolic state of the cell can regulate membrane potential and excitability thanks to K_{ATP} channels, which are inhibited by ATP and stimulated by nucleotide diphosphates (figure 1.15). An increase in the ATP/ADP ratio closes K_{ATP} channels (leading to depolarization), whereas a decrease in the ATP/ADP ratio opens K_{ATP} channels (leading to hyperpolarization).

The opening of K_{ATP} channels shifts the cell membrane potential more negatively (hyperpolarization) towards the E_K, leading to suppression of neuronal activity and excitability. Thus, opening K_{ATP} channels under metabolic stress can protect neurons against neuronal injury during cerebral ischemia and stroke.

The K_{ATP} channel contains four pore-lining subunits of the Kir 6 subfamily of inwardly rectifying potassium channels and four regulatory subunits the sulfonylurea receptor (SUR) proteins which confer channel sensitivity to numerous small-molecule inhibitors, such as adenosine triphosphate, and activators (Bhave et al. 2010). The SUR subunits are members of the ATP-binding cassette (ABC) protein superfamily and they are sensitive to the adenine nucleotides, Mg-ADP, so reducing the intracellular concentration of ATP or the ATP/ADP ratio gates the K_{ATP} channel.

Differences in endogenous K_{ATP} channel properties and pharmacology account for differences in subunit composition: Kir 6.2 and SUR 1 in pancreatic β cells, Kir 6.2 and SUR 2A in cardiac myocytes, Kir 6.2/Kir 6.1 and SUR 2B in vascular smooth muscles, or Kir 6.2 and SUR 1/2B in central neurons. SUR subunits are major pharmacological targets. K_{ATP} channels have distinctive pharmacology. Sulfonylureas are a type of potassium channel blocker that works by binding to SUR subunits. On the other hand K_{ATP} channels can be activated by a group of drugs called potassium channel openers. Some of these drugs are currently in use clinically for the treatment of a variety of disorders such as neonatal and adult-onset diabetes, hyperinsulinism, hypertension, cardiac arrhythmia, angina, alopecia, cerebral ischemia and stroke (Bhave et al. 2010).

1.5.4 K^+ - transport channels

Kir 1.1 is the founding member of the inward rectifier family, and it is commonly referred to as the renal outer medullary K^+ (ROMK) channel. Kir 1.1 cDNA is cloned from rat kidney outer medulla and is shown to encode a weakly rectifying K^+ channel located in epithelial cells of the thick ascending limb and collecting duct. Kir 1.1 in renal tubule conveys important function (figure 1.16): in thick ascending limb, luminal K^+ recycling by Kir 1.1 catalyzes Na^+ Cl^- reabsorption through Na^+ -K^+ -$2Cl^-$ co-transporter (NKCC2), which in turn promotes osmotic water reabsorption in the distal nephron. In the connecting tubule and collecting duct, Kir 1.1 constitutes a key physiological pathway for regulating K^+ secretion to match dietary intake (Bhave et al. 2010).

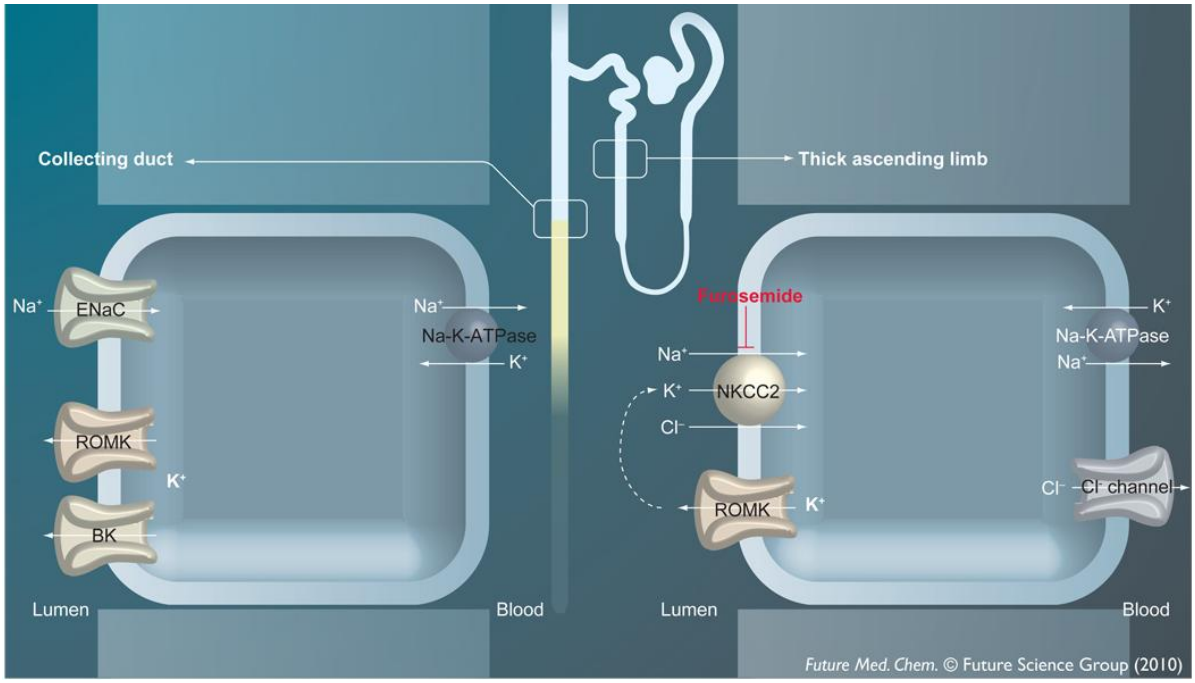

Figure 1.16 **Major functions of ROMK in the kidney tubule**.
ROMK provides substrate K^+ ions essential for transepithelial NaCl reabsorption by NKCC2, in the thick ascending limb of Henle's loop. NaCl reabsorption generates a hypertonic condition that promotes osmotic water reabsorption in the distal nephron. In the collecting duct, ROMK constitutes a key physiological pathway for K^+ secretion into the urinary fltrate. BK: Big or large conductance calcium-activated K^+ channel; ENaC: Epithelial Na^+ channel; NKCC2: Na+-K+-2Cl co-transporter intake. *From Bhave et al., Future.Med.Chem. 2010.*

Kir 4 & Kir 5

Simplicity and strong homology of the basic Kir channel subunit allow for both homomeric and heteromeric combinations. To form functional Kir channels, heteromerization generally occurs between members of the same subfamily (Hibino et al. 2010). An exception is the Kir 5 (Kir 5.1): it must co-assemble with Kir 4 to give a working ion channel. On the other hand, Kir 4 subunits (Kir 4.1 and 4.2) can form functional homomeric channels (Bhave et al. 2010).

Kir 4.x channels show an “intermediate” degree of inward rectification, different from the “strong” degree of Kir 2.x and Kir 3.x, and the “weak” one of Kir 1.1 and Kir 6.x. Moreover. Heteromeric assemblies confer distinct properties to particular channels, which can determine their location on a cell as well as extend the functional range of Kir channels in different cell types (Hibino et al. 2010).

Kir 4 and Kir 5 family members are expressed primarily in central nervous system and retinal glial cells, inner ear cochlear cells and kidney distal tubular epithelial cells (Bhave et al. 2010). In particular, Kir 4.1/5.1 channel is expressed in renal epithelial cells upon their basolateral membranes. The inwardly rectifying potassium channel Kir 4.1 is the principal K^+ conductance of mammalian Müller cells and participates in the generation of field potentials and regulation of extracellular K^+ in the retina (Hibino et al. 2010).

Kir 7.1 is the newest member of the Kir family and is expressed primarily in brain, intestine, kidney and retina (Bhave et al. 2010).

Its sequence is quite different from those of other types of Kir channel and shares only ~38% homology with its closest relative, Kir 4.2. Its working properties are different: the single-channel conductance of Kir 7.1 is extremely small, the sensitivity of the channel to main blockers such as Ba^{2+} and Cs^+ is very low, and inward rectification of Kir 7.1 is independent of $[K^+]_o$. Like other Kir channel subunits, Kir 7.1 is activated by PIP_2 (Hibino et al. 2010).

The physiological functions of Kir 7.1 are largely unknown, although their localization in diverse epithelial cells suggests a role in cellular ion transport mechanisms (Hibino et al. 2010).

Kir 7 mutations are found in patients with Snowflake vitreoretinal degeneration, for this reason the physiological rule of Kir 7 is being studied in K^+ homeostasis of the retinal pigmented epithelium (RPE). In polarized epithelial cells of the intestine and nephron, Kir 7.1 expression appears to be limited to the basolateral membrane. Based on their subcellular co-localization in the gut, it has been postulated that Kir 7.1 is functionally coupled to the Na^+/K^+-ATPase and $Na^+/K^+/2Cl^-$ co-transporter and thereby contributes to transepithelial Cl^- secretion (Bhave et al. 2010).

2 Materials and Methods

2.1 Animals

Experimental procedures were carried out so as to minimize animal suffering and the number of mice used. The procedures employed were in accordance with the Directive 86/609/EEC on the protection of animals used for experimental and other scientific purposes.

All experiments were performed using the transgenic mice TH-GFP/21–31 line carrying the eGFP gene under the control of the TH promoter: the transgene construct contained the 9.0 kb 5'-flanking region of the rat tyrosine hydroxylase (TH) gene, the second intron of the rabbit β-globin gene, cDNA encoding GFP, and polyadenylation signals of the rabbit β-globin and simian virus 40 early genes (Sawamoto et al. 2001, Matsushita et al. 2002). Transgenic mice were identified, at postnatal day 3 or 4, looking at the fluorescence of the olfactory bulbs trans-illuminated with a UV source (FBL/Basic-B & N-01; BLS, Hungary; FHS/F-01) and observed with an emission filter (FHS/EF-2G2; BLS, Budapest, Hungary) (fig.2.1). Transgenic lines were maintained as heterozygous by breeding with C57BL/6J inbred mice.

Figure 2.1 **Transgenic mice identification.** On the left UV source, and in the middle gloves with the emission filter used to detect GFP emission. On the right, picture of a P3 mouse: GFP+ olfactory bulbs are detect after directing UV source towards skull fontal bone.

2.2 Slice Preparation

The assumption in studying neuronal behaviour in the brain slice is that, neurons in this *in vitro* preparation reflect electrophysiological and pharmacological responses similar to those in the intact nervous system (Suter et al. 1999).

Once the animal is sacrificed, beheaded by laboratory guillotine, the brain is removed and submerged in ice-cold high sucrose carbogenated artificial cerebrospinal fluid (ACSF, see solutions). Keeping the tissue cold-throughout

sectioning minimizes damage from anoxia and improves the texture of the tissue for slicing. Brain is cut by hand caudally to the olfactory bulbs to maintain together the two ovoid structures. Tissue is embedded in agar (low gelling temperature agar, SIGMA-ALDRICH): the agar (4% dissolved in high sucrose ACSF) is cooled to below 37 °C before including the tissue; agar inclusion gives to tissue the mechanical stability which is essential for making thin slices. A thin film of cyanoacrylate glue (3M™ Vetbond™ Tissue Adhesive) is used for the instant attachment of the agar cube to the stage of the slicer. The slicing chamber is filled with ice high sucrose ACSF while slicing. A standard vibrating microslicer (Campden Instruments Ltd) is used to cut slices of 130 µm thickness.

After sectioning, each slice is immediately placed in carbogenated high sucrose ACSF where it remains until use (figure 2.2). Slices are transferred into and out of the holding chamber using a cut and fire polished pasteur pipette. A holding chamber is placed in the middle of a 50 ml beaker. A bubbler inserted in the beaker oxygenates the slices. Once slice is placed in the recording chamber, it is held in place with a grid of parallel nylon threads. The U-shaped frame of the grid is made from 0.5 mm platinum wire flattened, and between the two arms of the grid 50 µm diameter nylon threads are tense.

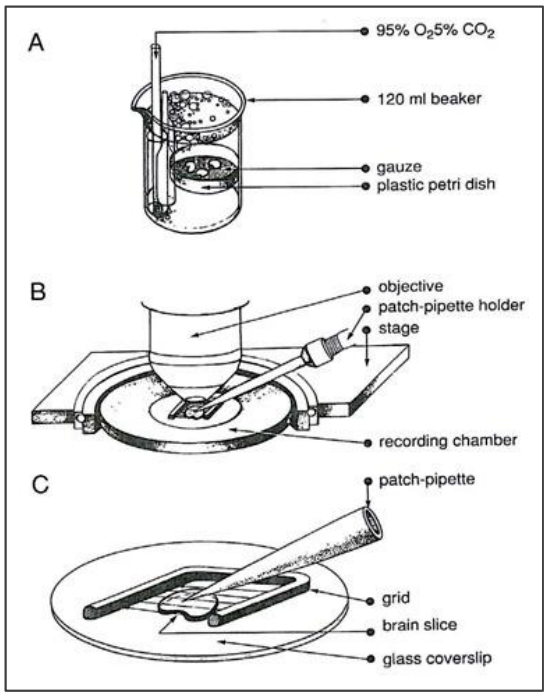

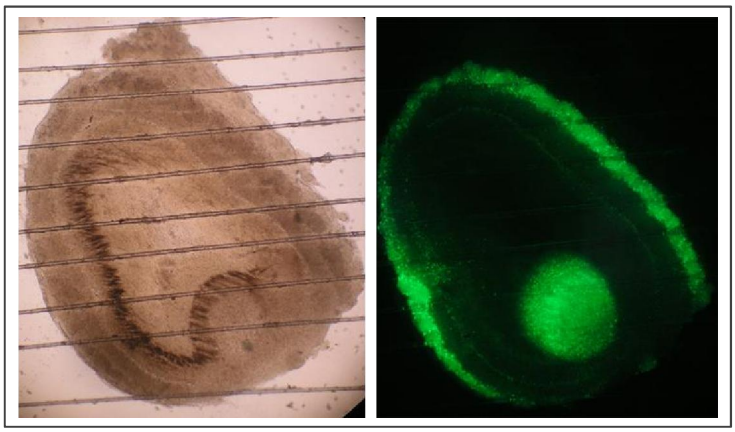

Figure 22 **Olfactory bulb slice preparation.** After sectioning, slice were maintained in a carbogenated high sucrose ACSF where it remains until use (A). In B, and C the recording chamber is shown: you can see microscope water immersion objective, the patch clamp pipette and the grid used to fixed the slice. On the right, pictures show coronal slices of olfactory bulb in bright field and in epifluorescence. Periglomerular layer with TH-GFP+ cells can be noted on the border of the slice and inner the accessory olfactory bulb.

2.3 Recording Conditions

One slice at a time is placed in the continuous perfusion recording chamber of microscope, where 2ml/min flux of saturated carbogenated solution perfuses slice. Continuously perfused chamber ensures constant oxygenation and heating and makes easily addition, and later washout of drugs. The recording chamber is fixed to the Olympus BX50WI microscope stage. The microscope focussing mechanism provides a moving objective and a fixed stage. A differential interference contrast optic technique (*Nomarski* optics) is used to enhance the contrast and to emphasize three-dimensional samples. Moreover, microscope was equipped of epifluorescence to detect GFP+ cells.

Patch-clamp pipettes

Patch pipettes were pulled from borosilicate glass with filament (Hilgenberg, Malsfeld, Germany): 1.5 mm outer diameter, 0.87 mm inner diameter and inner filament of 0.15 mm. Zeits-DMZ puller (Martinsried, Germany) produces two 5 cm long pipettes each pull, starting from 10 cm long glass capillary. These pipettes have a resistance of 4-5 MΩ when filled with standard intracellular solution (IC).

Positive pressure through the pipette was applied while advancing to prevent contaminating the tip with debris. Contact with a membrane can be detected by a sudden increase in resistance. The release of positive pressure and subsequent application of gentle suction after a detected increase in resistance results in *giga-seal* formation.

Patch-clamp technique

The *patch-clamp* technique, introduced by Erwin Neher and Bert Sakmann (Neher & Sakmann 1976) in the mid-1970s advanced the ability to study the membrane function of excitable cells, such as neurons. Ionic currents through single membrane channels were recorded after sealing a micropipette tip onto a clean membrane patch.

In the early 1980s, the technique evolved to allow recording of currents conveyed through membrane ionic channels in the whole cell: tight seals with high resistance in the GΩ range (*giga-seal*) were possible after drawing up a small patch of the membrane into the pipette tip by suction generated by application of gentle negative pressure (Hamill et al. 1981). Subsequent rupture of the patch with negative pressure or a voltage pulse allowed establishment of low-resistance electrical and physical access to the interior of the cell, thus allowing the recording of the entire population of ionic currents on the cellular membrane.

This constitutes the basis of the *whole-cell patch-clamp* technique.

Application of the conventional *whole-cell patch-clamp* method leads to a replacement of the intracellular fluid with the intracellular pipet solution. The speed of this replacement depends on the cell volume and electrode tip diameter. Although this mechanism can be used advantageously in many experiments, in my work there are conditions where such a dialysis interferes with the current response to be tested. In particular, in order to prevent washing of intracellular molecules, such as cAMP, and to avoid the response disappearance within minutes, *perforated patch-clamp* was performed in all experiments reported below. This technique does not involve the breaking of the patch membrane, ensuring physiological intracellular environment maintenance (figure 2.3, left). Amphotericin B (polyene antibiotics, SIGMA-ALDRICH) was used in order to gain electrical access to the cell interior by forming channels in the membrane. The channels produced are permeable to monovalent cations and chlorine ions (Cl^-) but do not allow passage of multivalent ions, such as Mg^{2+} or Ca^{2+}. Because of its limited water solubility, amphotericin B stock solutions of 25 mg/ml are prepared in DMSO; it is prepared just before use due to its loss of activity on prolonged storage. Stock solution is added directly to the pipette filling (IC) solution to a final concentration of 200 µg/ml, together with pluronic acid f-127 300 µg/ml.

Because patch pipettes can be readily visualized, microscope provides a 40X water immersion objective; in this way specific cells are identified by GFP emission presence, morphology, anatomical location around glomeruli, and selected for electrophysiological recordings.

Current-clamp and voltage clamp configuration

Changes in voltage underlie neuron excitability: action potentials, after potentials, and postsynaptic potentials can be determined thanks to the *patch-clamp* technique. The membrane voltage changes associated with these events are studied with the *current-clamp* configuration, where a known current is applied and changes in membrane potential are measured. Also changes in waveform and frequency of action potentials can be studied in response to the input current.

On the other hand, thanks to *voltage-clamp* recordings, examination of changes in voltage-dependent current is permitted. After the voltage step, the membrane potential changes rapidly and then there are no capacitative currents. Therefore, the remaining current is ionic and is proportional to the membrane conductance (figure 2.3, right).

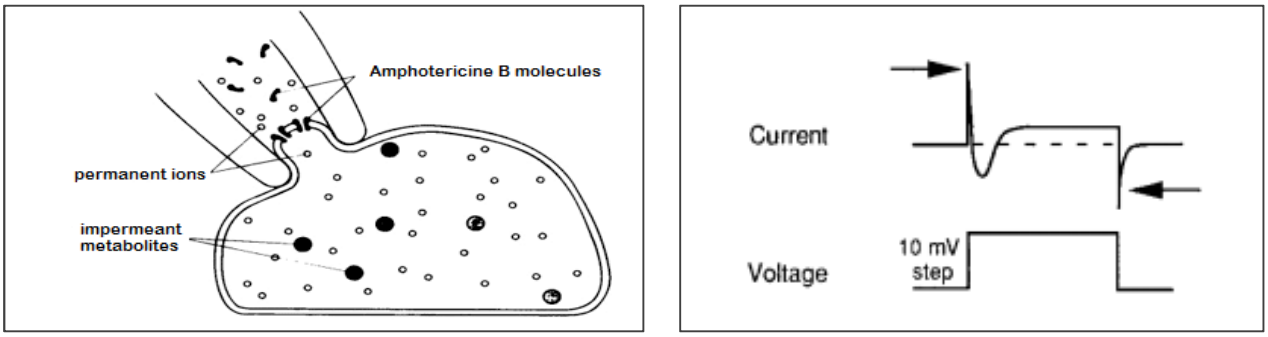

Figure 2.3 ***Patch-clamp*** **technique.** On the left, representation of perforated *patch-clamp* technique. On the right, Current response to a voltage-clamp pulse. Arrows indicate capacitative transients at the beginning and end of the pulse. Inward and outward currents follow the capacitative current.

2.4 Electrophysiological Experimental Set-up

Electrophysiological set-up provides different instruments:

- the optical microscope (Olympus BX50WI) with 5X and 40X moving objectives and a fixed stage;
- the electromechanical micromanipulator (Patch Man, Eppendorf) with dynamic joystick control, which ensures extra fine movement being able to approach pipette tip at membrane cell;
- the microelectrode amplifier (Axopatch™ 200B Capacitor Feedback Patch Clamp Amplifier, Axon Instrument, USA) optimizes membrane potential recordings. It allows correction for voltage errors due to pipette resistance, and it filters ultra-low noise of *patch-clamp* recordings. It permits some corrections such as pipette resistance compensation, cell capacitance compensation and in series resistance compensation.
- The analog-to-digital- and digital-to-analog converter (Digidata 1320A, Axon Instruments, USA), designed for electrophysiology experiments, sends and receives signals from microelectrode amplifiers.
- The Faraday cage blocks external static and non-static electric fields. It is formed by conducting material. All instruments used for electrophysiological recording were put inside the Faraday cage in order to prevent electrical noises.
- The anti-vibration table, with pneumatic auto-levelling mounts, isolates set-up instruments from vibrations.
- The temperature control system implies a Peltier element between the microscope stage and the recording chamber, and a temperature sensor put in the recording chamber. A high sensible thermoresistance corrects temperature changes, maintaining temperature in the recording chamber fixed to the set value.

2.5 Solutions

Intracellular solution

The standard pipette-filling intracellular (IC) solution used has the following composition (mM): 120 KCl, 10 NaCl, 2 $MgCl_2$, 0.5 $CaCl_2$, 5 EGTA (ethylene glycol tetraacetic acid), 10 HEPES (4-(2-hydroxyethyl)-1-piperazineethanesulfonic acid), 2 Na-ATP, 10 glucose. The free calcium concentration with this internal solution was calculated to be 16 nM. The pH is set equal to value 7.2 with KOH, and the osmolarity is adjusted at 295 mOsm.

Extracellular solution

Five extracellular solutions were used in order to performed different experiments. Standard extracellular solution provides physiological potassium concentration, but in order to better characterize Kir current also experiments with high potassium concentration were performed. Moreover, when tetraethylammonium (TEA) is present in the solution, sodium chloride concentration is recalculated in order to maintain osmolarity at the physiological value.

The solutions used had the following composition (mM):

- Standard ACSF extracellular (EC) saline, namely also as **EC0**: 125 NaCl, 2.5 KCl, 26 $NaHCO_3$, 1.25 NaH_2PO_4, 2 $CaCl_2$, 1 $MgCl_2$, and 15 glucose;
- High K^+ extracellular saline solution, namely also as **EC1**: 95 NaCl, 32.5 KCl, 26 $NaHCO_3$, 1.25 NaH_2PO_4, 2 $CaCl_2$, 1 $MgCl_2$, and 15 glucose.
- Standard K^+ and TEA extracellular saline solution, namely also as **EC2**: 100 NaCl, 2.5 KCl, 26 $NaHCO_3$, 1.25 NaH_2PO_4, 2 $CaCl_2$, 1 $MgCl_2$, and 20 TEA, and 10 mM glucose.
- High K^+ and TEA extracellular saline solution, namely also as **EC3**: 70 NaCl, 32.5 KCl, 26 $NaHCO_3$, 1.25 NaH_2PO_4, 2 $CaCl_2$, 1 $MgCl_2$, and 20 TEA, and 10 mM glucose.
- Medium K^+ and TEA extracellular saline solution, namely also as **EC4**: 90 NaCl, 10 KCl, 26 $NaHCO_3$, 1.25 NaH_2PO_4, 2 $CaCl_2$, 1 $MgCl_2$, and 20 TEA, and 10 mM glucose.

All extracellular saline solutions were continuously bubbled with 95% O_2 and 5% CO_2. Their composition were optimized to have pH set to the mammalian physiological value of 7.4, and solution osmolarity was adjusted at 305 mOsm with glucose.

The Kir current was recorded after blocking all other conductances active at the potentials of interest by adding at the external solution blockers (**BL1**) for the two main neurotransmitters in the OB, i.e. 1 mM kynurenic acid for glutamate and 10 μM bicuculline for GABA, and blockers (**BL2**) for the main voltage-dependent channels, i.e. TEA 20 mM, TTX 0.6 μM, Cd2+ 100 μM and ivabradine 10 μM for potassium, sodium, calcium and h-channels, respectively.

A particular extracellular solution was used during surgical procedures and slice preparation, which had the following composition:

- High sucrose extracellular saline solution: 3 KCl, 21 $NaHCO_3$, 1.25 NaH_2PO_4, 1.6 $CaCl_2$, 2 $MgCl_2$, 10 glucose and 215 sucrose.

2.6 Analysis of Current Recordings

In order to investigate Kir current in DA-PG cells, and provide current recordings at different voltage inputs the main protocol used was a *voltage clamp* step protocol. This protocol provided a holding potential of - 40 mV followed by a series of hyperpolarization voltage pulses, ranging from - 60 mV to - 130 mV in increments of 10 mV. Thanks to this protocol differences in current amplitude between recordings in control condition and in presence of drugs were tested. To compare control and treated recordings obtained from the same cell, before and after adding drug of interest, values are considered at steady state (SS) current and obtained by mediating a tract of the recording trace in a define interval of time. Analysis were performed using the software Clampfit 10.3 (pCLAMP) at each tested membrane potential.

To turn out rectification of Kir current in DA-PG cells, *voltage clamp* 220 mV/s ramp protocol has been used, starting from -180 mV to 40 mV, with a - 40 mV holding potential. In this way, I/V relation is obtained for a great range of potentials without stressing the cells. Currents were obtained by subtracting the *perforated-cell* currents in presence of Ba^{2+} 2mM from recordings in absence of Ba^{2+}, to isolate the barium sensitive component evoked by the ramp protocol and to exclude the leak component from analysis.

In order to fit experimental data to a theoretical trend defined by mathematical function, different equations were used: such as logistic equation for barium sensitivity description, exponentially decay function for Ba^{2+} and Cs^{+} voltage dependent block, Bolzmann Curve for Kir conductance, and exponentially modified Gaussian function for prevailing membrane potential. All equations are reported and explained in text (Chapter 3, Results) when used.

In some cases, box and whiskers graphs were used to better resume data from samples: this kind of representation gives several information about measurements of central tendency and probably distribution indexes. In this work, box and whisker charts identify the mean values whit full colour squares and the median values whit lines crossing the box. Standard errors values define the box range and between whiskers 80% of data were reported. In the other cases, data are presented as means ± S.E.M (standard error of mean).

Offline recording trace analysis was performed using version 10 of pClamp (Molecular Devices) and version 8 of Origin (OriginLab Corporation, Northampton, MA), and statistical analysis was performed using Prism 5 (GraphPad Software).

2.7 Statistical Analysis

D'Agostino-Pearson normality tests were used to determine if data sets are well-modelled by a normal distribution and to measure the goodness of fit of a normal model to data. Once verified assumptions about normality and independent errors, statistical parametrical analysis was performed.

Statistical significance of the results was assessed with Student's *t* test for paired samples and with two-way repeated measure analysis of variance (ANOVA) as indicated.

In order to compute post-tests following two-way ANOVA, multiple comparisons were performed using the Bonferroni method, as provided by Prism 5. The Bonferroni correction lowers the P value that one consider to be significant to 0.05 divided by the number of comparisons. This correction ensures that the 5 % probability applies to the entire family of comparisons, and not separately to each individual comparison.

P value of < 0.05 was considered significant; in figures, 1 to 4 asterisks represent differences significant at the 0.05, 0.01, 0.001, 0.0001 level, respectively.

3 Results

The data are based on recordings with *patch-clamp* technique in the *perforated-cell* configuration obtained from 285 TH-GFP+ periglomerular neurons in the glomerular layer.

Neurons are selected on the basis of their position around the glomeruli, dendritic arborization within the glomerular neuropil, membrane capacitance (8.54 ± 0.21 pF; n = 285) and input resistance (915.69 ± 31.31 MΩ; n = 248).

Dopaminergic PG cells can be differentiated from external tufted cells not only because of their large difference in membrane capacitance and input resistance, but also for their different modality of firing, regular in DA-PG cells (Pignatelli et al. 2005), in bursts in external tufted cells (Hayar et al. 2004).

Short-axon cells have membrane capacitance and input resistance very similar to PG cells, but usually they can be recognized in slice for their position between glomeruli, their fusiform shape and dendrites extending to different glomeruli (Shipley & Ennis 1996).

The transgenic mice used in these experiments express the green fluorescent protein under the tyrosine hydroxylase promoter (Sawamoto et al. 2001); it is a well-tested animal model for the study of dopaminergic neurons (Saino-Saito et al. 2004, Pignatelli et al. 2005, Pignatelli et al. 2009, Maher & Westbrook 2008) which provided a useful tool to examine dopaminergic cells in the rodent central nervous system.

3.1 Identification and Basic properties

3.1.1 Hyperpolarizing Step: Two Current Components

Hyperpolarizing steps evoke a measurable current in the experiments carried out using *perforated-patch* recordings, in slice at 34 °C. The used protocol, shown in figure 3.1, implies an holding potential of -40 mV and a series of hyperpolarizing steps ranging from -60 mV to -130 mV, with 10 mV increment to each step.

As you can see in A, the current evoked has different components: the *h*-current, the Kir current and the leakage current. A recent study proves the presence of I*h* in the dopaminergic periglomerular cells of the olfactory bulb (Pignatelli et al. 2013), arising in hyperpolarizing step protocols; the fraction of this current is suppressed by two organic compounds known as selective blockers of the *h*-current, ZD7288 30 μM (BoSmith et al. 1993) and the bradycardic agent S-16257 (ivabradine, 10 μM) (Bucchi et al. 2002, Bucchi et al. 2006). In figure 2.1 B, ivabradine 10 μM is added in the extracellular solution in order to subtract I*h* component.

After suppression of the *h*-current, the remaining current was identified as potassium inward rectifier (Kir) current, due to its time course, reversal potential and its sensitivity to Ba^{2+} (Hibino et al. 2010, Hibino et al. 2010) (figure 3.1 B).
In presence of ivabradine 10 µM and Ba^{2+} 2mM, to suppress I*h* and I_{Kir} respectively, only the leakage current is evoked by the used protocol (fig. 3.1C).

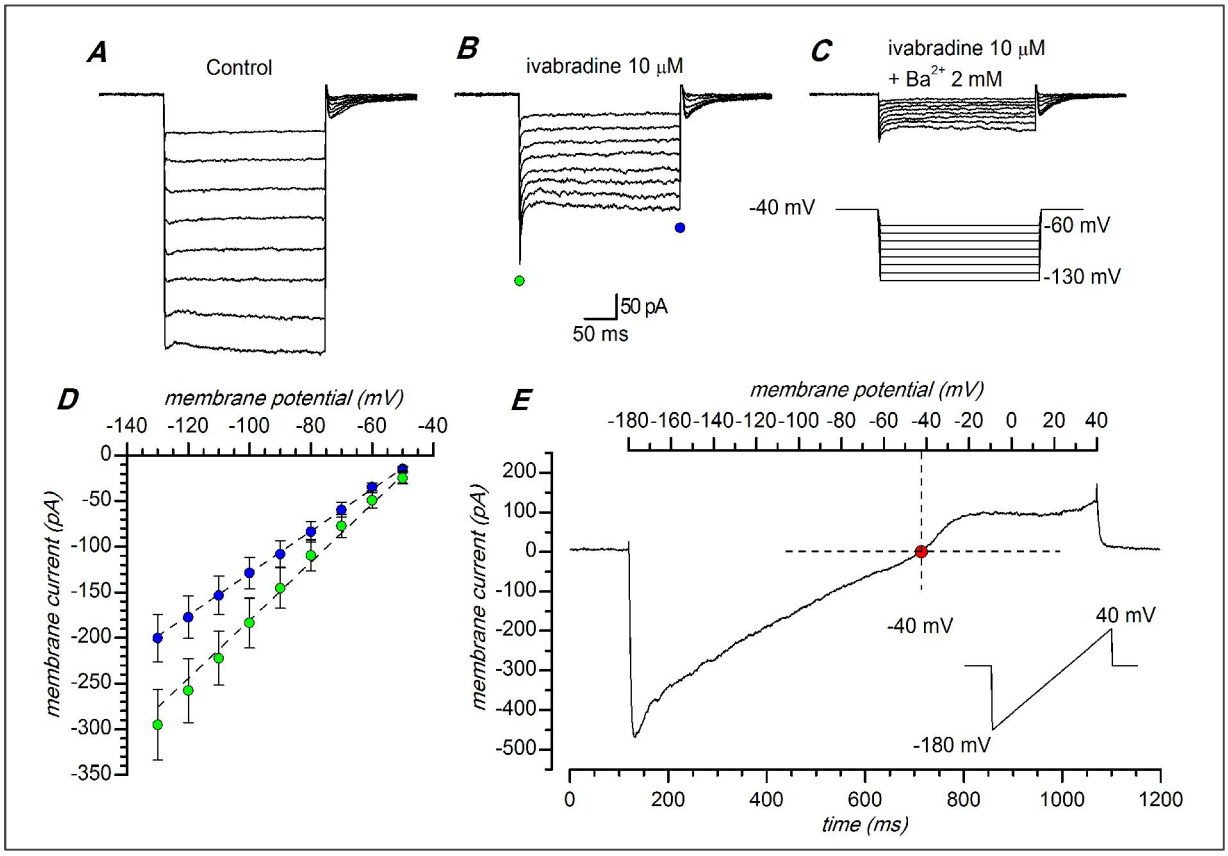

Figure 3.1 **General features.** *A)* Representative currents obtained in response to hyperpolarizing voltage step protocol from -60 mV to -130 mV, at a holding potential of - 40 mV in 32.5 mM external K^+ solution, containing bicuculline (10 µM), kynurenic acid (1 mM) for ligand-gated channels, TEA (20 mM), TTX (0.6 µM), Cd^{2+} (0.1 mM) for voltage-dependent channels, ivabradine (10 µM) in B and C in order to block I*h* current, and Ba^{2+} 2mM in C to block Kir current. D) I-V relationship of peak (green dots) and steady-state (blue dots) current: mean current amplitude of 81 cell recordings are reported. Vertical error bars represent standard errors. E) Instantaneous I/V curve during application of a 220 mV/s ramp protocol (from -180 mV to 40mV) in a DA PG cell perfused with solution used in B, after subtraction of the ohmic leak.

Kir current presents different amplitudes and time courses, if measured at peak or at steady-state (Hibino et al. 2010); in D, two different voltage-current relationship report mean current amplitudes of 81 cell recordings, both at peak (blue dots) and at steady-state (green dots).

In E the I/V relationship is obtained by 220 mV/s ramp protocol, which starts from an holding potential of -40 mV, than it forces the membrane from -180 mV to 40 mV in a second. The recorded trace shows great inward current evoked by hyperpolarization, reversal potential indicated as red dot (near to the Nernstian E_K

expected in this condition) and rectification, remarkable features of Kir current (Hibino et al. 2010).

3.1.2 Barium Sensitivity

Ba^{2+} cations are the most commonly used blockers to inhibit Kir channels, even if there are some differences between Kir subfamilies (Hibino et al. 2010). In order to verify barium sensitivity of TH-GFP+ Kir current, different concentrations of barium were added to the extracellular solution: some examples are reported in figure 3.2 A.

The Ba^{2+} dependent block of Kir current was assessed by measuring the decrease in steady-state current at − 120 mV. Each cell (n = 5) was exposed to bath solutions with external Ba^{2+} concentrations ranging from 1 µM to 10 mM; the inhibited current fraction is plotted against $[Ba^{2+}]_o$ (figure 3.2 B). The mean data are fitted by the logistic equation:

$$y = I_{max} / (1+ ([Ba^{2+}]_o/K_d)^p)$$

where I_{max} is the maximum current block, K_d is the concentration at half-block, and *p* is the slope of the dose-response curve, or Hill coefficient. This gives a K_d of 0.21 ± 0·10 mM and a *p* of 0.69 ± 0·229 (n = 5, −110 mV) for Ba^{2+} block of peak I_{Kir}.

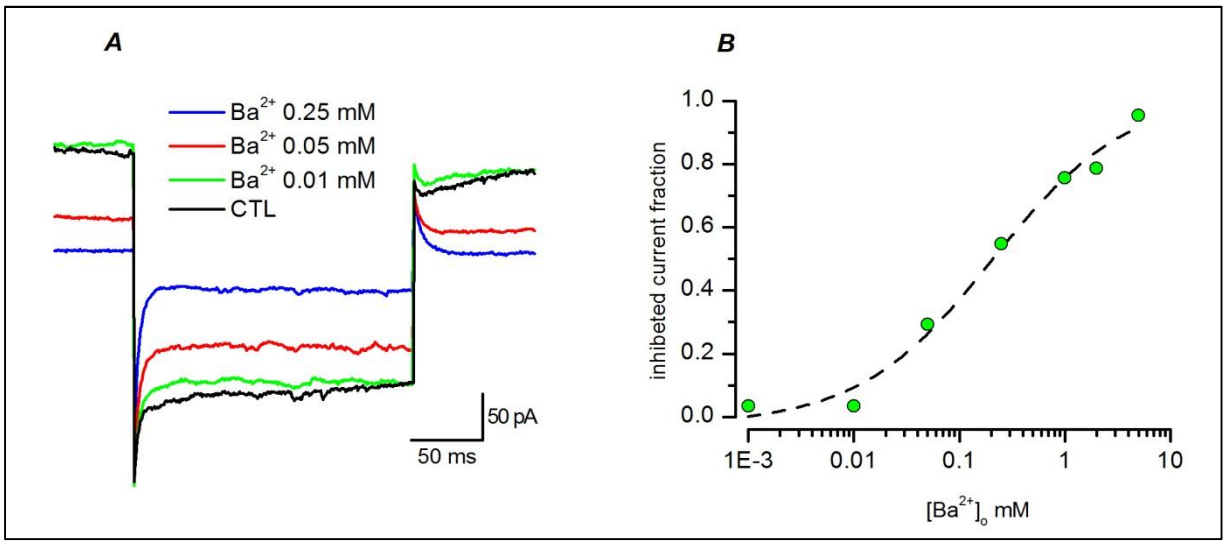

Figure 3.2 **Barium Sensitivity**
In A, recordings from the same cell are reported in different external barium concentration, as indicated by the legend of different color traces. The Kir current is evoked by a voltage step of - 120 mV with an holding potential of - 40 mV.
In B, inhibition of Kir current in different external concentration of Ba^{2+}. Data shown represents the means (n = 5) of steady state current evoked at - 110 mV, in 2.5 mM $[K^+]_{out}$ at 32 °C.

3.1.3 *Ba^{2+} and Cs^{+} Voltage Dependent Block*

Inorganic cations have been widely used to probe the permeation and gating mechanisms of potassium channels, indeed, it is well known that monovalent and divalent cations can bind Kir channels with high affinity (Hille 1992).

Protons like Na^{+}, Cs^{+}, Rb^{+} and Ag^{+}, and divalent cations, such as Ba^{2+}, Mg^{2+}, Ca^{2+} and Sr^{2+} block Kir channels (Standen & Stanfield 1978, Ohmori 1978, Doring et al. 1998, Dart et al. 1998). There are two different sites involved in the interaction of divalent cations with Kir channel: a shallow site that barely senses the membrane electric field, and a deeper one located approximately half-way within the membrane electrical field (Alagem et al. 2001).

As expected for deep-site blockers, the Ba^{2+} and Cs^{+} block is highly voltage dependent: figure 3.3 shows the effect induced by the application of Ba^{2+} 1 mM in TH-GFP+ PG cells (A-B), and of Cs^{+} 1 mM (C-D).

In E, the time required for the blocking reaction to reach steady state is calculated both in the case of barium and cesium by fitting the currents to an exponentially decaying function of the form:

$$I = A \exp(-t / \tau_{block}) + C$$

where A is the current amplitude, t is the independent variable, τ_{block} is the blocking time constant, and C is the steady-state current. The voltage dependence of the blocking time constants shows that Cs^{+} steady-state block is much faster than for Ba^{2+}. These results are in line with those reported in literature (Shioya et al. 1993, Hagiwara et al. 1976, Oliver et al. 1998).

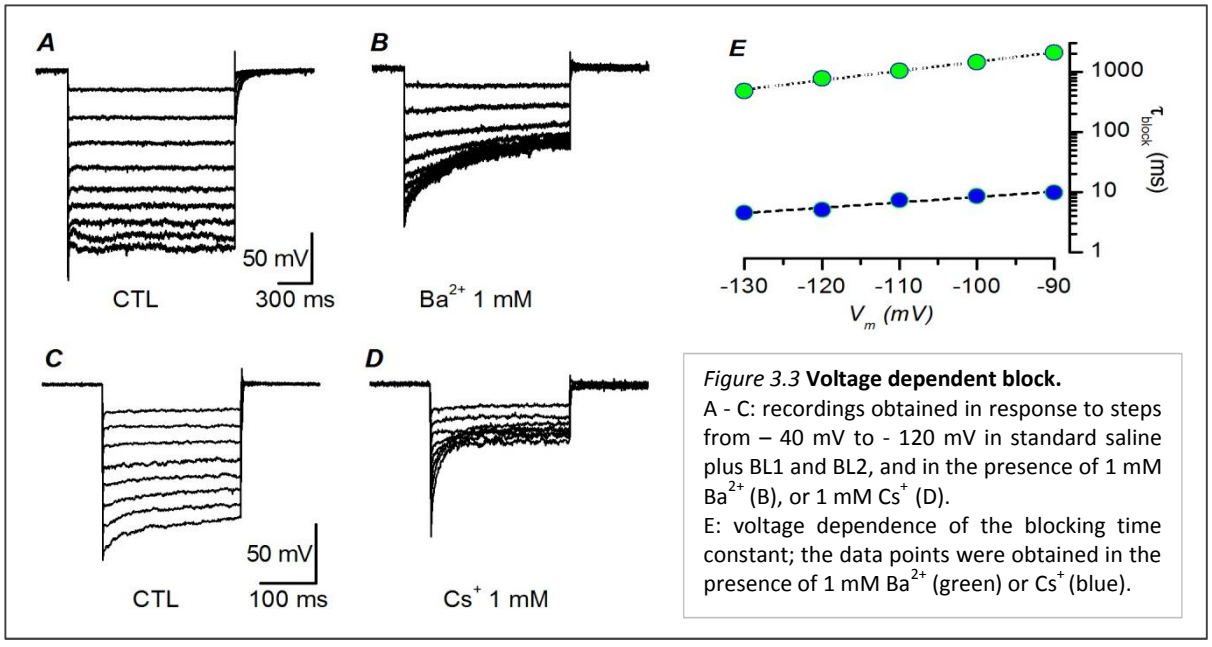

Figure 3.3 **Voltage dependent block.**
A - C: recordings obtained in response to steps from – 40 mV to - 120 mV in standard saline plus BL1 and BL2, and in the presence of 1 mM Ba^{2+} (B), or 1 mM Cs^{+} (D).
E: voltage dependence of the blocking time constant; the data points were obtained in the presence of 1 mM Ba^{2+} (green) or Cs^{+} (blue).

3.1.4 Potassium and Voltage Dependence of the I_{KIR}

Asymmetric channel pore block, which is caused by intracellular divalent cations and other molecules, is considered a hallmark of Kir current. Due to this feature Kir channels generate a large K^+ conductance at potential negative to E_K but less current flow is permitted at potential positive to E_K (Hibino et al. 2010). In figure 3.4 (A) are reported examples of ramp protocol recordings obtained in different external potassium concentration (each condition is represented by the mean of 8 ramp recordings). Currents were obtained by subtracting the *perforated-cell* currents in presence of Ba^{2+} 2mM from those in absence of Ba^{2+}, all this was made with the purpose of isolating the barium sensitive component evoked by the ramp protocol and to exclude the leak component from analysis.

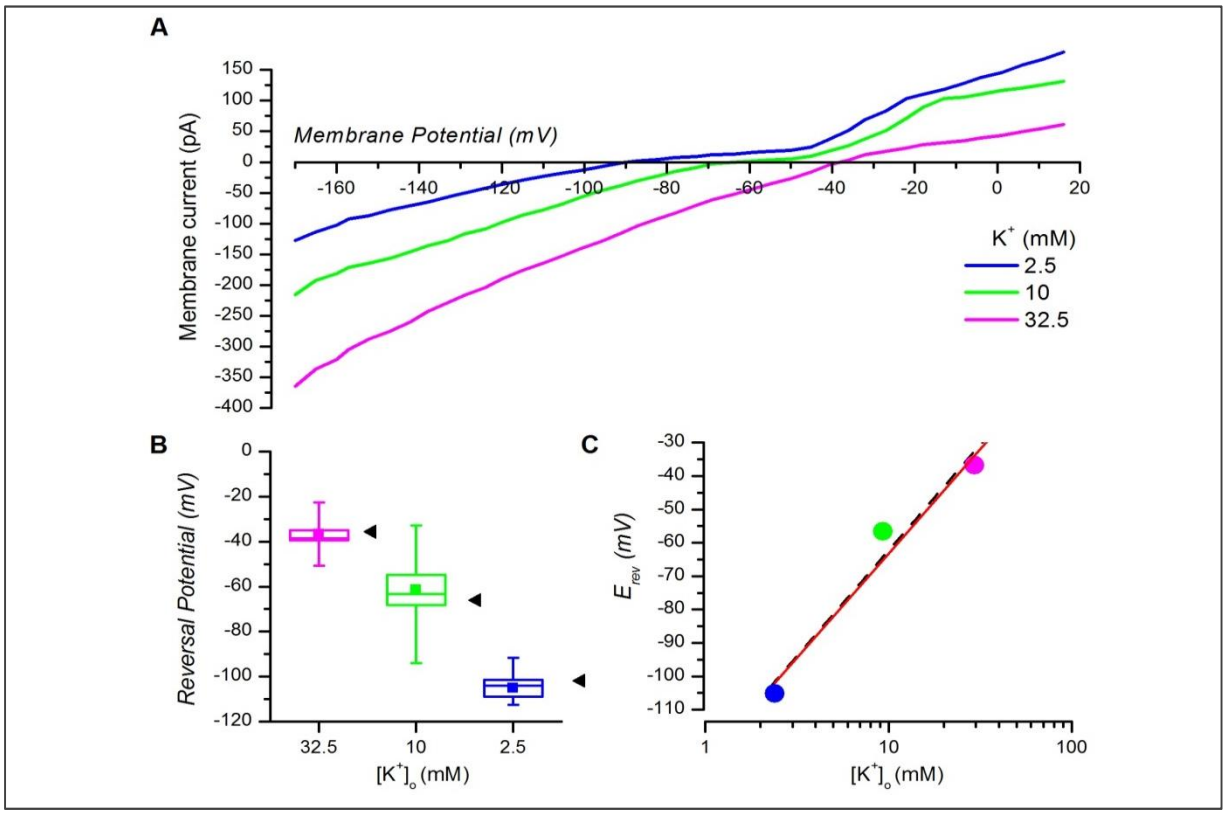

Figure 3.4 **K^+ and Voltage dependence of barium sensitive current in DA PG cells**
A) I/V curves of *perforated-cell* currents induced in a DA - PG cell by 220 mV/S voltage ramps between - 180 mV and 40 mV, starting from an holding potential of - 40 mV, at different external K^+ concentrations. Note that the inward currents increase in magnitude as well as slope conductances increase when the extracellular $[K^+]$ is raised.
B) Reversal potentials of inwardly rectifying current calculated at different extracellular potassium concentration; box-and-whisker charts identify the mean value with full color squares and the median value with lines crossing the box. Standard errors define the box range and whiskers represent the 10^{th} percentile and the 90^{th} percentile of data. Black arrow heads show expected reversal potential values which can be predicted by Nernst equation.
C) In this graph, external potassium concentration is set in a logarithmic scale on x-axis; the three full color points represent reversal potentials obtained in the three tested external potassium concentration, which are interpolated by black dashed line. Red line represents theoretical reversal potentials which are predicted by Nernst equation. Note the two lines are highly coincident.

The Kir conductance-voltage relationship shows an increase in its slope when the extracellular $[K^+]$ is increased (Hibino et al. 2010). This property is observed also in DA PG: note in figure 3.4 (A), the inward current increases in amplitude according to the extracellular potassium concentration.

The current-voltage relationship of the Kir current depends on the driving force for K^+ (as membrane potential minus equilibrium potential of K^+) (Hibino et al. 2010). In order to test K^+ selectivity of the barium sensitive current in TH-GFP+ PG cells, the reversal potentials of the inwardly rectifying current were calculated at different extracellular potassium concentrations (data are shown in figure 3.4 B).

When the $[K^+]_o$ changed from 2.5 mM to 10 mM and to 32.5 mM, the reversal potentials respectively were -105.12 ± 3.67 mV (n = 15), -56.67 ± 9.78 mV (n = 9), and -36.78 mV ± 1.89 mV (n = 27), not significantly different from the expected values predicted by the following Nernst equation:

$$E_K = -\frac{RTLn\,([K^+]_o/[K^+]_i)}{ZF}$$

where E_K is the theoretical membrane potential value expressed in volts, $[K^+]_o$ is the extracellular concentration of potassium ion, $[K^+]_i$ is the intracellular concentration of that ion, R is the ideal gas constant (joules per kelvin per mole), T is the temperature in kelvin, and F is Faraday's constant (coulombs per mole).

The plot (fig. 3.4 C) of those values against the logarithmic $[K^+]_o$ provides a linear relationship ($r^2 = 0.93$), with a slope of -61.9 mV, that is close to the theoretical level of -61.12 mV predicted by the Nernst equation used for the experimental conditions.

3.1.5 Kir Conductance

A Boltzmann function well describes the voltage dependence of the conductance: at negative membrane potentials, conductance reaches the maximal values, while the slope conductance changes are maximal around E_K, with g_{Kir} being approximately half maximal at E_K; at potentials positive to E_K conductance approaches to zero. In figure 3.5 conductance values are obtained using the equation:

$$g_{Kir} = I_{Kir} / (V_M - E_K)$$

where g_{Kir} is Kir conductance, I_{Kir} is the steady state current, V_M is the membrane potential in mV, and E_K is the Nernstian potassium equilibrium potential in mV.

In addition to exhibiting a K^+ selectivity, the voltage dependence of the Kir conductance is influenced by the potassium equilibrium potential. For this reason, the conductance (g_{Kir}) is examined at various external K^+ concentrations, from

physiological (2.5 mM) to high (32.5 mM), with an intermediate point (10 mM) as shown in figure 3.5 by different colour curves. When the external potassium concentration increases, also the maximal conductance raises, while the voltage-conductance relationship shifts to more depolarised potentials.

Fitting the experimental points with the Boltzman equation we obtained inflection points equal to -106.67 ± 1.29 mV, -74.54 ± 0.98 mV and -46.07 ± 1.81 mV, for 2.5 mM, 10 mM and 32.5 mM external potassium concentration respectively (fig. 3.5 A).

In figure 3.5 B, conductance is plotted as a function of the driving force (test potential (V_M) minus the measured E_K). Adopting this representation, for each $[K^+]_o$ the conductance curves become half maximal around zero value, reaching their minima and maxima at approximately the same voltage levels; that is to say, inflexion points of conductance curves are aligned at zero, i.e. at their own potassium equilibrium potentials, although there are differences in conductance magnitude.

In conclusion, the external potassium concentration affects both amplitude and voltage-dependence of the Kir conductance in DA PG cells. This result is similar to that found for Kir current in starfish egg cells (Hagiwara et al. 1976, Hagiwara & Jaffe 1979), frog skeletal muscle (Hestrin 1981, Leech & Stanfield 1981) and cat ventricular myocytes (Harvey & Ten Eick 1988).

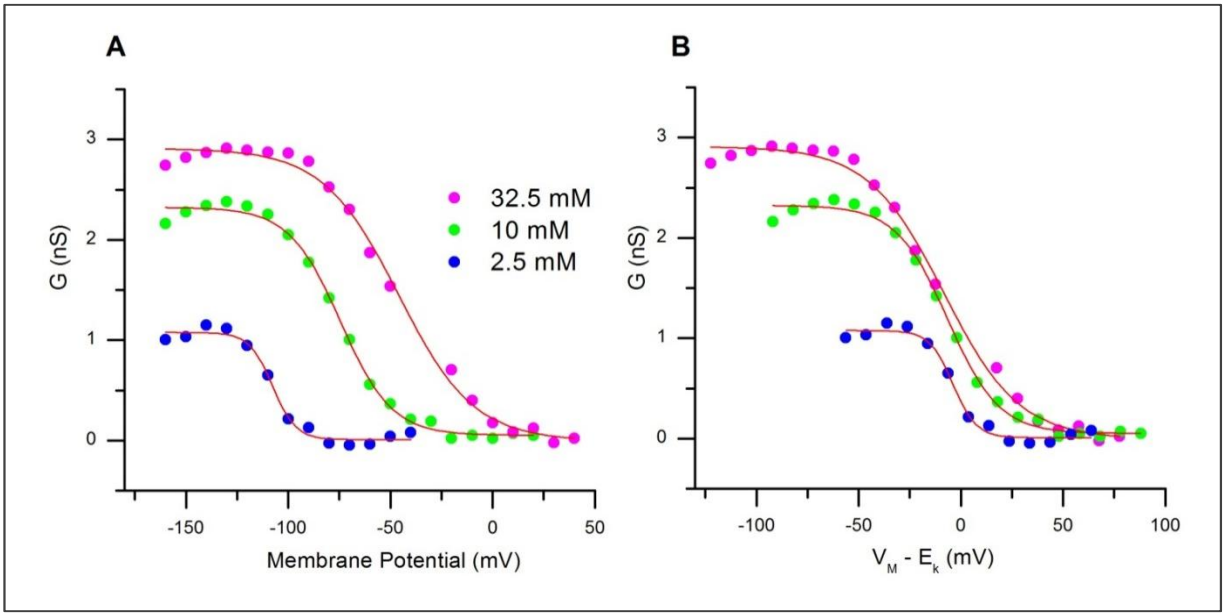

Figure 3.5 **K^+- and voltage-dependence of Kir chord conductance (g_{Kir})**
The chord conductance is calculated using the equation $g_{Kir} = I_{Kir} / (V_m - E_K)$, where I_{Kir} is the steady state current.
A: g_{Kir} plotted as a function of *voltage-clamp* tested potentials. Three are the studied conditions: 2.5, 10, and 32.5 mM $[K^+]_o$. B: Data in A are plotted again as a function of the driving force. Data points are fitted by Boltzmann curve using a least-squares method.

Since external potassium concentration influences the Kir current amplitude, modulation experiments were performed in a high (32.5 mM) external potassium concentration to obtain larger currents for a better characterization. Although this choice allows a more precise measure of the current amplitudes, it should be kept in mind that this manipulation causes a depolarizing shift of the reversal potential, as seen above.

3.1.6 Effect of I_{KIR} on Membrane Potential and Input Resistance

Barium sensitive inward current, in DA PG cells of olfactory bulb, presents properties that are coherent with a Kir current, such as potassium and voltage dependence of Kir current.

Once verified Kir current presence in TH-GFP+ periglomerular interneurons, how Kir current influences cell electrophysiological features has been studied.
It is of particular interest to understand how input resistance and resting potential could change after blocking Kir current with Ba^{2+}. Indeed, if Kir current is active at rest, modifications on Kir current conductances have great consequences on cellular electrophysiological profile.

A first verification is obtained by measuring the membrane impedance in response to hyperpolarizing current pulses in presence and absence of 0.3 and 2 mM Ba^{2+}. In these conditions, an increase in the membrane impedance and a large depolarization can be noticed in both cases.

Input Resistence

Current-clamp recordings are shown in figure 3.6: extracellular standard solution in presence of BL1 and BL2 is added of Ba^{2+} 0.3 mM (A), and Ba^{2+} 2 mM (B and D).
In these examples, hyperpolarizing current is applied in order to cause a step of at least 40 mV at regular time intervals of 10 seconds. For clarity, in A and B are shown only the control trace and the trace of maximum effect; in both cases the depolarization and also the rise in input resistance can be observed.

In figure 3.6 D, the experiment can be followed in time using all traces recorded each 10 seconds; input resistant values of D, calculated at the end of the step using Ohm law, are reported in E. This graph shows increase in input resistance caused by barium 2 mM application, starting from 120 s as indicated in figure by dot vertical line.

Membrane impedance changes significantly in Ba^{2+} 0.3 mM from 1079.65 ± 163.93 MΩ to 1260.86 ± 186.45 MΩ (n = 12, p = 0.00033, Paired Student *t* test),

and in Ba^{2+} 2 mM from 1061.55 ± 202.00 MΩ to 1621.23 ± 284.24 MΩ (n = 10, p = 0.0018, Paired Student *t* test) as shown in figure 3.6 C.

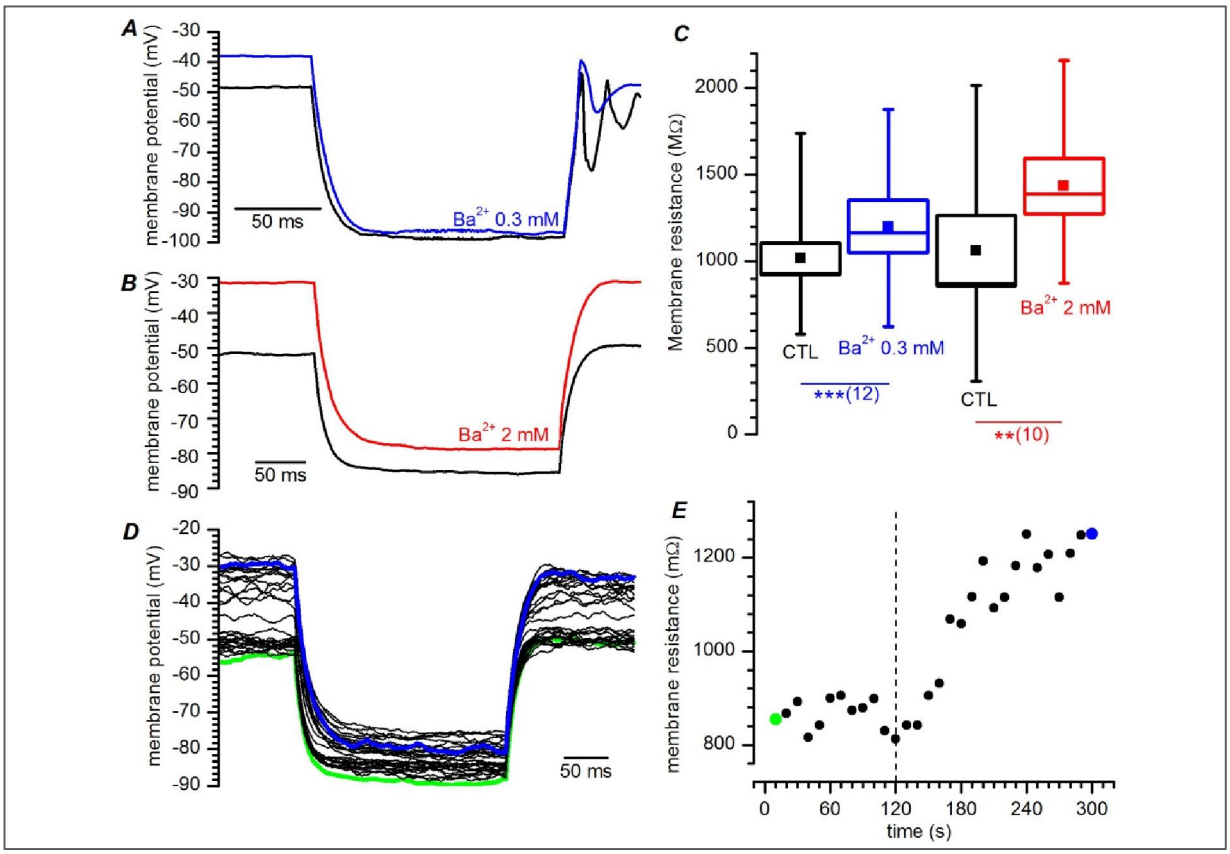

Figure 3.6 **Effect of different concentrations of Ba^{2+} on input resistance.** A, B: Sample tracings showing the response to the injection of - 40 pA in *current-clamp* conditions at different [Ba^{2+}]o. C: input resistance increase of 17.8 ± 3.2 %, n = 12, and 58.7 ± 14.2 %, n = 10 in barium 0.3, and 2 mM respect to controls. The data are summarized in a box structure. The square in the center of the box represents the mean value of the condition analyzed, the line that crosses the box indicates the median value of the data, the range of the box represents error standard and the whiskers define the 10 - 90% range of data sample. D: Family of tracings obtained in response to hyperpolarizing current pulses; green and blue traces are taken at the beginning and at the end of a 5' test. E: Time course of the variation of input resistance for the experiment shown in D. Green and blue dots mark the resistance of the traces with the same color in panel D.

Membrane potential

As seen before, Ba^{2+} induces important membrane depolarization correlating barium application with a Kir conductance closure. DA PG cells have spontaneous activity in a relatively strict range of membrane potentials: in a firing TH-GFP+ cell, 2 mM Ba^{2+} application induces a rapid and strong depolarization. In presence of depolarization, firing frequency increases before the complete disappearance of autorhythmic activity. Figure 3.7 A shows representative experiment in a cell.

Kir current is not essential to the pacemaker process, as the injection of hyperpolarizing current restores completely firing activity: fig. 3.7 A shows the injection of -40 pA at the time marked with a downward arrow.

Graphs B and D represent firing frequency and prevailing membrane potential of cell in A followed in time: the vertical dashed line indicates Ba^{2+} 2mM application, while yellow dots identify a condition similar to control obtained after injection of hyperpolarizing current.

To calculate the membrane potential in a cell characterized by autorhythmicity, we use the method illustrated in 3.7 C: frequency count histograms of the membrane potential were realized at 10 s intervals, and the distributions are fitted by an exponentially modified Gaussian function with the form:

$$f(x) = y_0 + \frac{A}{t_0}\, e^{\frac{1}{2}\left(\frac{w}{t_0}\right)^2 - \frac{x - x_c}{t_0}} \int_{-\infty}^{z} \frac{1}{\sqrt{2\pi}}\, e^{-\frac{y^2}{2}}\, dy$$

where $z = \frac{x - x_c}{w} - \frac{w}{t_0}$

and y_0 is the offset, A is the amplitude, x_c is the center of the peak (i.e. the prevailing potential, red dot in figure 3.7 C), w is the width of the peak and t_0 is the modification factor (skewness, $t_0 > 0$). Using this method, the variation of the prevailing membrane potential for two different external Ba^{2+} concentrations (0.3 and 2 mM) is measured.

In Ba^{2+} 0.3 mM the membrane potential increases from -59.06 ± 4.09 mV to -45.94 ± 3.95 mV (n = 14, p = 0.000025); and in Ba^{2+} 2 mM the mean value changes from -52.32 ± 3.73 mV to -16.18 ± 4.85 mV (n = 7 p = 0.0006 using Paired Student *t* test). Data are shown in figure 3.7 E.

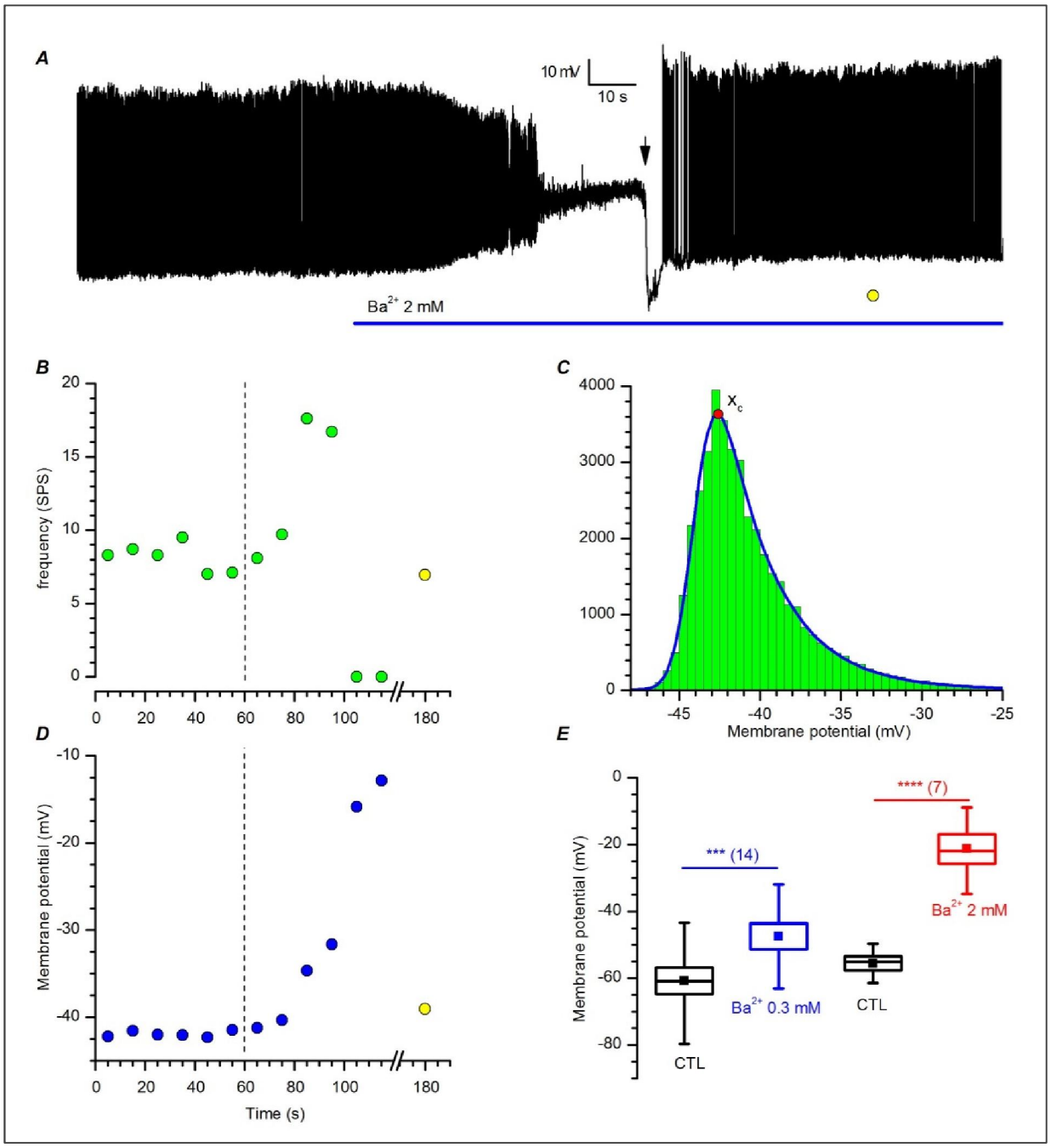

Figure 3.7 **Effect of Ba^{2+} on membrane potential.**
A: *Perforated patch* recording in standard saline (EC1 solution). The blue bar indicates the application of 2 mM Ba^{2+} into the bath; the downward arrow indicates the injection of a 40 pA hyperpolarizing current. B: Frequency analysis of action potentials (spike per second) for the experiment shown in panel A. The dashed line marks the time at which Ba^{2+} has been applied, while the yellow point (after the x-axis interruption) indicates the activity measured after the injection of a hyperpolarizing current. It corresponds to the time marked by a yellow point in panel A.
C: Illustration of the method used for the calculation of the prevailing membrane potential. The frequency count histogram of the membrane potential is built of 10 s intervals, whose distribution is fitted by an exponentially modified Gaussian function. The point marked by the red dot indicates the prevailing membrane potential (x_c).
D: Depolarization showed in panel A is followed in time using the analysis of the prevailing membrane potential.
E: Depolarization induced by two different concentrations of $[Ba^{2+}]_o$: 13. 33 ± 2.21 mV in barium 300 µM (n = 7), and 38.12 ± 6.01 mV in barium 2 mM (n = 14).

3.1.7 Effect of Temperature

Both I_{Kir} amplitude and kinetics are affected by temperature at which electrophysiological recordings are made; for this reason, temperature is one of the limiting factors in comparing results. Therefore, in this study most of the recordings reported were made at controlled temperature conditions. Figure 3.8 A shows recording traces from the same TH-GFP+ cell at 27 °C and 37 °C; in B current-voltage relationships, obtained from 8 cells, are presented for the two conditions.

Temperature influences Kir current directly: current amplitude raises 1.22 ± 0.0082 times with a 10°C temperature increase (Q_{10}, in C).

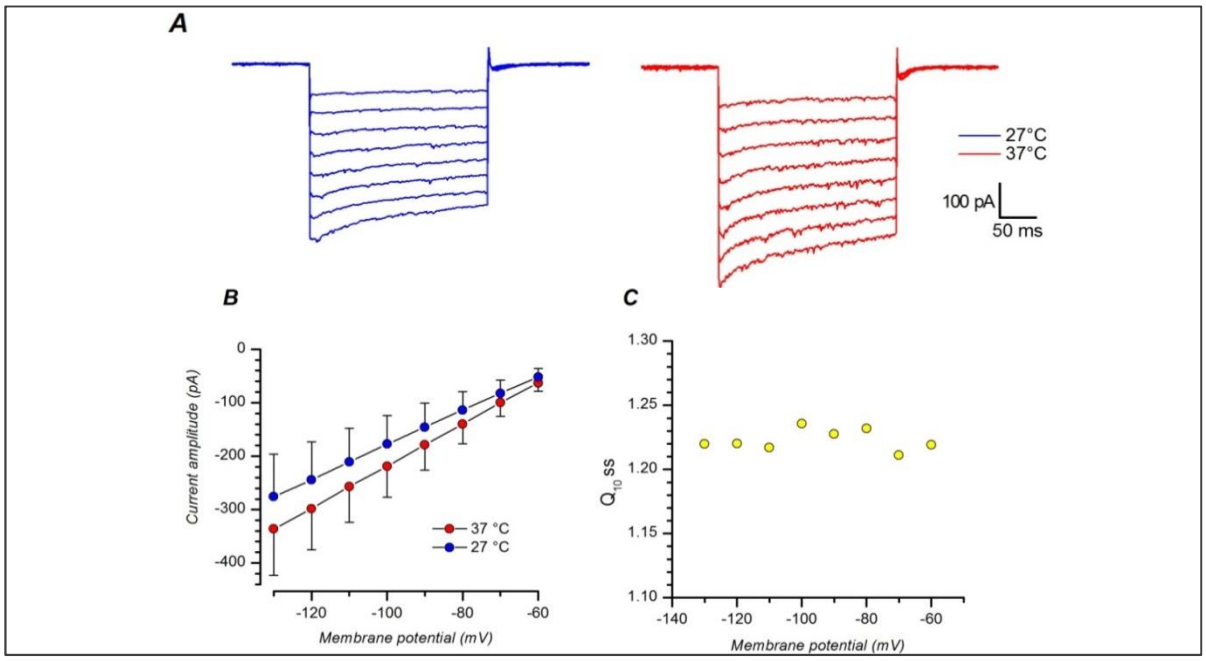

Figure 3.8 **Effect of temperature on I_{Kir}.** A: Current elicited by hyperpolarizing pulses from - 60 mV negative to - 130 mV starting from an holding potential of - 40 mV, recorded at 27 °C and 37 °C from DA periglomerular cell *in slice*. B: I-V curves of I_{Kir} measured at 27 °C and 37 °C. C: Q_{10} at the different voltages calculated at steady state current (ss). The mean value is 1.22 ± 0.0082. Data in B and C represent results obtained from 8 cells.

The Q_{10} coefficient measures the rate of change of a biological process as a consequence of increasing the temperature by 10 °C, and it is a useful way to express the temperature dependence of a physiological process. In our work, Q_{10} coefficient gives a measure of the temperature sensitivity of Kir current amplitude in DA PG neurons and it is measured using the following equation:

$$Q_{10} = \left(\frac{R_2}{R_1}\right)^{10/(T_2 - T_1)}$$

where R is the current amplitude, R_1 current at 27 °C and R_2 current at 37 °C, T is the temperature in Celsius degrees (T_1 =27 °C and T_2 =37 °C).

Our results show that the effect of temperature on current is substantially stable at different voltages.

3.2 Pharmacology

3.2.1 Blockers

The most commonly blockers of Kir channels are Ba^{2+} and Cs^{+} (Hibino et al. 2010). In literature (Hagiwara et al. 1976, Orkand et al. 1966), Tetraethylammonium (TEA) and 4-aminopyridine (4-AP) are reported to have little effects on Kir channels, although they are main inhibitors of other potassium channels, such as K_v channels.

On the bright side, Ba^{2+} and Cs^{+} block the majority of Kir channels: they suppress all Kir conductance without distinguishing between the several Kir subfamilies, for this reason they are often used to examine physiological roles of Kir channels in native cells and tissues. On the other hand, applications of Ba^{2+} and Cs^{+} suppress Kir currents in a voltage-dependent manner, to be precise they inhibit Kir channels more strongly when cell membrane is hyperpolarized. In addition, it is reported that the blocking effect of Cs^{+} and Ba^{2+} decreases substantially as $[K^{+}]_o$ increases (Hagiwara et al. 1976, Hagiwara et al. 1978). Moreover, as seen before the time required to reach the state block is different for the two blockers, in particular it is faster for Cs^{+} than Ba^{2+}.

In spite of a limited number of broad blockers of Kir channels, pharmacological and physiological assays have revealed other compounds that can affect particular types of Kir channels.

Tertiapin

Tertiapin is a toxic 21-amino acid peptide isolated from the honey bee (*Apis mellifera*). It binds specifically to different subunits of the inward rectifier potassium channel. Tertiapin acts as an inhibitor, it induces a dose-dependent block of the potassium current of two members of the inward-rectifier K^{+} channel family, namely GIRK1 (Kir 3.1), GIRK4 (Kir 3.4) and ROMK1 (Kir 1.1), although other closely related channel is insensitive to Tertiapin, such as IRK1 (Kir 2.1). The structure shows that tertiapin is a highly compact molecule with a high density of positively charged residues (Jin & Lu 1998).

Both channel families have an important role in physiological activity: GIRK 1 and GIRK 4 are subunits of the muscarinic potassium channels (K_{ACh}), they are important in the slowing down of the heart rate in response to parasympathetic stimulation via acetylcholine. An inhibition by tertiapin will result in a shorter cardiac action potential with loss of parasympathetic control, resulting in a faster

heart rate (Bhave et al. 2010). Moreover their presence is also reported in SNC, and in particular they are present in the periglomerular layer of the MOB (Karschin et al. 1996), for this reason it is of some interest to test the efficacy of the drug in our cells.

ROMK is found in the kidneys where it contributes to K^+ recycling. ROMK inhibition results in loss of potassium, as observed in Bartter syndrome caused by mutations in the ROMK channels (Asteria 1997). Due to their exclusive renal outer medullary potassium channels (Bhave et al. 2010), they are not issue of this study.

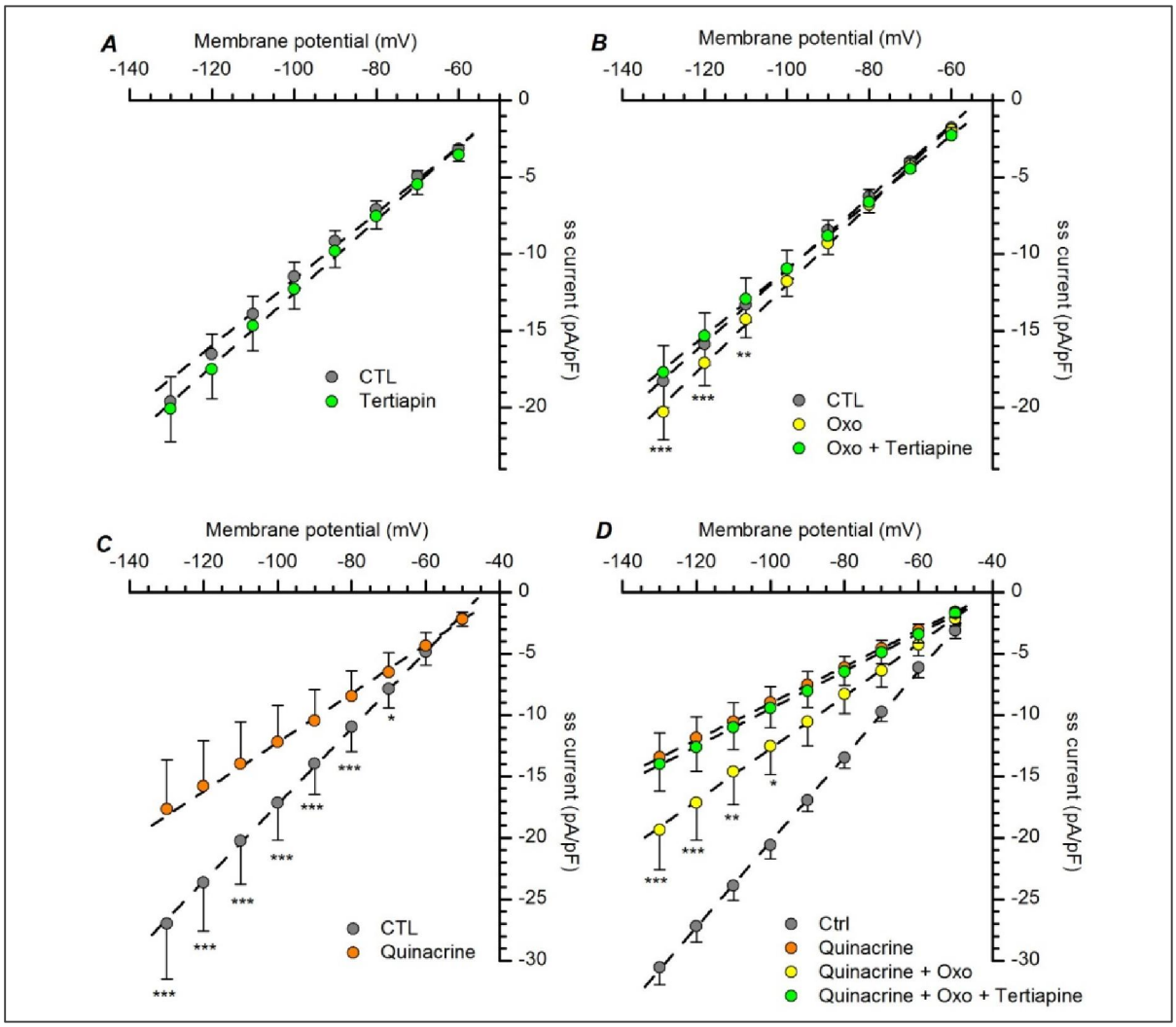

Figure 3.9 **Organic blockers of the Kir channels**.
A, B: Tertiapin-Q (1 µM) application in EC0. This GIRK channel blocker does not change the amplitude of hyperpolarization-activated (HPA) current when applied alone (A; n = 13). On the other hand, tertiapin completely suppresses the GIRK current fraction, which is activated by a cholinergic muscarinic agonist (oxotremorine 10 µM) (B; n = 11).
C: Quinacrine (100 µM), a blocker of Kir 2.x channels, suppresses a 40.2 % of HPA current at - 100 mV (n = 15).
D: With the KIR 2.x channels blocked by quinacrine, a muscarinic cholinergic agonist (oxotremorine 10 µM) can activate a GIRK current (yellow dots), and this fraction can be completely suppressed by tertiapin (green dots; n = 7).

When oxidation-resistant tertiapin-Q is added to extracellular bath in *perforated-patch* recordings of DA PG cells, no significant changes in Kir current amplitude occur. Tertiapin-Q is ineffective on TH-GFP+ cell Kir current when tested alone at concentrations ranging from 100 nM to 3 μM (fig. 3.9 A).

Voltage-clamp experiments, reported in figure 3.9, are obtained using a series of hyperpolarization pulses ranging from -60 mV to -130 mV in increments of 10 mV, and starting from an holding potential of -40 mV in EC2 external solution, at 34 °C. Statistical analysis was performed with a *two-way repeated measure ANOVA,* and *Bonferroni test* was used as *post-hoc* test.

In rest condition, GIRK channels do not allow K^+ ions movement, indeed their activation depends on the binding of the G protein βγ subunit. When G protein-coupled receptor ligands are present, dissociation of G protein occur, and GIRK channels are active (Walsh 2011). For this reason, the effect of tertiapin is tested also after activation of GIRK dependent current with oxotremorine (Oxo). This metabotropic cholinergic receptor activator is used to evoke K_{Ach} current (see also below). In presence of Oxo 10 μM, 1 μM tertiapin completely abolished the current increment promoted by the muscarinic receptor activation (fig. 3.9 B). These data suggest that functional GIRK channels are actually present in DA-PG cells.

Moreover, in order to confirm that the inhibitor effect of tertiapin concerns the GIRK current fraction, the same experiment shown in B was reproduced in presence of quinacrine (100 μM) (fig. 3.9 D). These results reinforced the idea that current amplitude increase depends on GIRK channels activation.

Quinacrine

Quinacrine inhibits Kir channels, differentially Kir 6.2 ~ Kir 2.3 > Kir 2.1 (Lopez-Izquierdo et al. 2011). Quinacrine, a cationic amphiphilic molecule, is originally developed as anti-malarial agent, but it has also effect on different ionic currents, like the I_A (Kehl 1991), the L-type Ca^{2+} current (Nagano et al. 1996), besides inward rectifier K^+ current (Evans & Surprenant 1993).

Quinacrine 100 μM suppresses a significant fraction of the hyperpolarization-activated current in DA PG cells (fig. 3.9 C, D).

As seen above, barium is a potent blocker of Kir current, in *current clamp* recordings it causes a depolarization of membrane potential until the complete disappearance of the spontaneous firing activity, which can be restored by applying a hyperpolarization current. The reappearance of the activity in the presence of a Kir blocker would suggest the absence of any role of the current in the pacemaker process, however the barium block is voltage-dependent. This result leaves open

question of whether the restore of spontaneous activity upon repolarization is due to barium block removal or not.

We looked for an answer to this question using quinacrine, a drug exerting a non voltage-dependent block of the Kir current.

Quinacrine 100 µM was applied in *current-clamp* recordings to verify its capacity to reproduce the barium effect on membrane potential, results are shown in figure 3.10. Like barium, quinacrine blocks the Kir current causing a large membrane depolarization leading also to a complete stop of firing activity. At the end of trace shown in A, the membrane was reported to a resting potential comparable to control conditions by injecting hyperpolarizing current. The activity was resumed: this result confirms that the Kir current plays an important role in maintaining membrane potential of DA PG cells, but is not an essential component of the pacemaker mechanism in these cells.

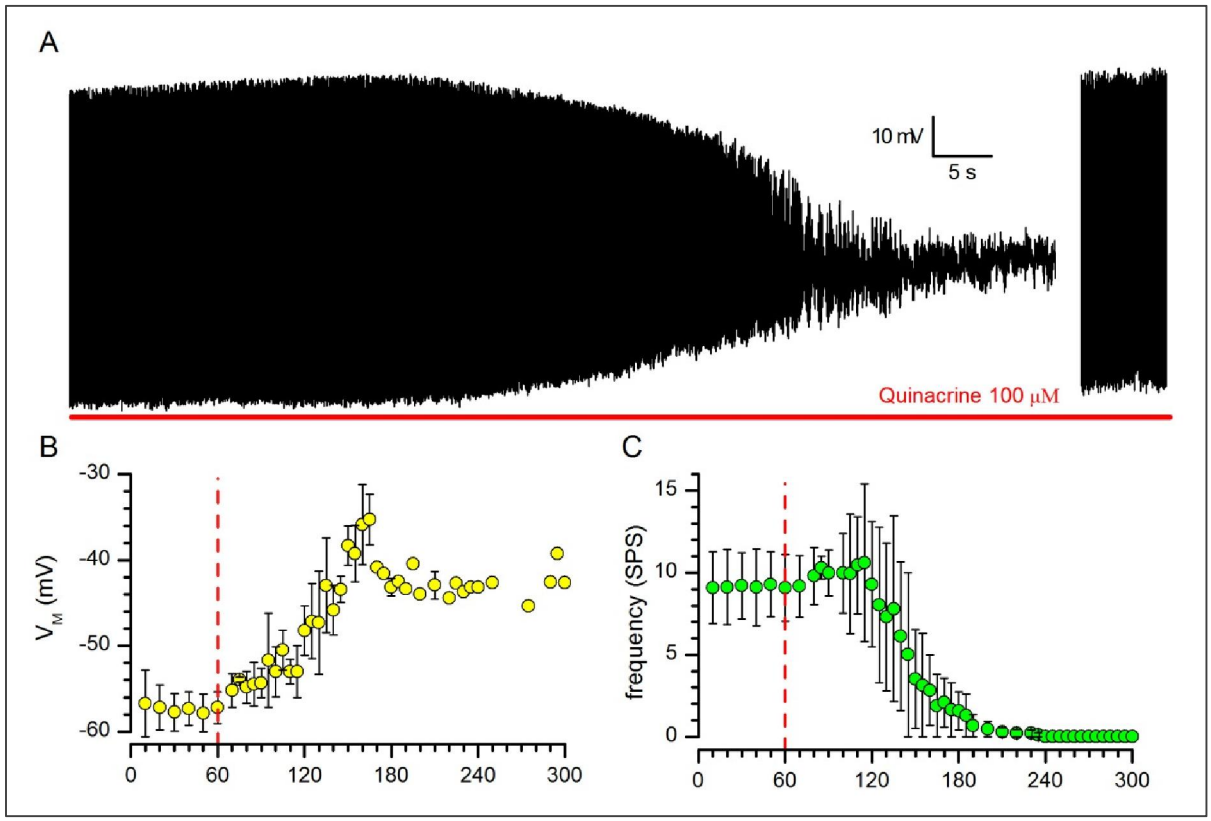

Figure 3.10 **Quinacrine effect on membrane potential.** In A, *current-clamp* recording in EC1 external solution in presence of quinacrine 100 µM. In B and C are reported changes in prevailing membrane potential and spike frequency respectively, of the cell recorded in A followed in time. Points represent mean values each 10 seconds, and bars represent standard errors. Quinacrine is applied after 60 second, as reported by red vertical dashed bars.

3.3 DA PG cell Kir current modulation

Once the presence of an inwardly rectifying K^+ current was verified in DA PG cells, both through the identification of the main electrophysiological properties of the Da PG cell barium sensitive current and using specific blockers, it was of some interest the study of current modulation. Cyclic AMP influence and the effects of different neurotransmitters or receptor agonists are studied on DA PG cell Kir current.

In the following experiments, Kir current is evoked by hyperpolarizing voltage step protocol, and it is recorded with *perforated patch-clamp* technique, in 32 mM external K^+ solution at controlled temperature conditions. The Kir current was recorded after blocking all the other conductances active at the potentials of interest by adding at the external solution blockers for the two main neurotransmitters in the OB, i.e. 1 mM kynurenic acid for glutamate and 10 μM bicuculline for GABA, and blockers for the main voltage-dependent channels, i.e. TEA 20 mM, TTX 0.6 μM, Cd2+ 100 μM and ivabradine 10 μM for potassium, sodium, calcium and h-channels, respectively.

The voltage clamp protocol provided a holding potential of -40 mV, followed by a series of hyperpolarization voltage pulses ranging from -60 mV to -130 mV in increments of 10 mV. Statistical analysis was performed with a *two way repeated measure ANOVA*, and *Bonferroni test* was used as *post-hoc* test.

3.3.1 Kir modulation by cAMP

The inward rectifier potassium current is modulated by cAMP, which can either inhibit (Xu et al. 2002, Podda et al. 2010) or enhance the current (Bolton & Butt 2006, Park et al. 2005).

A first series of experiments were performed in presence of 10 μM forskolin and 0.1 mM IBMX, in order to test amplitude variation of DA PG cell current induced by change in intracellular concentration of cAMP. Forskolin is a classical activator of adenylyl cyclase (Seamon & Daly 1981). Moreover, IBMX (3-isobutyl-1-methylxanthine) is added in the external solution in order to inhibit phosphodiesterase (Beavo et al. 1970). In this way, intracellular level of cAMP is increased and its half-life time is made longer.

High level of cAMP induces a decrease of the Kir current (fig. 3.11): the stimulation of the cAMP synthesis reduces the I_{Kir} amplitude of 12.3 ± 0.22 % in the range from -80 to -130 mV (n=12).

These data have been further enriched by reproducing the experiment using 10 µM 8Br-cAMP. 8-Bromoadenosine 3',5'-cyclic monophosphate is a brominated derivative of cyclic adenosine monophosphate, which is a useful tool to investigate cAMP dependent effect. It is long-acting because it is resistant to degradation by cyclic AMP phosphodiesterase. The effect was more marked, with a 36.9 ± 0.15 % reduction of current amplitude (n=6). In both cases, the difference between control and test was significant in the range of potentials more negative than -80 mV.

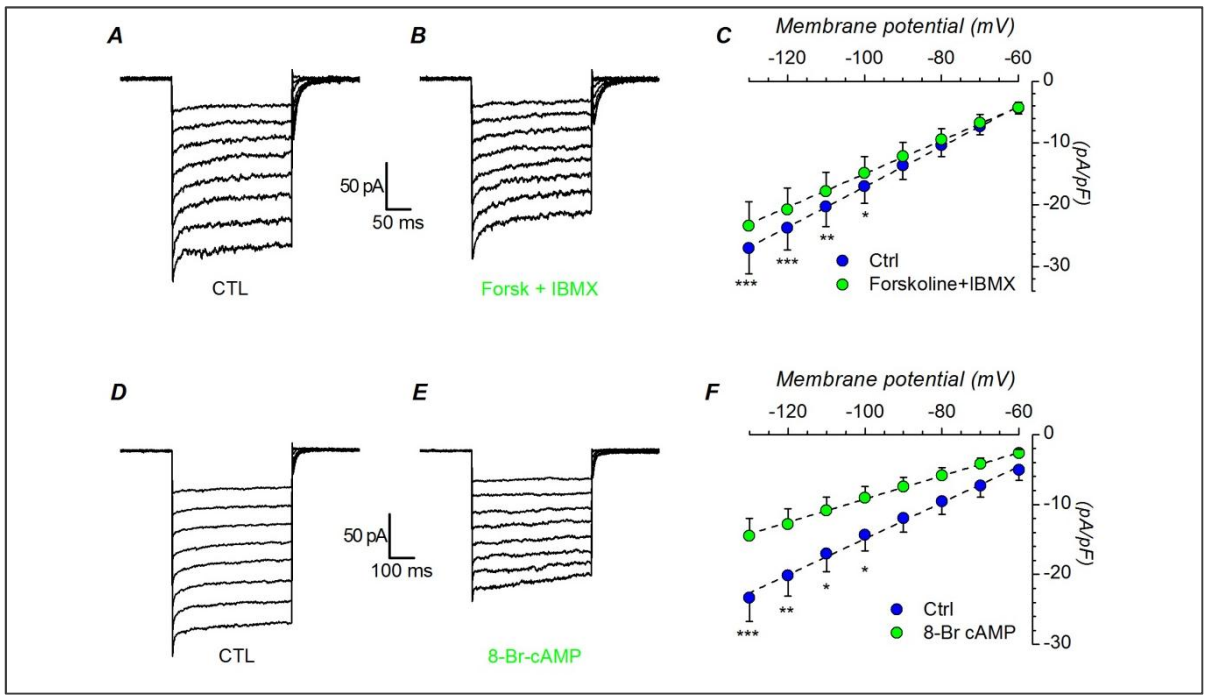

Figure 3.11 **cAMP effect on DA PG cell Kir current amplitude.** A and B: *voltage-clamp perforated-patch* recordings in control and in the presence of forskolin and IBMX from the same cell.
C: comparison of the I/V curves recorded in control (blue dots) and in the presence of 10 µM forskolin plus 100 µM IBMX (green dots); n=12.
D and E: *voltage-clamp perforated-patch* recordings in control and in the presence of 8Br-cAMP from the same cell.
F: comparison of the I/V curves recorded in control (blue dots) and in the presence of 10 µM 8Br-cAMP (green dots); n=6. All recordings were realized in EC2 with the addition of BL1 and BL2, at 34 °C.

3.3.2 Kir modulation by Neurotransmitters

Dopaminergic cells in the olfactory bulb are the target of numerous afferents releasing a variety of neurotransmitters, many of which are known to affect the cAMP pathway, and therefore potentially capable of a modulation of the Kir current.

Among the others, there are serotoninergic afferents from the ventral and dorsal raphe nuclei (Araneda et al. 1980, Araneda et al. 1980, Halász et al. 1977), noradrenergic input from the locus cœruleus (Halász & Shepherd 1983, Macrides et al. 1981, McLean et al. 1989), cholinergic inputs from the nucleus of the horizontal limb of the diagonal band (Carson 1984, Carson 1984, Zaborszky et al. 1986,

Carson 1984, Matsutani & Yamamoto 2008) , and histaminergic inputs from hypothalamus (Panula et al. 1989).

Furthermore, bulbar dopaminergic cells have been shown to express D2 receptors (Gutierrez-Mecinas et al. 2005), which could be activated by the dopamine released by the cell itself (Maher & Westbrook 2008).

We tested the effects on the Kir current amplitude of 5-10 min applications of 5-HT (50 µM), dopamine (100 µM, + 1 mM ascorbic acid), quinpirole (D2 agonist, 30 µM), noradrenaline (100 µM, + 1 mM ascorbic acid), phenylephrine (α1 agonist, 10 µM), clonidine (α2 agonist, 10 µM), histamine (10 µM), oxotremorine (muscarinic agonist, 10 µM), GABA (100 µM), muscimol (GABAA 50 µM) and baclofen (GABAB agonist, 30 µM), with protocol and in the conditions explained above. Results are shown in figure 3.12.

	Delta (pA/pF)	*S.E.*	*p-value*	*% variation (pA/pF)*	*S.E.*	*N*
5HT	3.40	1.09	P < 0.01	- 15.83	3.51	18.00
Histamine	4.89	1.71	P < 0.05	- 24.22	6.90	8.00
DA	- 2.96	0.66	P < 0.01	22.08	7.46	5.00
DA (Ago D1)	0.15	0.46	P > 0.05	0.64	4.89	9.00
DA (Ago D2)	- 2.82	1.00	P < 0.05	19.32	7.51	9.00
NA	4.30	0.81	P < 0.001	- 23.72	3.77	10.00
Phenylephrine	3.11	2.62	P < 0.05	- 22.71	16.83	8.00
Clonidine	1.03	1.07	P > 0.05	- 7.79	10.91	4.00
Oxotremorine	- 1.55	0.48	P < 0.01	17.80	5.95	13.00
Baclofen	0.99	1.40	P > 0.05	- 3.85	3.87	11.00

Table 2 **NT and agonist effects on DA PG cell Kir current.** Data resume the analysis performed at – 100 mV.
Delta defines changing in current amplitude caused by administration of NT and agonists in the extracellular solution. Percent variation estimates effects on Kir current caused by the different compounds.

Noradrenaline

Noradranaline (NA) is a catecholamine and it can acts both as hormone and neurotransmitter.

Both α and β NA receptors are present in the olfactory bulb (Woo and Leon 1995, Shipley and Ennis 1996). It is reported that NA-containing fibers arise from locus coeruleus and terminate on granule cells in the internal plexiform layer (Macrides et al. 1981, Halász 1990). Moreover, it is note that α1 activated NA receptors inhibit rectifying and non-rectifying leak potassium currents (Nai et al. 2010, Pan et al. 1994).

In a first series of experiments (n=10), NA (100 µM) has been tested on DA-PG cells in slice at 31 °C. NA leads to a 24.6 % reduction of the Kir amplitude: the current evoked at -100 mV dropped from -17.51 ± 1.62 pA/pF in control conditions to -13.20 ± 1.23 pA/pF with NA. Data are shown in figure 3.12 A.

A further characterization of the NA induced effect consisted in the identification the subtype of α-receptor involved. Clonidine 10 μM, an α2 agonist, was added to the external solution without causing significant effect: the current amplitude evoked at-100 mV was equal to -15.14 ± 1.40 pA/pF in control conditions and -14.11 ± 1.65 pA/pF in presence of clonidine (n = 4). On the other hand, phenylephrine 10 μM, a α1 agonist, induced a 24.1 % inhibition: at -100 mV, the evoked current amplitude changes from -12.88 ± 1.27 pA/pF in control conditions to -9.77 ± 0.92 pA/pF in presence of phenylephrine (n = 8); it should be observed that the phenylephrine dependent inhibition was quantitatively almost identical to that of NA. Data are shown in figure 3.12 (B and C).

This kind of voltage-clamp experiments were conducted in high external potassium concentration (EC3), and in presence of BL1 and BL2 to isolate Kir current. In order to confirm these data and prove a physiological relevance of the effect induced by NA, experiments were performed in current clamp configuration. In particular, it is of some interest to confirm that NA dependent reduction of Kir current causes some change in resting potential.

7 cells were recorded in current-clamp configuration and in standard extracellular solution (EC0) in presence of only BL1, before and during phenylephrine application. Phenylephrine 10 μM induced a depolarization of 8.13 ± 3.0 mV; this result confirms the expected depolarization following a reduction of a current which is hyperpolarizing.

Dopamine

Dopamine (DA) is an excitatory aminoacid released by centrifugal fibers termini. Dopaminergic neurons present autoreceptors, for this reason the effect of dopamine is tested in DA PG cells, in order to verify DA effect on Kir current.

Dopamine (100 μM) induced an increase of the Kir current: in slice, at 34 °C a -100 mV stimulus current amplitude changed from -16.96 ± 2.95 pA/pF (ctrl) to -19.92 ± 2.33 pA/pF. This change is significant at 0.001 level (figure 3.12 D).

The effect is mimicked by the D2 agonist quinpirole 30 μM (figure 3.12 E), which promotes an increase in current amplitude from -15.47 ± 0.85 pA/pF (ctrl) to -18.29 ± 1.20 pA/pF. This change is also significant at 0.001 level (*Bonferroni post-hoc test,* n = 9); on the contrary, the D1 agonist SKF 38393 (Sibley & Monsma, Jr. 1992) remains ineffective (15 μM, n= 4, fig. 3.12 F).

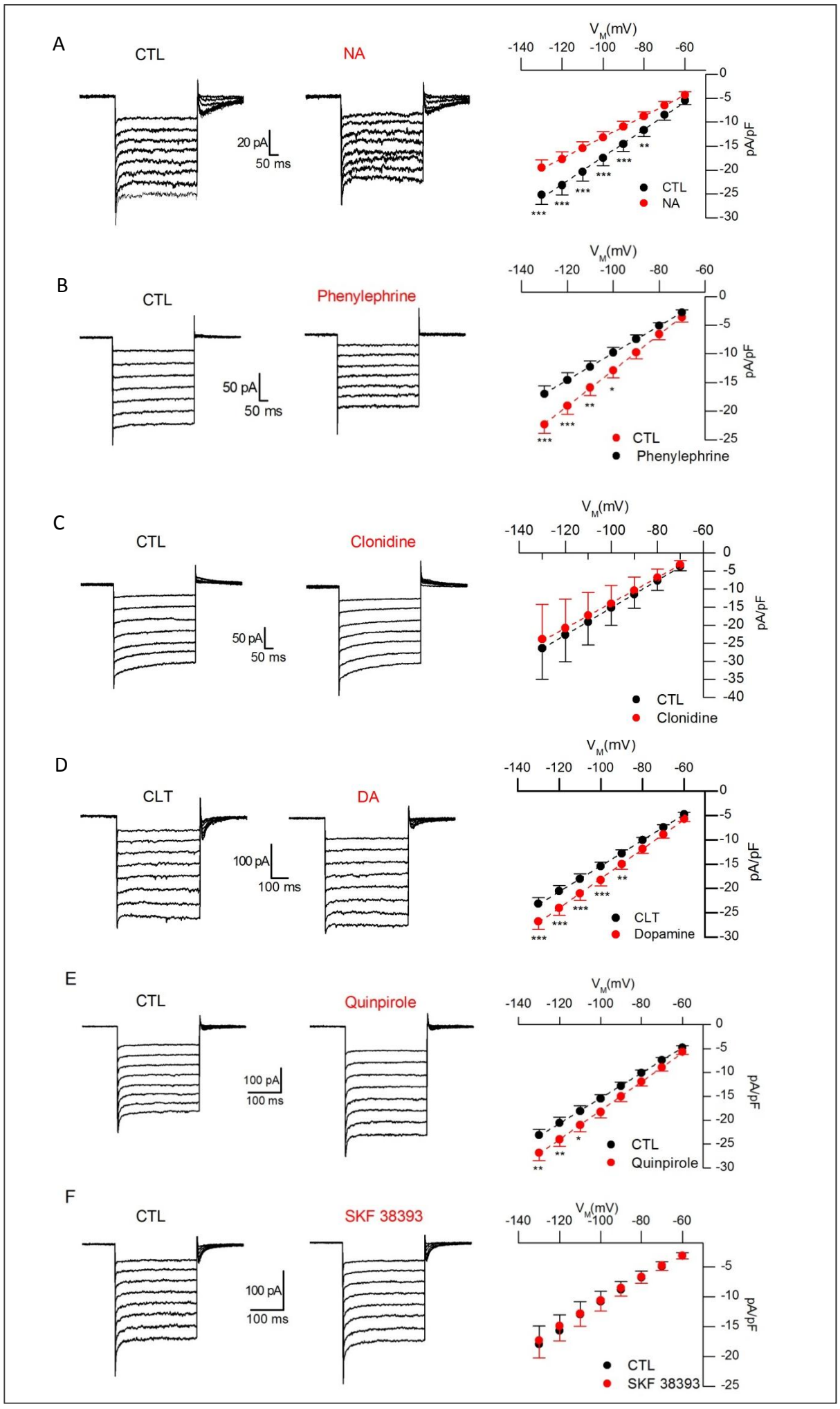
A
CTL
NA
20 pA
50 ms
V_M(mV)
-140 -120 -100 -80 -60
0 -5 -10 -15 -20 -25 -30
pA/pF
CTL
NA
B
CTL
Phenylephrine
50 pA
50 ms
V_M(mV)
-140 -120 -100 -80 -60
0 -5 -10 -15 -20 -25
pA/pF
CTL
Phenylephrine
C
CTL
Clonidine
50 pA
50 ms
V_M(mV)
-140 -120 -100 -80 -60
0 -5 -10 -15 -20 -25 -30 -35 -40
pA/pF
CTL
Clonidine
D
CLT
DA
100 pA
100 ms
V_M(mV)
-140 -120 -100 -80 -60
0 -5 -10 -15 -20 -25 -30
pA/pF
CLT
Dopamine
E
CTL
Quinpirole
100 pA
100 ms
V_M(mV)
-140 -120 -100 -80 -60
0 -5 -10 -15 -20 -25 -30
pA/pF
CTL
Quinpirole
F
CTL
SKF 38393
100 pA
100 ms
V_M(mV)
-140 -120 -100 -80 -60
-5 -10 -15 -20 -25
pA/pF
CTL
SKF 38393

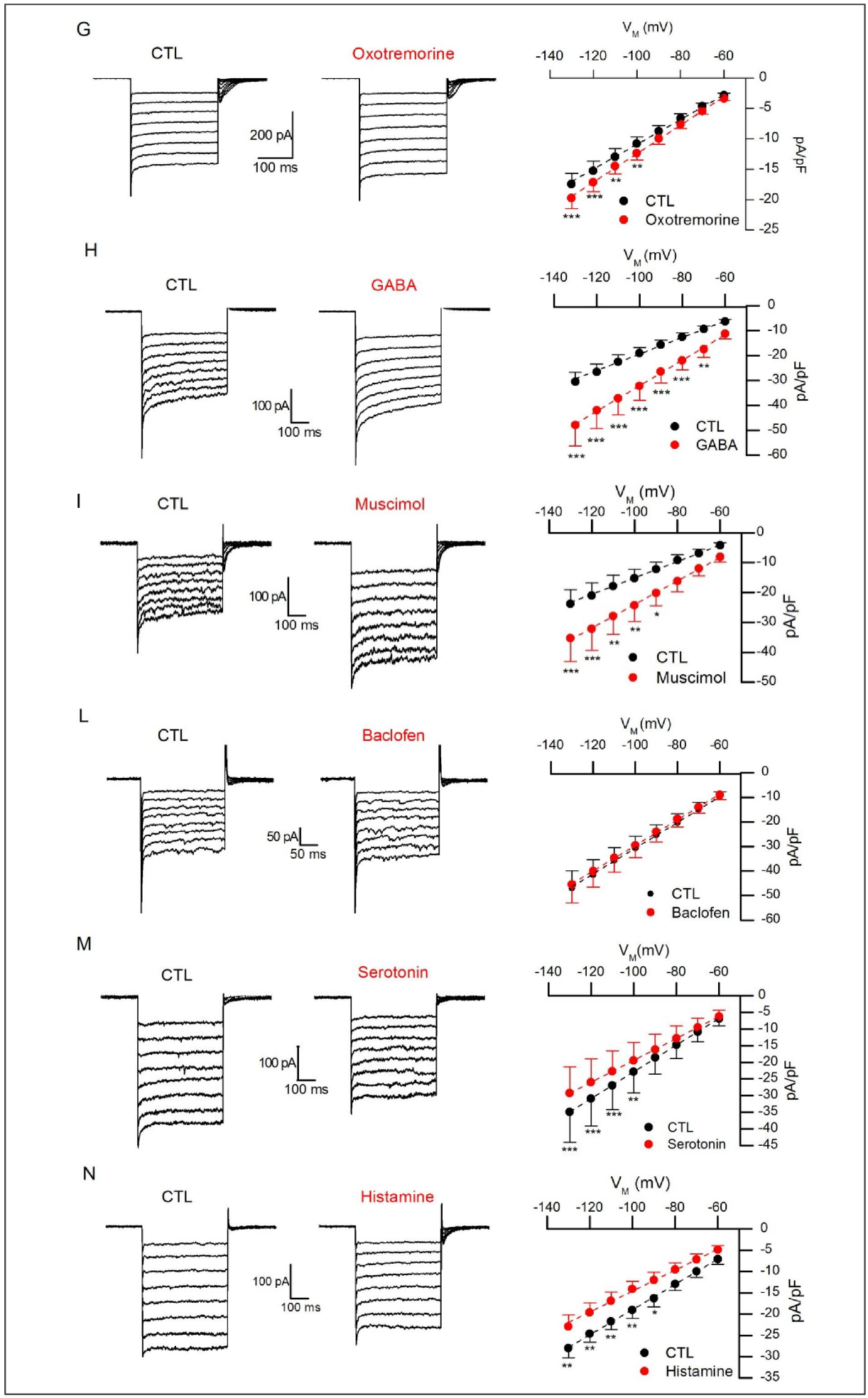

Figure 3.12 **NT effects on DA PG cell Kir current amplitude.** On the left, *voltage-clamp perforated-patch* recordings in control and in the presence of different NT or agonists (red), as specified in figure. On the right, comparison of the I/V curves recorded in control (black dots) and in the presence of the different compounds tested (red dots).

Acetylcholine

Acetylcholine (ACh) is an ester of acetic acid and choline, which acts as neurotransmitter both on peripheral nervous system (PNS) and central nervous system (CNS).

Extensive cholinergic fibers, from the horizontal limb of the diagonal band of Broca, project to all bulbar layers with the heaviest density occurring in the granular layer and external plexiform layer (Macrides et al. 1981, Zaborszky et al. 1986, El-Etri et al. 1999, Matsutani & Yamamoto 2008), while the existence of cholinergic interneurons in the OB has been controversial.

Only recent studies provide clear evidence of the presence of a significant number of intrinsic cholinergic interneurons in the mouse OB: these experiments imply olfactory peduncle lesion in order to reduce cholinergic centrifugal projection to the OB, and to unmask intrinsic elements (Krosnowski et al. 2012). These results suggest that olfactory information processing is modulated by dual cholinergic systems of local interneuron networks and centrifugal projections (Krosnowski et al. 2012).

Both muscarinic and nicotinic ACh receptors are expressed in the olfactory bulb (Shipley & Ennis 1996), but in DA PG cells it is reported that the activation of M2 metabotropic cholinergic receptors induce a hyperpolarization mediated by a K^+ conductance (Pignatelli & Belluzzi 2008). Due to this previous evidence, the effect of the M2 agonist (oxotremorine, 10 µM) is only tested on the Kir current. The experiments shown in figure 3.12 G, confirm the involvement of ACh M2 receptor in change of DA PG cell Kir current amplitude.

Oxotremorine (10 µM) is added to the external solution EC3 in presence of BL1 and BL2 to isolate Kir current. In *voltage clamp* recordings at -100 mV stimulus, oxotremorine increases current amplitude from -10.83 ± 1.15 pA/pF (control) to -12.38 ± 1.14 pA/pF (n=11); change is significant with a $p < 0.001$ (*Bonferroni post-hoc test*).

In order to confirm that change in Kir current amplitude is dependent on ACh M2 receptor activation, *current clamp* recordings were made. In EC0 solution with BL1, oxotremorine (10 µM) induced a change in prevailing membrane potential equal to a 4.52 ± 0.8 mV hyperpolarization ($n = 9$; $p < 0.001$ pair student *t* test).

GABA

In the olfactory bulb, GABA (γ-aminobutiric acid) is a neurotransmitter released by centrifugal axons (Zaborszky et al. 1986), and by the majority of interneurons (Kosaka & Kosaka 2008). GABA is an important neurotransmitter in the OB, moreover GABAergic terminals impinge on DA-PG cells.

Like other compounds tested, GABA 100 μM was added to the external solution (EC3) in presence of BL1 and BL2: GABA induces a large increase in Kir current amplitude, which changed from -19.16 ± 2.35 pA/pF to -32.35 ± 5.70 pA/pF, at -100 mV input (figure 3.12 H) a difference statistically significant at the 0.01 level (*Bonferroni post-hoc test,* n = 13).

There are two kind of GABA receptors: ligand-activated chloride channels ($GABA_A$ - $GABA_C$) where the receptor and the ion channel are parts of the same complex, and, $GABA_B$ which are G protein-coupled metabotropic receptors. Due to the great change in Kir current amplitude following GABA application, it was of some interest to identify the receptor involved.

Kir 3 channel family (GIRK) has been shown to be functionally regulated by $GABA_B$ receptors in numerous systems (Sodickson & Bean 1996, Tabata et al. 2005), including dopaminergic neurons (Lacey et al. 1988).

Following $GABA_B$ agonist baclofen (Bowery et al. 1980) 10 μM addition to the external solution we failed to observe any change in the current amplitude (from -30.53 ± 4.68 pA/pF to -29.54 ± 5.03 pA/pF, n = 11; p > 0.5, figure 3.12 L). On the contrary, the GABA effect could be mimicked by the $GABA_A$ agonist muscimol 50 μM (Johnston et al. 1968): at -100 mV, the Kir current changed from -15.26 ± 3.01 pA/pF to -24.33 ± 5.31 pA/pF (figure 3.12 I), a change statistically significant (p < 0.05*, Bonferroni post-hoc test,* n = 7*).*

These data suggest that, contrary to the other neurotransmitters studied, there is not a metabotropic receptor mediated modulation of GABA on the Kir current. Moreover, the observed increase of the current more likely depends on $GABA_A$ channel opening, an effect which should be further studied using chloride channels blockers.

Serotonin

Serotonin or 5-hydroxytryptamine (5-HT) is a monoamine neurotransmitter, which reachs the olfactory bulb only by the projection from the raphe nuclei (Araneda et al. 1980, McLean & Shipley 1987). 5-HT receptors are present both in bulbar interneurons, periglomerular and granular cells (Morilak et al. 1993), and in principal cells such as mitral and tufted cells (Pompeiano et al. 1994, McLean et al. 1995).

Serotonin (50 µM) induces a significant decrease of the K_{ir} current amplitude: at -100 mV the inward current is reduced from -22.83 ± 6.32 pA/pF (CTL) to -19.43 ± 5.37 pA/pF (5-HT; n=18, $p<0.01$ *Bonferroni post-hoc test*). Data are shown in figure 3.12 M. In order to confirm this result, and to emphasize the physiological role of DA PG cell Kir current *current clamp* experiments are recorded. In the same cell prevailing membrane potential is calculate before and in presence of 5-HT 50 µM: serotonin, which reduces Kir current amplitude, causes a depolarization of 12.8 ± 3.2 mV (n=8, $p < 0.001$ Paired Student *t* test).

Histamine

Histamine is an organic nitrogen compound involved in local immune responses, as well as playing an important role as neurotransmitter .

Olfactory bulb receives histaminergic inputs primarily from the caudal tuberal and postmammillary magnocellular hypothalamus (Auvinen & Panula 1988, Panula et al. 1989). Due to the presence of this innervation, it was of some interest to investigate the presence of a Kir current modulation depending on histamine.

In *voltage-clamp* conditions, histamine (10 µM) induces a significant reduction of the Kir current amplitude, which at -100 mV decreases from -19.03 ± 2.01 pA/pF (CTL) to -14.13 ± 1.84 pA/pF. The presented mean values come from 8 recorded cells, and the difference is statistically significant with a $p < 0.01$, using *Bonferroni post-test*. Data are showed in figure 3.12 N.

In *current-clamp* recordings, prevailing membrane potential changes from -69.11 ± 2.47 mV in control, to -58.22 ± 7.52 mV in presence of histamine 10 µM. This effect is coherent with the expected depolarization following a Kir conductance closure.

3 DISCUSSION

The olfactory system recognizes a great number of odor substances and discriminates chemical signals with fine differences in structural properties, which come from outdoor environment and can profoundly influence animal behavior, for this reason the olfactory system provides essential information for animal survival (Lledo et al. 2005).

The olfactory bulb is an excellent model for understanding the neural mechanisms of sensory information processing, moreover it constitutes a site in which interneurons are added in postnatal and adult life. OB is the first relay station for the transmission of olfactory information, indeed, it receives and processes the information coming from the olfactory sensory neurons in the nasal mucosa, and it sends this information to different parts of the primary olfactory cortex in the forebrain (Lledo et al. 2005).

In the olfactory bulb principal output neurons, such as mitral cells and tufted cells ensure a vertical flux of information. It arrives from the outdoor environment and is processed and refined within the olfactory bulb, before the transmission to upstream cortex centers (Lledo et al. 2005).

Firing activity of output neurons is controlled both by sensory excitatory inputs and intra-bulbar circuit stimuli. Two distinct connections are implied in the intra-bulbar circuit stimuli: the first occurs between primary dendrites and periglomerular cells (PG), the second between secondary dendrites and granule cells (Gr) (Shipley & Ennis 1996). Granule cells and periglomerular cells are interneurons which extend their projections within the olfactory bulb.

PG cells constitute a high chemically heterogeneous cell population as T. Kosaka and K. Kosaka morphological and immunocytochemical studies reveal (Kosaka & Kosaka 2007). To recognize dopaminergic interneurons within the olfactory bulb in living preparations, transgenic mice have been used. The transgenic mouse strain harbours an eGFP (enhanced green fluorescent protein) reporter construct under the promoter of tyrosine hydroxylase, which is the rate-limiting enzyme for cathecolamine synthesis (Sawamoto et al. 2001, Matsushita et al. 2002).

Electrophysiological and functional properties of TH-GFP+ PG cells in mouse olfactory bulb are mainly described in a Pignatelli's work (Pignatelli et al. 2005): five voltage-dependent currents have been identified and kinetically characterized in order to understand the mechanism of spontaneous firing, which is considered a hallmark of these cells. Recently, two hyperpolarization-activated currents have been found in TH-GFP+ neurons: the first is the *h* current (also named I*f* in cardiac tissue), a mixed cation current with a reversal potential substantially positive to E_K,

insensitive to Ba^{2+}, and blocked by highly selective drugs such as ivabradine and ZD7288 (Pignatelli et al. 2013).

The second hyperpolarization-activated current has fast kinetics, it is permeable primarily to K^+, is blocked by extracellular Ba^{2+} and Cs^+, has a voltage-dependence influenced by extracellular K^+ concentration, and has been identified as a classical potassium inward rectifier current (Kir): this current is the subject of my work.

For the first time Kir current is identified and characterized in dopaminergic periglomerular interneurons of the mouse olfactory bulb. The investigation of Kir current electrophysiological properties, provided with my studies, has been further enriched with the analysis of the effects on Kir current of several neuromodulators.

The purpose of this research is to complete the electrophysiological characterization of DA PG cells in order to have a better understanding of their properties and to shed light on their physiological role, which still remain unknown.

Although Kir current does not directly participate at the spontaneous firing, it has a key role in maintaining membrane potential in the proper range of values where spikes can occur. Moreover, this study points out that several neurotransmitters can regulate Kir current amplitude: an increment or decrease of potassium inward current has important consequences on cell membrane potential, and in turn on cell firing frequency. In this way, Kir current provides additional flexibility of DA-PG cell signaling.
For this reason Kir current is important in these cells.

4.1 Barium Sensitive Current in DA-PG Cells

Kir current effect on membrane potential and input resistance

Kir current first evidence in DA-PG cells is due to barium effect on membrane potential: barium, a potent blocker of Kir current, in *current clamp* recordings causes a depolarization of membrane potential until a complete disappearance of the spontaneous firing activity. The large depolarization caused by barium application suggested the presence of a barium sensitive current. The application of barium at the external bath solution causes a membrane potential depolarization of 13. 33 ± 2.21 mV in 300 μM $[Ba^{2+}]_o$ in 7 cells tested, and of 38.12 ± 6.01 mV in 2 mM $[Ba^{2+}]_o$ in 14 cells.
The depolarization observed could be caused by the opening of a depolarizing conductance or by the closure of an hyperpolarizing conductance, active at rest.

In order to discriminate between these two possibilities, analysis on input resistance was performed. Variations of DA-PG cell input resistance, in response to

hyperpolarizing current pulses, were tested in *current clamp* recordings in presence of the two barium concentrations seen before. In both cases membrane impedance increases: from 1079.6 ± 163.9 to 1260. ± 186.5 MΩ and from 1061.6 ± 202.0 MΩ to 1621.2 ± 284.2 MΩ in 0.3 mM and 2mM $[Ba^{2+}]_o$ respectively.

Membrane impedance increase agrees with a closure of hyperpolarizing conductance.

Identification and basic properties of Kir current

Inward rectification was originally termed *anomalous* rectification because it is opposite to the normal outward rectification that is seen in delayed rectifier K^+ channels (Nichols & Lopatin 1997). In general, inward rectification refers to the ability of an ion channel to allow greater influx than efflux of ions. Inward rectifier potassium channels allow small amounts of outward current at membrane potential (V_M) positive to the potassium equilibrium potential (E_K) compared to currents generated at stimuli negative to the potassium equilibrium potential (Hibino et al. 2010).

Although K^+ ions could pass selectively in both direction in Kir channels, cytoplasm Mg^{2+} and polyamines with pore channel interactions block K^+ efflux at membrane potentials, which are more positive than the E_K (Bichet et al. 2003).

Four identical (homotetrameric) or homologous (heterotetrameric) Kir subunits are organized in a tetrameric structure in the membrane in order to surround a water-fill pore, through which K^+ ions can move following their electrochemical gradient. Each subunit includes two transmembrane helices, a pore forming region and a cytoplasmic domain formed by the amino (N) and carboxy (C) terminals (Bichet et al. 2003).

The transmembrane domain is formed by two transmembrane helices M1 and M2 separated by an extracellular loop that form a K^+ selectivity filter (van der Heyden et al. 2013). The intracellular domain is organized in order to give the "*cytoplasmic pore"*, which is 30 Å long and 7-15 Å in diameter (Bichet et al. 2003).

Hyperpolarizing steps evoke a measurable current in experiments carried out using *perforated-patch* recordings, in slice at 34 °C. The *voltage clamp* protocol provides a holding potential of -40 mV followed by a series of hyperpolarization voltage pulses, ranging from -60 mV to -130 mV in increments of 10 mV.

The current evoked has different components: the *h*-current, the Kir current and the leakage current. After the suppression of the *h*-current in presence of ivabradine 10 μM, the remaining current was identified as potassium inward rectifier (Kir) current, thanks to its time course, reversal potential and sensitivity to Ba^{2+} (Hibino et al. 2010).

Due to asymmetric channel pore block, Kir channels generate a large K^+ conductance at potentials negative to E_K, but a less current flow is permitted at potential positive to E_K (Hibino et al. 2010). With the purpose of turning out this feature in DA PG cells, current-to-voltage relationship was also investigated by eliciting Kir current whit a 220 mV/s voltage ramp protocol, from -180 mV to 40 mV. In this way, I/V relation was obtained for a great range of potentials without stressing the cells. Moreover, the voltage ramp protocol has made possible the study of DA PG cell barium sensitive current in different potassium external concentration, to analyze potassium and voltage dependence of this current.

Current recordings from DA PG cells showed strong rectification at all external potassium concentrations examined (physiological 2.5 mM, high 32.5 mM, and intermediate 10 mM); In addition, for the three different tested conditions, the obtained reversal potentials agree whit values predicted for a pure K^+ current by Nernst equation. Indeed, plotting those reversal potential values against the logarithmic $[K^+]_o$ provided a linear relationship ($r^2 = 0.93$) with a slope of -61.9 mV, close to the theoretical level of -61.12 mV predicted by the Nernst equation in the experimental conditions used.

These results reinforce the idea that Kir current is present in DA-PG cells: Kir channels are selective for K^+ ions, consequently the reversal potentials in different extracellular K^+ concentrations should always follow the Nernstian equilibrium potential for potassium.

What is more, in DA PG cells the inward current increases in amplitude according to the extracellular potassium concentration: this result agrees with a Kir conductance-voltage relationship, which shows an increase in its slope when the extracellular $[K^+]$ is increased (Hibino et al. 2010). Chord conductance of DA-PG neurons was further examined at various external K^+ concentrations in order to prove voltage dependence of barium sensitive current of TH-GFP+ cells.

The potential dependence of the cord conductance exhibited a sigmoidal relationship, increasing as the membrane potential became more negative, with g_{Kir} being approximately half-maximal at E_K. Increasing $[K^+]_o$, Kir conductance increased at negative membrane potentials and shifted the voltage-conductance relationship to more positive potentials. When conductance is plotted as a function of the driving force (V_M - E_K: membrane potential minus Nernstian equilibrium potential for potassium), conductances at each selected $[K^+]_o$ reach a minimum and a maximum at approximately the same voltage levels.

This indicates that Kir current conductance in DA-PG cells depends on both $[K^+]_o$ and membrane potential, where the membrane potential is described as V_M - E_K in

analogy to what has been found for Kir current in several other preparations (Hestrin 1981, Leech & Stanfield 1981, Harvey & Ten Eick 1988).

From this series of experiments we can conclude that barium and cesium sensitive current of DA-PG cells is primarily permeable to K^+. The external potassium concentration has a great effect on barium sensitive current of DA-PG cells affecting largely both amplitude and voltage-dependence of the inwardly conductance in DA PG cells. All these features suggest that the current described in this work belongs to inwardly potassium rectifier current family.

4.2 Different Kir Channels in DA-PG Cells

Although inward rectifier potassium channels have been postulated as therapeutic targets for several common disorders, including hypertension, cardiac arrhythmias and pain, the pharmacology of this family is virtually limited to barium, cesium, and few poorly selective cardiovascular and neurologic drugs with off-target activity toward inward rectifiers (Bhave et al. 2010, Hibino et al. 2010).

Tertiapin and Quinacrine have been used to identify which Kir channel family members are present in DA-PG cells of the olfactory bulb.

Tertiapin can inhibit GIRK 1 (Kir 3.1), GIRK 4 (Kir 3.4) and ROMK1(Kir 1.1)(Jin & Lu 1998, Jin & Lu 1999). In DA-PG cell barium sensitive current, the oxidation-resistant form of the drug tertiapin-Q was ineffective when tested alone at concentrations ranging from 100 nM to 3 μM. If Kir 1.1 are present in DA-PG cells, and active at rest, Tertiapin blocks their contribute to Kir current when applied in extracellular bath. Moreover, you can exclude presence of ROMK 1 in DA-PG cells because they are commonly localized on renal outer medulla, where they convey important functions in regulating K^+ secretion (Bhave et al. 2011).

On the other hand, GIRK channels become activated only following the binding of ligands to their cognate G protein-coupled receptors, which causes the dissociation of the βγ subunits of pertussis toxin-sensitive G proteins which subsequently bind to and activate the GIRK channel (Walsh, 2011). For this reason, we tested the effect of tertiapin after activation of K_{ACh} current with oxotremorine. In these conditions, tertiapin completely abolished the current increment promoted by the muscarinic receptor activation suggesting that functional GIRK channels are actually present in DA-PG cells.

Quinacrine is chosen in order to investigate the presence of strongly rectifier channel members such as Kir 2.x, also known as classical Kir channels. Quinacrine is reported to block Kir 6.2 ~ Kir 2.3 > Kir 2.1 (Lopez-Izquierdo et al. 2011). Data

obtained from 15 cells show that Quinacrine 100 μM suppresses a significant fraction of the hyperpolarization-activated current in DA PG cells. Of the 2.x family, Kir 2.1 is highly expressed in periglomerular cells (Pruss et al. 2005), as well as Kir 2.2 (Karschin et al. 1996). Kir 2.3 is also present in the OB (Inanobe et al. 2002); no immunoreactivity was found in the glomerular layer for this subunit (Inanobe et al. 2002), but the Allen Brain Atlas shows a weak positivity. For this reason, it is thought that Quinacrine inhibits Kir 2.x channels present in DA-PG cells. Moreover, in DA-PG cells working K_{ATP} channel presence can be excluded: although, 6.2 subunit weak positivity is reported in PG layer, SURx proteins are not detected in the OB (Allen Brain Atlas). Kir 6.x subunits constitute the pore forming structure of K_{ATP} channel, which needs the presence of SUR subunits to work.

In conclusion, at hyperpolarizing potentials negative to E_K, DA-PG cells display a Ba^{2+} sensitive inward rectifying current supported by Kir 2.x channels, which contribute to the resting K^+ conductance and are constitutively active. In presence of different neuromodulators, also Kir 3.x channels can open following G protein activation.

4.3 Kir Current Role in DA-PG Cells Intrinsic Firing Activity

Current clamp experiments prove the presence of a barium sensitive current. Ba^{2+} is a blocker commonly used for Kir channels. Adding barium to the extracellular solution causes changes of the electrical properties of the membrane. At first it was noted a significant membrane resistance increase in presence of barium, due to the closing of Kir conductance. Moreover, an important depolarization occurred after blocking Kir current. This depolarization causes the disappearance of spontaneous activity in dopaminergic periglomerular neurons. This effect is reversible, and it has been shown that in presence of the barium block, the injection of a hyperpolarizing current causes a temporary reactivation of spontaneous activity followed by a progressive depolarization that ends with a new block of the spontaneous activity.

The reappearance of the activity in presence of a Kir blocker would suggest the absence of any role of the current in the pacemaker process, but the barium block is voltage-dependent, and this leaves open question of whether the restore of spontaneous activity upon repolarization is caused by the barium block removal or not.

We searched an answer to this question using quinacrine, a drug exerting a non-voltage dependent block of the Kir current. Quinacrine 100 μM was applied in *current-clamp* recordings to verify its capacity to reproduce the barium effect on

membrane potential. Like barium, quinacrine blocks the Kir current causing a large membrane depolarization and also leading to a complete stop of firing activity. When the membrane was reported to a resting potential comparable to control conditions by injecting hyperpolarizing current, the activity was resumed. This result confirms that Kir current plays an important role in maintaining the membrane potential of DA PG cells, but it is not an essential component of the pacemaker mechanism in these cells.

4.4 Effect of Kir Current Modulation on DA-PG Cells

The OB is the first central relay station in the vertebrate olfactory system (Mori et al. 1999, Shepherd & Greer 1998). It receives rich afferent sensory information encoding odor molecule structure and concentration as well as spatiotemporal aspects of odor stimulation (Buck 1996, Wachowiak & Cohen 2001, Spors et al. 2006). This sensory information is processed and refined substantially by a diverse array of local interneurons that differ in spatial distribution, neurochemical expression and synaptic connections (Wachowiak & Shipley 2006, Cave & Baker 2009, Kosaka & Kosaka 2011).

In the OB, different stimuli, which come from neurotransmitter release, modulate a great number of activities: such as glomerular microcircuits rearrangement, the dendrodendritic reciprocal synapses between interneurons and mitral/tufted cells, and excitability of principal neurons. These modulatory activities are important for odor discrimination, odor-guided behaviors and perceptual learning (Krosnowski et al. 2012).

The olfactory bulb is unique among primary sensory centers in receiving centrifugal projection: SNC controls and adjusts the incoming flow of information and the processing of afferent signals via centrifugal projections. Two major groups of axons project to the bulb from brain: the first is composed by afferent fibers which arise from primary cortex, the second is given of axons originating in non-olfactory structures of the basal forebrain and brainstem (Kratskin & Belluzzi 2003).

The most prominent projections to the olfactory bulb originate in the anterior olfactory nucleus (AON), whose afferents predominantly terminate in the granule cell layer, and in less extent in EPL and GL. The piriform cortex is another great source of projections to the olfactory bulb, whose axons terminate in granule cell layer.

The nucleus of the horizontal limb of the diagonal band (NHDB) is the major source of bulbar centrifugal projection arising from non-olfactory brain structures.

NHDB innervates neocortex and hippocampus and plays an important role in learning and memory. NHDB projects to the glomerular layer, the granule cell layer and EPL. Also dorsal and median raphe nuclei are the source of bilateral projection to the olfactory bulb: these axons largely terminate around and within glomeruli (Kratskin & Belluzzi 2003).

In general centrifugal innervation of mammalian OB implies centrifugal afferent fibers having both olfactory and non-olfactory brain structure origin. The position of centrifugal neurons in the brain does not correspond clearly to the location of its terminal field in the bulb. Centrifugal fiber axons largely project to the ipsilateral olfactory bulb. Fibers from all brain contact different parts of granule cells, while the projections from the AON and non-olfactory brain structures reach interneurons in the glomerular layer.

Centrifugal inputs to the olfactory bulb may influence bulbar processing by modulating the activity of local interneurons (Linster & Gervais 1996, Linster & Hasselmo 1997). The presence of reciprocal connections between the bulb and secondary olfactory centers, thanks to multiple feedback loops, ensure a coordinate signaling processing and self-regulation in the olfactory system (Kratskin & Belluzzi 2003); neuromodulator such as noradrenaline, acetylcholine, serotonin and dopamine serve important function in this kind of communication.

Dopaminergic cells in the olfactory bulb are the target of numerous afferents releasing a variety of neurotransmitters: there are serotoninergic afferents from the ventral and dorsal raphe nuclei (Araneda et al. 1980, Araneda et al. 1980, Halász et al. 1977), noradrenergic input from the locus cœruleus (Halász & Shepherd 1983, Macrides et al. 1981, McLean et al. 1989), cholinergic inputs from the nucleus of the horizontal limb of the diagonal band (Carson 1984, Carson 1984, Zaborszky et al. 1986, Carson 1984, Matsutani & Yamamoto 2008), and histaminergic inputs from hypothalamus (Panula et al. 1989). Furthermore, bulbar dopaminergic cells have been shown to express D2 receptors (Gutierrez-Mecinas et al. 2005), which could be activated by the dopamine released by the cell itself (Maher & Westbrook 2008).

Many of these neurotransmitters are known to affect the cAMP pathway, and therefore they are potentially capable of a modulation of the Kir current. Moreover, data reported in this work show that in DA-PG cells neurotransmitter modulation on Kir channels is able to increase or decrease the amplitude of Kir current. For this reason, it is of some interest studying how a current, which plays such an important role in the resting membrane potential of DA-PG cells, is modulated by different neurotransmitters.

We tested the effects on the Kir current amplitude of 5-10 min applications of serotonin (50 μM), dopamine (100 μM and 1 mM ascorbic acid), quinpirole (D2 agonist, 30 μM), SKF 38393 (D1 agonist, 15 μM), noradrenaline (100 μM and 1 mM ascorbic acid), phenylephrine (α1 agonist, 10 μM), clonidine (α2 agonist, 10 μM), histamine (10 μM), oxotremorine (muscarinic agonist, 10 μM), GABA (100 μM), muscimol ($GABA_A$ 50 μM) and baclofen ($GABA_B$ agonist, 30 μM) on Kir current. In these experiments we evoked the inward rectifier K^+ current through hyperpolarizing voltage step protocol, and recorded it using the *perforated patch clamp* technique, in 32 mM external K^+ solution and in controlled temperature conditions (fig.4.1).

The responses induced by neurotransmitters shown and discussed in this work are the results of the direct activation of receptors on bulbar DA-PG cells, since all recordings were made in conditions of block of synaptic transmission.

Data obtained in this work show that acetylcholine - via M2 muscarinic receptor activation, and dopamine - via D2 receptor activation increase the amplitude of Kir current in DA-PG cells.

Acetylcholine present in the bulbar structure comes both from extensive cholinergic fibers of the horizontal limb of the diagonal band of Broca (Macrides et al. 1981, Zaborszky et al. 1986, El-Etri et al. 1999, Matsutani & Yamamoto 2008), and from cholinergic interneurons in the OB (Krosnowski et al. 2012).

In olfactory bulb, the resulting effect of cholinergic modulation is excitatory (Elaagouby & Gervais 1992) and the multiple action of ACh seems to be orchestrated towards an enhancement of specificity and temporal precision of mitral cell responses to odors (Elaagouby & Gervais 1992, Mandairon et al. 2006, D'Souza & Vijayaraghavan 2012).

The increase of Kir current amplitude, correlated with a 4.5 mV hyperpolarization in *current clamp* condition, can imply a variation on frequency of the firing activity of DA - PG cells, which in turn could inhibit principal neurons less intensely.

Dopamine administration increases Kir current; this effect is mimicked by quinpirole: the compound acts as agonist for D2 receptor. DA-PG cells present autoreceptors, for this reason the increase of an hyperpolarizing conductance in presence of DA release is supposed to have great importance in excitatory self-regulation.

On the other hand, serotonin, histamine and noradrenaline administration present opposite effect on Kir current amplitude.

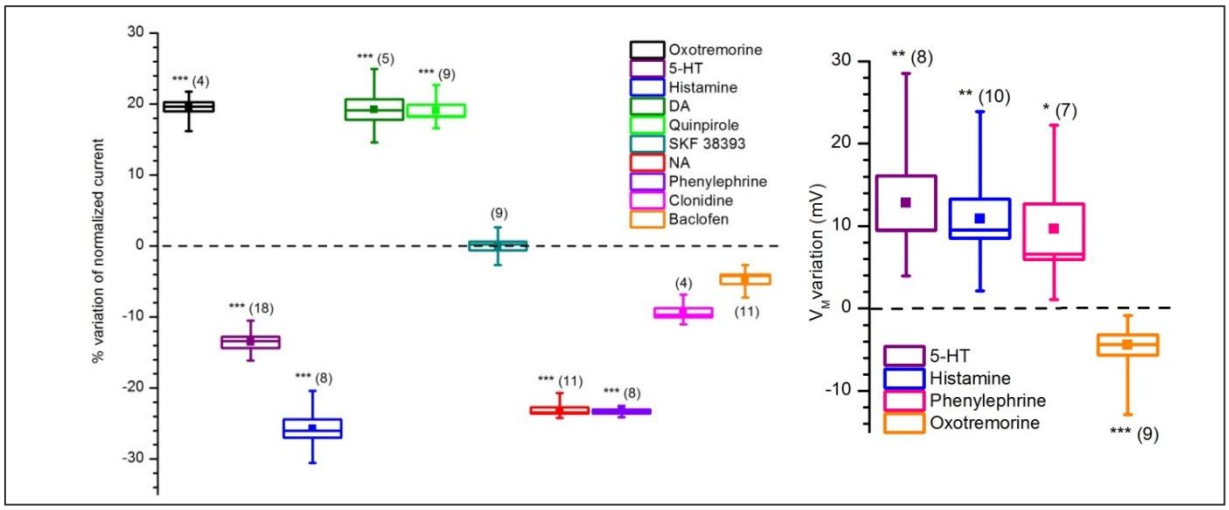

Figure 4.1 **Effect of various neurotransmitters and agonists acting on Kir current.**
On the left, agonist and NT effects on current amplitude in *voltage clamp* conditions are resumed.
On the right, effect on membrane potential in *current clamp* conditions are shown.

Both α and β NA receptors are present in the olfactory bulb (Woo and Leon 1995, Shipley and Ennis 1996). NA, acting via α1 receptors, has been reported to inhibit inward rectifying potassium currents in several systems (Hayar et al. 2001, Nai et al. 2010). Also in DA-PG cells, NA - via α1 receptor agonist (phenylephrine) - induces a significant decrease of Kir current amplitude, an effect which is paralleled by a 8.13 mV depolarization in *current-clamp* conditions.

A dense serotonergic innervation of the OB, and in particular of the glomerular region is provided by projections from the dorsal and median raphe nuclei (Araneda et al. 1980, McLean & Shipley 1987). 5-HT receptors are present both in bulbar interneurons, periglomerular and granular cells (Morilak et al. 1993), and in principal cells such as mitral and tufted cells (Pompeiano et al. 1994, McLean et al. 1995). Data presented in this study show that serotonin administration, which decreases Kir current amplitude, causes a large depolarization of 12.8 mV. Serotonin has great effect on regulating DA-PG cells exitability profile.

Hystaminergic inputs are also present in the olfactory bulb, which receives caudal tuberal and postmammillary magnocellular hypothalamus hystaminirgi centrifugal fibers (Auvinen & Panula 1988, Panula et al. 1989). In DA-PG cells, histamine reduces Kir current amplitude causing a depolarization of 10.89 mV. Data are coherent with a previous evidence: in a unidentified fraction of periglomerular cells, H1-receptor activation causes a block of a potassium current (Jahn et al. 1995).

In order to confirm data obtained in *voltage clamp* recordings, and proving a physiological relevance of the effects induced by the neurotransmitters described above, experiments in *current clamp* configuration were performed. In particular, it

was interesting to analyze the changes occurred in the membrane potential induced by the neuromodulation of the Kir current, caused by drugs previously tested in *voltage clamp*.

In conclusion, data provided from this work contribute to understand better how neurotransmitters modulate Kir current. The presence of two different ways to modulate potassium hyperpolarizing conductance, increasing or decreasing Kir current amplitude, suggests a fine regulatory pathway. Although Kir current is present at rest, several mechanisms contribute to refine the amplitude of Kir current, which can be largely change in different physiological conditions.

Moreover, it is worth noting that Kir current deeply influences the resting potential. Pointed this, we should expect that any modification in the amplitude of the current is paralleled by a variation of the membrane potential. Data provided from this study show a close correlation between change of Kir current amplitude and the variation of membrane potential, this in turn produces a fine modulation of DA - PG cell excitatory profile.

4 CONCLUSION

Dopaminergic (DA) periglomerular (PG) neurons are critically placed at the entry of the bulbar circuitry, directly in contact with both the terminals of olfactory sensory neurons and the apical dendrites of projection neurons. They are autorhythmic and the target of numerous afferents releasing a variety of neurotransmitters. Despite the centrality of their position suggests a critical role in the sensory processing, their properties and their role remain elusive.

In this study, the *perforated-patch* technique was adopted to record the current mediated by Kir channels in DA-PG cells in thin slice in order to preserve intracellular environment. *Patch clamp* recordings were performed both in *current clamp* and in *voltage clamp* configuration to show the presence of Kir current and describe its modulation in DA-PG cells. In controlled conditions, DA-PG cells display an inward rectifying current at hyperpolarizing potentials around E_K. A first component is sustained by Ba^{2+}-sensitive KIR2.x channels. On the other hand, this background activity could also receive the contribution of KIR3.x channels open in response to G protein activation by different neuromodulators.

Dopamine has been shown to modulate several aspects of olfactory information processing, for this reason, it is important to understand the physiological role of dopaminergic periglomerular interneurons. Moreover, spontaneous firing activity of TH-GFP+ interneurons, which due to their location ensure horizontal flux of information in the bulbar structure, suggest a key role in processing sensory information.

The study of the Kir current completes the electrophysiological characterization of these cells and reinforce the physiological importance of these bulbar interneurons: changes in firing frequency of DA-PG cells can regulate bulbar intrinsic neuron activity, and in turn, modulate signal transmission to high cortex centres.

Although the absence of any role of the Kir current in the pacemaker process of TH-GFP+ PG cells, Kir current largely influences prevailing membrane potential of these cells, and in turn, I_{Kir} amplitude is widely influenced by several neurotransmitters. This characteristic of the Kir current provides the basis for additional flexibility and function of DA-PG cells.

It is interesting to observe the important role of Kir current in DA-PG cells: resting membrane potential of cells - strategically placed at the entry of the bulbar circuitry - is highly influenced by Kir current and can be modulated in different directions by a variety of neurotransmitters.

References

Literature Cited

1. Alagem N, Dvir M, Reuveny E. 2001. Mechanism of Ba(2+) block of a mouse inwardly rectifying K+ channel: differential contribution by two discrete residues. *J. Physiol* 534(Pt. 2):381-93
2. Altman J. 1963. Autoradiographic investigation on cell proliferation in the brains of rats and cats. *Anat. Rec.* 145:573-91
3. Altman J. 1969. Autoradiographic and histological studies of postnatal neurogenesis. IV. Cell proliferationand migration in the anterior forebrain, with special reference to persisting neurogenesis in the olfactory bulb. *J. Comp. Neurol.* 137:433-58
4. Altman J, Das GD. 1965. Autoradiographic and histological evidence of postnatal hippocampal neurogenesis in rats. *J. Comp. Neurol.* 124(3):319-35
5. Araneda S, Bobillier P, Buda M, Pujol JF. 1980. Retrograde axonal transport following injection of [3H]serotonin in the olfactory bulb. I. Biochemical study. *Brain Res.* 196(2):405-15
6. Araneda S, Gamrani H, Font C, Calas A, Pujol JF, Bobillier P. 1980. Retrograde axonal transport following injection of [3H]-serotonin into the olfactory bulb. II. Radioautographic study. *Brain Res.* 196(2):417-27
7. Armstrong CM. 1969. Inactivation of the potassium conductance and related phenomena caused by quaternary ammonium ion injection in squid axons. *J. Gen. Physiol* 54(5):553-75
8. Aroniadou-Anderjaska V, Ennis M, Shipley MT. 1997. Glomerular synaptic responses to olfactory nerve input in rat olfactory bulb slices. *Neuroscience* 79(2):425-34
9. Aroniadou-Anderjaska V, Zhou FM, Priest CA, Ennis M, Shipley MT. 2000. Tonic and synaptically evoked presynaptic inhibition of sensory input to the rat olfactory bulb via GABA(B) heteroreceptors. *J. Neurophysiol.* 84(3):1194-203
10. Asteria C. 1997. Molecular basis of Bartter's syndrome: new insights into the correlation between genotype and phenotype. *Eur. J. Endocrinol.* 137(6):613-5
11. Aungst JL, Heyward PM, Puche AC, Karnup SV, Hayar A et al. 2003. Centre-surround inhibition among olfactory bulb glomeruli. *Nature* 426(6967):623-9
12. Auvinen S, Panula P. 1988. Development of histamine-immunoreactive neurons in the rat brain. *J. Comp Neurol.* 276(2):289-303
13. Baker H, Liu N, Chun HS, Saino S, Berlin R et al. 2001. Phenotypic differentiation during migration of dopaminergic progenitor cells to the olfactory bulb. *J Neurosci.* 21(21):8505-13
14. Beavo JA, Rogers NL, Crofford OB, Hardman JG, Sutherland EW, Newman EV. 1970. Effects of xanthine derivatives on lipolysis and on adenosine 3',5'-monophosphate phosphodiesterase activity. *Mol. Pharmacol.* 6(6):597-603
15. Berkowicz DA, Trombley PQ, Shepherd GM. 1994. Evidence for glutamate as the olfactory receptor cell neurotransmitter. *J. Neurophysiol.* 71:2557-61
16. Betarbet R, Zigova T, Bakay RA, Luskin MB. 1996. Dopaminergic and GABAergic interneurons of the olfactory bulb are derived from the neonatal subventricular zone. *Int. J. Dev. Neurosci.* 14(7-8):921-30
17. Bhave G, Chauder BA, Liu W, Dawson ES, Kadakia R et al. 2011. Development of a selective small-molecule inhibitor of Kir1.1, the renal outer medullary potassium channel. *Mol. Pharmacol.* 79(1):42-50
18. Bhave G, Lonergan D, Chauder BA, Denton JS. 2010. Small-molecule modulators of inward rectifier K+ channels: recent advances and future possibilities. *Future. Med. Chem.* 2(5):757-74
19. Bichet D, Haass FA, Jan LY. 2003. Merging functional studies with structures of inward-rectifier K(+) channels. *Nat. Rev. Neurosci.* 4(12):957-67
20. Bolton S, Butt AM. 2006. Cyclic AMP-mediated regulation of the resting membrane potential in myelin-forming oligodendrocytes in the isolated intact rat optic nerve. *Exp. Neurol.* 202(1):36-43
21. BoSmith RE, Briggs I, Sturgess NC. 1993. Inhibitory actions of ZENECA ZD7288 on whole-cell hyperpolarization activated inward current (If) in guinea-pig dissociated sinoatrial node cells. *Br. J. Pharmacol.* 110(1):343-9
22. Bowery NG, Hill DR, Hudson AL, Doble A, Middlemiss DN et al. 1980. (-)Baclofen decreases neurotransmitter release in the mammalian CNS by an action at a novel GABA receptor. *Nature* 283(5742):92-4

23. Bucchi A, Baruscotti M, DiFrancesco D. 2002. Current-dependent block of rabbit sino-atrial node I(f) channels by ivabradine. *J. Gen. Physiol* 120(1):1-13
24. Bucchi A, Tognati A, Milanesi R, Baruscotti M, DiFrancesco D. 2006. Properties of ivabradine-induced block of HCN1 and HCN4 pacemaker channels. *J. Physiol* 572(Pt 2):335-46
25. Buck LB. 1996. Information coding in the mammalian olfactory system. *Cold Spring Harb. Symp. Quant. Biol.* 61:147-55
26. Calof AL, Rim PC, Askins KJ, Mumm JS, Gordon MK et al. 1998. Factors regulating neurogenesis and programmed cell death in mouse olfactory epithelium. *Ann. N. Y. Acad. Sci.* 855:226-9
27. Carr VM, Farbman AI. 1993. The dynamics of cell death in the olfactory epithelium. *Exp. Neurol.* 124(2):308-14
28. Carson KA. 1984. Quantitative localization of neurons projecting to the mouse olfactory bulb. *Brain Res. Bull.* 12:629-34
29. Cave JW, Baker H. 2009. Dopamine Systems in the Forebrain. In *Development and Engineering of Dopamine Neurons*, ed. RJ Pasterkamp, MP Smidt, JPH Burbach, Landes Bioscience and Springer Science+Business Media.
30. Chen WR, Shepherd GM. 1997. Membrane and synaptic properties of mitral cells in slices of rat olfactory bulb. *Brain. Res.* 745(1-2):189-96
31. Coetzee WA, Amarillo Y, Chiu J, Chow A, Lau D et al. 1999. Molecular diversity of K+ channels. *Ann. N. Y. Acad. Sci.* 868:233-85
32. D'Souza RD, Vijayaraghavan S. 2012. Nicotinic receptor-mediated filtering of mitral cell responses to olfactory nerve inputs involves the alpha3beta4 subtype. *J. Neurosci.* 32(9):3261-6
33. Dart C, Leyland ML, Barrett-Jolley R, Shelton PA, Spencer PJ et al. 1998. The dependence of Ag+ block of a potassium channel, murine kir2.1, on a cysteine residue in the selectivity filter. *J. Physiol* 511 (Pt 1):15-24
34. De Marchis S, Bovetti S, Carletti B, Hsieh YC, Garzotto D et al. 2007. Generation of distinct types of periglomerular olfactory bulb interneurons during development and in adult mice: implication for intrinsic properties of the subventricular zone progenitor population. *J Neurosci.* 27(3):657-64
35. Doring F, Derst C, Wischmeyer E, Karschin C, Schneggenburger R et al. 1998. The epithelial inward rectifier channel Kir7.1 displays unusual K+ permeation properties. *J. Neurosci.* 18(21):8625-36
36. Du X, Zhang H, Lopes C, Mirshahi T, Rohacs T, Logothetis DE. 2004. Characteristic interactions with phosphatidylinositol 4,5-bisphosphate determine regulation of kir channels by diverse modulators. *J. Biol. Chem.* 279(36):37271-81
37. El-Etri MM, Ennis M, Griff ER, Shipley MT. 1999. Evidence for cholinergic regulation of basal norepinephrine release in the rat olfactory bulb. *Neuroscience* 93(2):611-7
38. Elaagouby A, Gervais R. 1992. ACh-induced long-lasting enhancement in excitability of the olfactory bulb. *Neuroreport* 3(1):10-2
39. Ennis M, Zimmer LA, Shipley MT. 1996. Olfactory nerve stimulation activated rat mitral cells via NMDA and non NMDA receptors *in vitro*. *Neuroreport* 7(5):989-92
40. Evans RJ, Surprenant A. 1993. Effects of phospholipase A2 inhibitors on coupling of alpha 2-adrenoceptors to inwardly rectifying potassium currents in guinea-pig submucosal neurones. *Br. J. Pharmacol.* 110(2):591-6
41. Fan Z, Makielski JC. 1997. Anionic phospholipids activate ATP-sensitive potassium channels. *J. Biol. Chem.* 272(9):5388-95
42. Firestein S. 1996. Olfaction: scents and sensibility. *Curr. Biol.* 6(6):666-7
43. Gage FH. 2000. Mammalian neural stem cells. *Science* 287(5457):1433-8
44. Grace AA, Onn SP. 1989. Morphology and electrophysiological properties of immunocytochemically identified rat dopamine neurons recorded in vitro. *J Neurosci.* 9(10):3463-81
45. Graziadei PP, Levine RR, Graziadei GA. 1978. Regeneration of olfactory axons and synapse formation in the forebrain after bulbectomy in neonatal mice. *Proc. Natl. Acad. Sci. U. S. A* 75(10):5230-4
46. Guo D, Lu Z. 2003. Interaction mechanisms between polyamines and IRK1 inward rectifier K+ channels. *J. Gen. Physiol* 122(5):485-500
47. Gutierrez-Mecinas M, Crespo C, Blasco-Ibanez JM, Gracia-Llanes FJ, Marques-Mari AI et al. 2005. Distribution of D2 dopamine receptor in the olfactory glomeruli of the rat olfactory bulb. *Eur. J. Neurosci.* 22(6):1357-67
48. Hagiwara S, Jaffe LA. 1979. Electrical properties of egg cell membranes. *Annu. Rev. Biophys. Bioeng.* 8:385-416
49. Hagiwara S, Miyazaki S, Moody W, Patlak J. 1978. Blocking effects of barium and hydrogen ions on the potassium current during anomalous rectification in the starfish egg. *J. Physiol* 279:167-85
50. Hagiwara S, Miyazaki S, Rosenthal NP. 1976. Potassium current and the effect of cesium on this current during anomalous rectification of the egg cell membrane of a starfish. *J. Gen. Physiol* 67(6):621-38

51. Halász N. 1990. *The vertebrate olfactory system: chemical neuroanatomy, function and development.,* Budapest: Académiai Kiadó.
52. Halasz N, Greer CA. 1993. Terminal arborizations of olfactory nerve fibers in the glomeruli of the olfactory bulb. *J Comp Neurol.* 337(2):307-16
53. Halász N, Johansson O, Hokfelt T, Ljungdahl A, Goldstein M. 1981. Immunohistochemical identification of two types of dopamine neuron in the rat olfactory bulb as seen by serial sectioning. *J. Neurocytol.* 10(2):251-9
54. Halász N, Ljungdahl A, Hökfelt T, Johansson O, Goldstein M, Park D, Biberfeld P. Transmitter histochemistry of the rat olfactory bulb. I. Immunohistochemical localization of monoamine synthesizing enzymes. Support for intrabulbar, periglomerular dopamine neurons. Brain Res. 126[3], 455-474. 1977.
55. Halász N, Shepherd GM. 1983. Neurochemistry of the vertebrate olfactory bulb. *Neuroscience* 10(3):579-619
56. Hamill OP, Marty A, Neher E, Sakmann B, Sigworth FJ. 1981. Improved patch clamp techniques for high-resolution current recording from cells and cell-free membrane patches. *Pflügers Archiv-European Journal of Physiology* 391:85-100
57. Harvey RD, Ten Eick RE. 1988. Characterization of the inward-rectifying potassium current in cat ventricular myocytes. *J. Gen. Physiol* 91(4):593-615
58. Harvey RD, Ten Eick RE. 1988. Characterization of the inward-rectifying potassium current in cat ventricular myocytes. *J Gen Physiol* 91(4):593-615
59. Hayar A, Heyward PM, Heinbockel T, Shipley MT, Ennis M. 2001. Direct excitation of mitral cells via activation of alpha1-noradrenergic receptors in rat olfactory bulb slices. *J. Neurophysiol.* 86(5):2173-82
60. Hayar A, Karnup S, Shipley MT, Ennis M. 2004. Olfactory bulb glomeruli: external tufted cells intrinsically burst at theta frequency and are entrained by patterned olfactory input. *J Neurosci* 24(5):1190-9
61. Heginbotham L, Lu Z, Abramson T, MacKinnon R. 1994. Mutations in the K+ channel signature sequence. *Biophys J* 66(4):1061-7
62. Hestrin S. 1981. The interaction of potassium with the activation of anomalous rectification in frog muscle membrane. *J. Physiol* 317:497-508
63. Hestrin S. 1981. The interaction of potassium with the activation of anomalous rectification in frog muscle membrane. *J Physiol* 317:497-508
64. Hibino H, Inanobe A, Furutani K, Murakami S, Findlay I, Kurachi Y. 2010. Inwardly rectifying potassium channels: their structure, function, and physiological roles. *Physiol Rev.* 90(1):291-366
65. Hibino H, Inanobe A, Furutani K, Murakami S, Findlay I, Kurachi Y. 2010. Inwardly rectifying potassium channels: their structure, function, and physiological roles. *Physiol Rev.* 90(1):291-366
66. Hilgemann DW, Ball R. 1996. Regulation of cardiac Na+,Ca2+ exchange and KATP potassium channels by PIP2. *Science* 273(5277):956-9
67. Hille B. 1992. *Ionic channels of excitable membranes,* pp. -426. Sunderland, MA, USA: Sinauer Associates Inc.
68. Hinds JW. 1968. Autoradiographic study of histogenesis in the mouse olfactory bulb. II. Cell proliferation and migration. *J Comp Neurol.* 134(3):305-22
69. Hsia AY, Vincent JD, Lledo PM. 1999. Dopamine depresses synaptic inputs into the olfactory bulb. *J Neurophysiol.* 82(2):1082-5
70. Inanobe A, Fujita A, Ito M, Tomoike H, Inageda K, Kurachi Y. 2002. Inward rectifier K+ channel Kir2.3 is localized at the postsynaptic membrane of excitatory synapses. *Am. J. Physiol Cell Physiol* 282(6):C1396-C1403
71. Inanobe A, Nakagawa A, Kurachi Y. 2011. Interactions of cations with the cytoplasmic pores of inward rectifier K(+) channels in the closed state. *J. Biol. Chem.* 286(48):41801-11
72. Jahn K, Haas HL, Hatt H. 1995. Patch-clamp study of histamine activated potassium currents on rabbit olfactory bulb neurons. *Naunyn-Schmied. Arch. Pharmacol.* 352:386-93
73. Jin W, Lu Z. 1998. A novel high-affinity inhibitor for inward-rectifier K+ channels. *Biochemistry* 37(38):13291-9
74. Jin W, Lu Z. 1998. A novel high-affinity inhibitor for inward-rectifier K+ channels. *Biochemistry* 37(38):13291-9
75. Jin W, Lu Z. 1999. Synthesis of a stable form of tertiapin: a high-affinity inhibitor for inward-rectifier K+ channels. *Biochemistry* 38(43):14286-93
76. Johnston GA, Curtis DR, De Groat WC, Duggan AW. 1968. Central actions of ibotenic acid and muscimol. *Biochem Pharmacol* 17(12):2488-9
77. Kaplan MS. 1983. Proliferation of subependymal cells in the adult primate CNS: differential uptake of DNA labelled precursors. *J Hirnforsch.* 24(1):23-33
78. Karschin C, Dissmann E, Stuhmer W, Karschin A. 1996. IRK(1-3) and GIRK(1-4) inwardly rectifying K+ channel mRNAs are differentially expressed in the adult rat brain. *J Neurosci* 16(11):3559-70
79. Kasowski HJ, Kim H, Greer CA. 1999. Compartmental organization of the olfactory bulb glomerulus. *J. Comp. Neurol.* 407(2):261-74

80. Kehl SJ. 1991. Quinidine-induced inhibition of the fast transient outward K+ current in rat melanotrophs. *Br. J. Pharmacol.* 103(3):1807-13
81. Keller A, Yagodin S, Aroniadou-Anderjaska V, Zimmer LA, Ennis M et al. 1998. Functional organization of rat olfactory bulb glomeruli revealed by optical imaging. *J. Neurosci.* 18(7):2602-12
82. Kendrick KM, Keverne EB, Chapman C, Baldwin BA. 1988. Intracranial dialysis measurement of oxytocin, monoamine and uric acid release from the olfactory bulb and substantia nigra of sheep during parturition, suckling, separation from lambs and eating. *Brain Res.* 439(1-2):1-10
83. Kobal G, Kettenmann B. 2000. Olfactory functional imaging and physiology. *Int. J. Psychophysiol.* 36(2):157-63
84. Kohwi M, Petryniak MA, Long JE, Ekker M, Obata K et al. 2007. A subpopulation of olfactory bulb GABAergic interneurons is derived from Emx1- and Dlx5/6-expressing progenitors. *J Neurosci.* 27(26):6878-91
85. Kosaka K, Aika Y, Toida K, Heizmann CW, Hunziker W et al. 1995. Chemically defined neuron groups and their subpopulations in the glomerular layer of the rat main olfactory bulb. *Neurosci. Res.* 23(1):73-88
86. Kosaka K, Kosaka T. Chemical properties of type 1 and type 2 periglomerular cells in the mouse olfactory bulb are different from those in the rat olfactory bulb. Brain Res. 1167, 42-55. 2007.
87. Kosaka K, Toida K, Aika Y, Kosaka T. 1998. How simple is the organization of the olfactory glomerulus?: the heterogeneity of so-called periglomerular cells. *Neurosci Res.* 30(2):101-10
88. Kosaka K, Toida K, Margolis FL, Kosaka T. 1997. Chemically defined neuron groups and their subpopulations in the glomerular layer of the rat main olfactory bulb .2. Prominent differences in the intraglomerular dendritic arborization and their relationship to olfactory nerve terminals. *Neuroscience* 76(3):775-86
89. Kosaka T, Kosaka K. Tyrosine hydroxylase-positive GABAergic juxtaglomerular neurons are the main source of the interglomerular connections in the mouse main olfactory bulb. Neurosci Res. 60[3], 349-354. 2008.
90. Kosaka T, Kosaka K. 2008. Tyrosine hydroxylase-positive GABAergic juxtaglomerular neurons are the main source of the interglomerular connections in the mouse main olfactory bulb. *Neurosci. Res.* 60(3):349-54
91. Kosaka T, Kosaka K. 2011. "Interneurons" in the olfactory bulb revisited. *Neurosci. Res.* 69(2):93-9
92. Kratskin I, Belluzzi O. 2003. Anatomy and neurochemistry of the olfactory bulb. In *Handbook of Olfaction and Gustation*, ed. RL Doty, 7:139-164. New York - Basel: Marcel Dekker.
93. Krosnowski K, Ashby S, Sathyanesan A, Luo W, Ogura T, Lin W. 2012. Diverse populations of intrinsic cholinergic interneurons in the mouse olfactory bulb. *Neuroscience* 213:161-78
94. Kukekov VG, Laywell ED, Suslov O, Davies K, Scheffler B et al. 1999. Multipotent stem/progenitor cells with similar properties arise from two neurogenic regions of adult human brain. *Exp. Neurol.* 156(2):333-44
95. Kuo A, Gulbis JM, Antcliff JF, Rahman T, Lowe ED et al. 2003. Crystal structure of the potassium channel KirBac1.1 in the closed state. *Science* 300(5627):1922-6
96. Kurata HT, Akrouh A, Li JB, Marton LJ, Nichols CG. 2013. Scanning the topography of polyamine blocker binding in an inwardly rectifying potassium channel. *J. Biol. Chem.* 288(9):6591-601
97. Kurata HT, Marton LJ, Nichols CG. 2006. The polyamine binding site in inward rectifier K+ channels. *J. Gen. Physiol* 127(5):467-80
98. Kurata HT, Phillips LR, Rose T, Loussouarn G, Herlitze S et al. 2004. Molecular basis of inward rectification: polyamine interaction sites located by combined channel and ligand mutagenesis. *J. Gen. Physiol* 124(5):541-54
99. Lacey MG, Mercuri NB, North RA. 1988. On the potassium conductance increase activated by GABAB and dopamine D2 receptors in rat substantia nigra neurones. *J. Physiol* 401:437-53
100. Leech CA, Stanfield PR. 1981. Inward rectification in frog skeletal muscle fibres and its dependence on membrane potential and external potassium. *J. Physiol* 319:295-309
101. Leech CA, Stanfield PR. 1981. Inward rectification in frog skeletal muscle fibres and its dependence on membrane potential and external potassium. *J Physiol* 319:295-309
102. Linster C, Gervais R. 1996. Investigation of thr role of interneurons and their modulation by centrifugal fibers in a neural model of the olfactory bulb. *J. Comp. Neurosci.* 3:225-46
103. Linster C, Hasselmo M. 1997. Modulation of inhibition in a model of olfactory bulb reduces overlap in the neural representation of olfactory stimuli. *Behav. Brain Res.* 84(1-2):117-27
104. Liou HH, Zhou SS, Huang CL. 1999. Regulation of ROMK1 channel by protein kinase A via a phosphatidylinositol 4,5-bisphosphate-dependent mechanism. *Proc. Natl. Acad. Sci. U. S. A* 96(10):5820-5

105. Lledo PM, Alonso M, Grubb MS. 2006. Adult neurogenesis and functional plasticity in neuronal circuits. *Nat Rev. Neurosci.* 7(3):179-93
106. Lledo PM, Gheusi G. 2003. Olfactory processing in a changing brain. *Neuroreport* 14(13):1655-63
107. Lledo PM, Gheusi G, Vincent JD. 2005. Information processing in the Mammalian olfactory system. *Physiol. Rev.* 85(1):281-317
108. Lledo PM, Gheusi G, Vincent JD. 2005. Information processing in the mammalian olfactory system. *Physiol Rev.* 85(1):281-317
109. Lledo PM, Merkle FT, Alvarez-Buylla A. 2008. Origin and function of olfactory bulb interneuron diversity. *Trends Neurosci.* 31(8):392-400
110. Logothetis DE, Jin T, Lupyan D, Rosenhouse-Dantsker A. 2007. Phosphoinositide-mediated gating of inwardly rectifying K(+) channels. *Pflugers Arch.* 455(1):83-95
111. Logothetis DE, Lupyan D, Rosenhouse-Dantsker A. 2007. Diverse Kir modulators act in close proximity to residues implicated in phosphoinositide binding. *J. Physiol* 582(Pt 3):953-65
112. Lois C, Alvarez-Buylla A. 1994. Long-distance neuronal migration in the adult mammalian brain. *Science* 264(5162):1145-8
113. Lopatin AN, Makhina EN, Nichols CG. 1994. Potassium channel block by cytoplasmic polyamines as the mechanism of intrinsic rectification. *Nature* 372(6504):366-9
114. Lopatin AN, Makhina EN, Nichols CG. 1995. The mechanism of inward rectification of potassium channels: "long-pore plugging" by cytoplasmic polyamines. *J. Gen. Physiol* 106(5):923-55
115. Lopes CM, Zhang H, Rohacs T, Jin T, Yang J, Logothetis DE. 2002. Alterations in conserved Kir channel-PIP2 interactions underlie channelopathies. *Neuron* 34(6):933-44
116. Lopez-Izquierdo A, Arechiga-Figueroa IA, Moreno-Galindo EG, Ponce-Balbuena D, Rodriguez-Martinez M et al. 2011. Mechanisms for Kir channel inhibition by quinacrine: acute pore block of Kir2.x channels and interference in PIP2 interaction with Kir2.x and Kir6.2 channels. *Pflugers Arch.* 462(4):505-17
117. Lu Z, Klem AM, Ramu Y. 2001. Ion conduction pore is conserved among potassium channels. *Nature* 413(6858):809-13
118. Luo M, Fee MS, Katz LC. 2003. Encoding pheromonal signals in the accessory olfactory bulb of behaving mice. *Science* 299(5610):1196-201
119. Luskin MB. 1993. Restricted proliferation and migration of postnatally generated neurons derived from the forebrain subventricular zone. *Neuron* 11(1):173-89
120. Macrides F, Davis BJ. 1983. The olfactory bulb. In *Chemical Neuroanatomy*, ed. PC Emson,391-426. New York: Raven.
121. Macrides F, Davis BJ, Youngs WM, Nadi NS, Margolis FL. 1981. Cholinergic and catecholaminergic afferents to the olfactory bulb in the hamster: a neuroanatomical, biochemical, and histochemical investigation. *J. Comp Neurol.* 203(3):495-514
122. Macrides F, Schneider SP. 1982. Laminar organization of mitral and tufted cells in the main olfactory bulb of the adult hamster. *J Comp Neurol.* 208(4):419-30
123. Maher BJ, Westbrook GL. 2008. Co-transmission of dopamine and GABA in periglomerular cells. *J. Neurophysiol.* 99(3):1559-64
124. Malnic B, Hirono J, Sato T, Buck LB. 1999. Combinatorial receptor codes for odors. *Cell* 96(5):713-23
125. Mandairon N, Ferretti CJ, Stack CM, Rubin DB, Cleland TA, Linster C. 2006. Cholinergic modulation in the olfactory bulb influences spontaneous olfactory discrimination in adult rats. *European Journal of Neuroscience* 24(11):3234-44
126. Matsuda H. 1991. Magnesium gating of the inwardly rectifying K+ channel. *Annu. Rev. Physiol* 53:289-98
127. Matsuda H, Saigusa A, Irisawa H. 1987. Ohmic conductance through the inwardly rectifying K channel and blocking by internal Mg2+. *Nature* 325(7000):156-9
128. Matsuda H, Stanfield PR. 1989. Single Inwardly Rectifying Potassium Channels in Cultured Muscle Cells from Rat and Mouse. *J. Physiol. (Lond.)* 414:111-24
129. Matsushita N, Okada H, Yasoshima Y, Takahashi K, Kiuchi K, Kobayashi K. 2002. Dynamics of tyrosine hydroxylase promoter activity during midbrain dopaminergic neuron development. *J Neurochem.* 82(2):295-304
130. Matsutani S, Yamamoto N. 2008. Centrifugal innervation of the mammalian olfactory bulb. *Anat. Sci. Int.* 83(4):218-27
131. McLean JH, Darby-King A, Paterno G. 1995. Localization of 5-HT2A receptor mRNA by in situ hybridization in the olfactory bulb of the postnatal rat. *J. Comp. Neurol.* 353(3):371-8
132. McLean JH, Shipley MT. 1987. Serotonergic afferents to the rat olfactory bulb: I. Origins and laminar specificity of serotoninergic inputs in the adult rat. *J. Neurosci.* 7:3029-39
133. McLean JH, Shipley MT. 1988. Postmitotic, postmigrational expression of tyrosine hydroxylase in olfactory bulb dopaminergic neurons. *J. Neurosci.* 8(10):3658-69
134. McLean JH, Shipley MT, Nickell WT, Aston-Jones G, Reyher CK. 1989. Chemoanatomical organization of the noradrenergic input from locus coeruleus to the olfactory bulb of the adult rat. *J. Comp. Neurol.* 285:339-49

135. Mori K, Kishi K, Ojima H. 1983. Distribution of dendrites of mitral, displaced mitral, tufted and granule cells in the rabbit olfactory bulb. *J. Comp. Neurol.* 219:339-55
136. Mori K, Nagao H, Yoshihara Y. 1999. The olfactory bulb: coding and processing of odor molecule information. *Science* 286(5440):711-5
137. Morilak DA, Garlow SJ, Ciaranello RD. 1993. Immunocytochemical localization and description of neurons expressing serotonin2 receptors in the rat brain. *Neuroscience* 54(3):701-17
138. Moulton DG. 1974. Dynamics of cell populations in the olfactory epithelium. *Ann. N. Y. Acad. Sci.* 237(0):52-61
139. Murphy GJ, Darcy DP, Isaacson JS. 2005. Intraglomerular inhibition: signaling mechanisms of an olfactory microcircuit. *Nat. Neurosci.* 8(3):354-64
140. Murphy GJ, Isaacson JS. 2003. Presynaptic cyclic nucleotide-gated ion channels modulate neurotransmission in the mammalian olfactory bulb. *Neuron* %20;37(4):639-47
141. Nagano N, Imaizumi Y, Watanabe M. 1996. Novel blockade of Ca2+ current by quinacrine in smooth muscle cells of the guinea pig. *Jpn. J. Pharmacol.* 71(1):51-60
142. Nai Q, Dong HW, Linster C, Ennis M. 2010. Activation of alpha1 and alpha2 noradrenergic receptors exert opposing effects on excitability of main olfactory bulb granule cells. *Neuroscience* 169(2):882-92
143. Neher E, Sakmann B. 1976. Single-channel currents recorded from membrane of denervated frog muscle fibres. *Nature* 260(5554):799-802
144. Neuhoff H, Neu A, Liss B, Roeper J. I(h) channels contribute to the different functional properties of identified dopaminergic subpopulations in the midbrain. J Neurosci. 22[4], 1290-1302. 2002.
145. Nichols CG, Lopatin AN. 1997. Inward rectifier potassium channels. *Annu. Rev. Physiol* 59:171-91
146. Nieuwenhuys R. 1967. Comparative anatomy of olfactory centres and tracts. *Prog. Brain Res.* 23:1-64
147. Ohmori H. 1978. Inactivation kinetics and steady-state current noise in the anomalous rectifier of tunicate egg cell membranes. *J. Physiol* 281:77-99
148. Oliver D, Baukrowitz T, Fakler B. 2000. Polyamines as gating molecules of inward-rectifier K+ channels. *Eur. J. Biochem.* 267(19):5824-9
149. Oliver D, Hahn H, Antz C, Ruppersberg JP, Fakler B. 1998. Interaction of permeant and blocking ions in cloned inward-rectifier K+ channels. *Biophys. J.* 74(5):2318-26
150. Orkand RK, Nicholls JG, Kuffler SW. 1966. Effect of nerve impulses on the membrane potential of glial cells in the central nervous system of amphibia. *J. Neurophysiol.* 29(4):788-806
151. Orona E, Rainer EC, Scott JW. 1984. Dendritic and axonal organisation of mitral and tufted cells in the rat olfactory bulb. *J. Comp. Neurol.* 226:346-56
152. Pan WJ, Osmanovic SS, Shefner SA. 1994. Adenosine Decreases Action Potential Duration by Modulation of A- Current in Rat Locus Coeruleus Neurons. *J. Neurosci.* 14:1114-22
153. Panula P, Pirvola U, Auvinen S, Airaksinen MS. 1989. Histamine-immunoreactive nerve fibers in the rat brain. *Neuroscience* 28(3):585-610
154. Park WS, Han J, Kim N, Ko JH, Kim SJ, Earm YE. 2005. Activation of inward rectifier K+ channels by hypoxia in rabbit coronary arterial smooth muscle cells. *Am. J. Physiol Heart Circ. Physiol* 289(6):H2461-H2467
155. Pearson WL, Nichols CG. 1998. Block of the Kir2.1 channel pore by alkylamine analogues of endogenous polyamines. *J. Gen. Physiol* 112(3):351-63
156. Pencea V, Bingaman KD, Freedman LJ, Luskin MB. 2001. Neurogenesis in the subventricular zone and rostral migratory stream of the neonatal and adult primate forebrain. *Exp. Neurol.* 172(1):1-16
157. Peretto P, Merighi A, Fasolo A, Bonfanti L. 1999. The subependymal layer in rodents: a site of structural plasticity and cell migration in the adult mammalian brain. *Brain Res. Bull.* 49(4):221-43
158. Pignatelli A, Ackman JB, Vigetti D, Beltrami AP, Zucchini S, Belluzzi O. 2009. A potential reservoir of immature dopaminergic replacement neurons in the adult mammalian olfactory bulb. *Pflugers Arch.* 457(4):899-915
159. Pignatelli A, Belluzzi O. 2008. Cholinergic modulation of dopaminergic neurons in the mouse olfactory bulb. *Chem. Senses.* 33(4):331-8
160. Pignatelli A, Borin M, Fogli IA, Gambardella C, Belluzzi O. 2013. The h-current in periglomerular dopaminergic neurons of the mouse olfactory bulb. *PLoS. ONE.* 8(2):e56571
161. Pignatelli A, Kobayashi K, Okano H, Belluzzi O. 2005. Functional properties of dopaminergic neurones in the mouse olfactory bulb. *J. Physiol* 564(2):501-14
162. Pinching AJ, Powell TPS. 1971. The neuron types of the glomerular layer of the olfactory bulb. *J. Cell Sci.* 9:305-45
163. Pinching AJ, Powell TPS. 1971. The neuropil of the periglomerular region of the olfactory bulb. *J. Cell Sci.* 9:379-409

164. Podda MV, Riccardi E, D'Ascenzo M, Azzena GB, Grassi C. 2010. Dopamine D1-like receptor activation depolarizes medium spiny neurons of the mouse nucleus accumbens by inhibiting inwardly rectifying K+ currents through a cAMP-dependent protein kinase A-independent mechanism. *Neuroscience* 167(3):678-90
165. Pompeiano M, Palacios JM, Mengod G. 1994. Distribution of the serotonin 5-HT2 receptor family mRNAs: comparison between 5-HT2A and 5-HT2C receptors. *Brain Res. Mol. Brain Res.* 23(1-2):163-78
166. Price JL, Powell TP. 1970. The mitral and short axon cells of the olfactory bulb. *J Cell Sci.* 7(3):631-51
167. Price JL, Powell TPS. 1970. The synaptology of the granule cells of the olfactory bulb. *J. Cell Sci.* 764:125-55
168. Pruss H, Derst C, Lommel R, Veh RW. 2005. Differential distribution of individual subunits of strongly inwardly rectifying potassium channels (Kir2 family) in rat brain. *Brain Res. Mol. Brain Res.* 139(1):63-79
169. Puopolo M, Belluzzi O. 1998. Functional heterogeneity of periglomerular cells in the rat olfactory bulb. *Eur. J. Neurosci.* 10(3):1073-83
170. Ramon y Cajal S. 1911. *Histologie du Sistème Nerveux de l'Homme et des Vertébrés.,* Paris: Maloine.
171. Rato C, Amirova SR, Bates DG, Stansfield I, Wallace HM. 2011. Translational recoding as a feedback controller: systems approaches reveal polyamine-specific effects on the antizyme ribosomal frameshift. *Nucleic Acids Res.* 39(11):4587-97
172. Rohacs T, Lopes C, Mirshahi T, Jin T, Zhang H, Logothetis DE. 2002. Assaying phosphatidylinositol bisphosphate regulation of potassium channels. *Methods Enzymol.* 345:71-92
173. Rolls ET. 2001. The rules of formation of the olfactory representations found in the orbitofrontal cortex olfactory areas in primates. *Chem. Senses* 26(5):595-604
174. Sadja R, Alagem N, Reuveny E. 2003. Gating of GIRK channels: details of an intricate, membrane-delimited signaling complex. *Neuron* 39(1):9-12
175. Saino-Saito S, Sasaki H, Volpe BT, Kobayashi K, Berlin R, Baker H. 2004. Differentiation of the dopaminergic phenotype in the olfactory system of neonatal and adult mice. *J Comp Neurol.* 479(4):389-98
176. Sawamoto K, Nakao N, Kakishita K, Ogawa Y, Toyama Y et al. 2001. Generation of dopaminergic neurons in the adult brain from mesencephalic precursor cells labeled with a nestin-GFP transgene. *J. Neurosci.* 21(11):3895-903
177. Sawamoto K, Nakao N, Kobayashi K, Matsushita N, Takahashi H et al. 2001. Visualization, direct isolation, and transplantation of midbrain dopaminergic neurons. *Proc. Natl. Acad. Sci. U. S. A* 98(11):6423-8
178. Schneider SP, Macrides F. 1978. Laminar distributions of interneurons in the main olfactory bulb of the adult hamster. *Brain Res. Bull.* 3(1):73-82
179. Schoenfeld T, Macrides F. 1984. Topographic organization of connections between the main olfactory bulb and pars externa of the anterior olfactory nucleus in the hamster. *J. Comp. Neurol.* 227:121-35
180. Schoenfeld T, Marchand JE, Macrides F. 1985. Topographic organization of tufted cell axonal projections in the hamster main olfactory bulb: an intrabulbar associational system. *J. Comp. Neurol.* 235:503-18
181. Schulze D, Krauter T, Fritzenschaft H, Soom M, Baukrowitz T. 2003. Phosphatidylinositol 4,5-bisphosphate (PIP2) modulation of ATP and pH sensitivity in Kir channels. A tale of an active and a silent PIP2 site in the N terminus. *J. Biol. Chem.* 278(12):10500-5
182. Scott JW, McBride RL, Schneider SP. 1980. The organization of projections from the olfactory bulb to the piriform cortex and olfactory tubercle in the rat. *J. Comp. Neurol.* 194:519-34
183. Seamon KB, Daly JW. 1981. Forskolin: a unique diterpene activator of cyclic AMP-generating systems. *J. Cyclic. Nucleotide. Res.* 7(4):201-24
184. Shepherd GM, Greer CA. 1998. Olfactory bulb. In *The synaptic organisation of the brain*, ed. GM Shepherd,159-203. New York: Oxford University Press.
185. Shin HG, Lu Z. 2005. Mechanism of the voltage sensitivity of IRK1 inward-rectifier K+ channel block by the polyamine spermine. *J. Gen. Physiol* 125(4):413-26
186. Shioya T, Matsuda H, Noma A. 1993. Fast and slow blockades of the inward-rectifier K+ channel by external divalent cations in guinea-pig cardiac myocytes. *Pflugers Arch.* 422(5):427-35
187. Shipley MT, Ennis M. 1996. Functional organisation of olfactory system. *J. Neurobiol.* 30:123-76
188. Shyng SL, Barbieri A, Gumusboga A, Cukras C, Pike L et al. 2000. Modulation of nucleotide sensitivity of ATP-sensitive potassium channels by phosphatidylinositol-4-phosphate 5-kinase. *Proc. Natl. Acad. Sci. U. S. A* 97(2):937-41
189. Sibley DR, Monsma FJ, Jr. 1992. Molecular biology of dopamine receptors. *Trends Pharmacol. Sci.* 13(2):61-9

190. Slesinger PA. 2001. Ion selectivity filter regulates local anesthetic inhibition of G-protein-gated inwardly rectifying K+ channels. *Biophys. J.* 80(2):707-18
191. Smith TC, Jahr CE. 2002. Self-inhibition of olfactory bulb neurons. *Nat. Neurosci.* 5(8):760-6
192. Sodickson DL, Bean BP. 1996. GABAB receptor-activated inwardly rectifying potassium current in dissociated hippocampal CA3 neurons. *J. Neurosci.* 16(20):6374-85
193. Spassova M, Lu Z. 1998. Coupled ion movement underlies rectification in an inward-rectifier K+ channel. *J. Gen. Physiol* 112(2):211-21
194. Spors H, Wachowiak M, Cohen LB, Friedrich RW. 2006. Temporal dynamics and latency patterns of receptor neuron input to the olfactory bulb. *J. Neurosci.* 26(4):1247-59
195. Standen NB, Stanfield PR. 1978. Inward rectification in skeletal muscle: a blocking particle model. *Pflugers Arch.* 378(2):173-6
196. Suter KJ, Smith BN, Dudek FE. 1999. Electrophysiological recording from brain slices. *Methods* 18(2):86-90
197. Tabata T, Haruki S, Nakayama H, Kano M. GABAergic activation of an inwardly rectifying K+ current in mouse cerebellar Purkinje cells. The Journal of Physiology Online 563[2], 443-457. 2005.
198. Tabor CW, Tabor H. 1984. Polyamines. *Annu. Rev. Biochem.* 53:749-90
199. Temple S. 2001. The development of neural stem cells. *Nature* 414(6859):112-7
200. Temple S, Alvarez-Buylla A. 1999. Stem cells in the adult mammalian central nervous system. *Curr. Opin. Neurobiol.* 9(1):135-41
201. Toida K, Kosaka K, Aika Y, Kosaka T. 2000. Chemically defined neuron groups and their subpopulations in the glomerular layer of the rat main olfactory bulb. IV. Intraglomerular synapses of tyrosine hydroxylase-immunoreactive neurons. *Neuroscience* 101(1):11-7
202. Toida K, Kosaka K, Heizmann CW, Kosaka T. 1998. Chemically defined neuron groups and their subpopulations in the glomerular layer of the rat main olfactory bulb: III. Structural features of calbindin D28K-immunoreactive neurons. *J Comp Neurol.* 392(2):179-98
203. van der Heyden MA, Stary-Weinzinger A, Sanchez-Chapula JA. 2013. Inhibition of cardiac inward rectifier currents by cationic amphiphilic drugs. *Curr. Mol. Med.* 13(8):1284-98
204. Ventura RE, Goldman JE. 2007. Dorsal radial glia generate olfactory bulb interneurons in the postnatal murine brain. *J Neurosci.* 27(16):4297-302
205. Wachowiak M, Cohen LB. 2001. Representation of odorants by receptor neuron input to the mouse olfactory bulb. *Neuron* 32(4):723-35
206. Wachowiak M, Shipley MT. 2006. Coding and synaptic processing of sensory information in the glomerular layer of the olfactory bulb. *Semin. Cell Dev. Biol.* 17(4):411-23
207. Walsh KB. 2011. Targeting GIRK Channels for the Development of New Therapeutic Agents. *Front Pharmacol.* 2:64
208. Wang C, Delcros JG, Cannon L, Konate F, Carias H et al. 2003. Defining the molecular requirements for the selective delivery of polyamine conjugates into cells containing active polyamine transporters. *J. Med. Chem.* 46(24):5129-38
209. Weickert CS, Webster MJ, Colvin SM, Herman MM, Hyde TM et al. 2000. Localization of epidermal growth factor receptors and putative neuroblasts in human subependymal zone. *J Comp Neurol.* 423(3):359-72
210. Wichterle H, Turnbull DH, Nery S, Fishell G, Alvarez-Buylla A. 2001. In utero fate mapping reveals distinct migratory pathways and fates of neurons born in the mammalian basal forebrain. *Development* 128(19):3759-71
211. Xie LH, John SA, Ribalet B, Weiss JN. 2005. Long polyamines act as cofactors in PIP2 activation of inward rectifier potassium (Kir2.1) channels. *J. Gen. Physiol* 126(6):541-9
212. Xie LH, John SA, Ribalet B, Weiss JN. 2007. Activation of inwardly rectifying potassium (Kir) channels by phosphatidylinositol-4,5-bisphosphate (PIP2): interaction with other regulatory ligands. *Prog. Biophys. Mol. Biol.* 94(3):320-35
213. Xie LH, John SA, Weiss JN. 2002. Spermine block of the strong inward rectifier potassium channel Kir2.1: dual roles of surface charge screening and pore block. *J. Gen. Physiol* 120(1):53-66
214. Xie LH, John SA, Weiss JN. 2003. Inward rectification by polyamines in mouse Kir2.1 channels: synergy between blocking components. *J. Physiol* 550(Pt 1):67-82
215. Xu R, Zhao Y, Chen C. 2002. Growth hormone-releasing peptide-2 reduces inward rectifying K+ currents via a PKA-cAMP-mediated signalling pathway in ovine somatotropes. *J. Physiol* 545(Pt 2):421-33
216. Yang J, Yu M, Jan YN, Jan LY. 1997. Stabilization of ion selectivity filter by pore loop ion pairs in an inwardly rectifying potassium channel. *Proc. Natl. Acad. Sci. U. S. A* 94(4):1568-72
217. Yang Z, Xu H, Cui N, Qu Z, Chanchevalap S et al. 2000. Biophysical and molecular mechanisms underlying the modulation of heteromeric Kir4.1-Kir5.1 channels by CO2 and pH. *J. Gen. Physiol* 116(1):33-45

218. Yu CR, Power J, Barnea G, O'Donnell S, Brown HE et al. 2004. Spontaneous neural activity is required for the establishment and maintenance of the olfactory sensory map. *Neuron* 42(4):553-66
219. Yung WH, Hausser MA, Jack JJ. 1991. Electrophysiology of dopaminergic and non-dopaminergic neurones of the guinea-pig substantia nigra pars compacta in vitro. *J Physiol.* 436:643-67
220. Zaborszky L, Carlsen J, Brashear HR, Heimer L. 1986. Cholinergic and GABAergic afferents to the olfactory bulb in the rat with special emphasis on the projection neurons in the nucleus of the horizontal limb of the diagonal band. *J Comp Neurol.* 243(4):488-509
221. Zaborszky L, Carlsen J, Brashear HR, Heimer L. 1986. Cholinergic and GABAergic afferents to the olfactory bulb in the rat with special emphasis on the projection neurons in the nucleus of the horizontal limb of the diagonal tract. *J. Comp. Neurol.* 243(4):488-509
222. Zeng WZ, Li XJ, Hilgemann DW, Huang CL. 2003. Protein kinase C inhibits ROMK1 channel activity via a phosphatidylinositol 4,5-bisphosphate-dependent mechanism. *J. Biol. Chem.* 278(19):16852-6
223. Zhang X, Firestein S. 2002. The olfactory receptor gene superfamily of the mouse. *Nat. Neurosci.* 5(2):124-33
224. Zou DJ, Feinstein P, Rivers AL, Mathews GA, Kim A et al. 2004. Postnatal refinement of peripheral olfactory projections. *Science* 304(5679):1976-9